ISSN 2463-6029 (Print)
ISSN 2350-3432 (Online)

Feasibility of Water Quality Monitoring by Remote Sensing in the Waikato Region

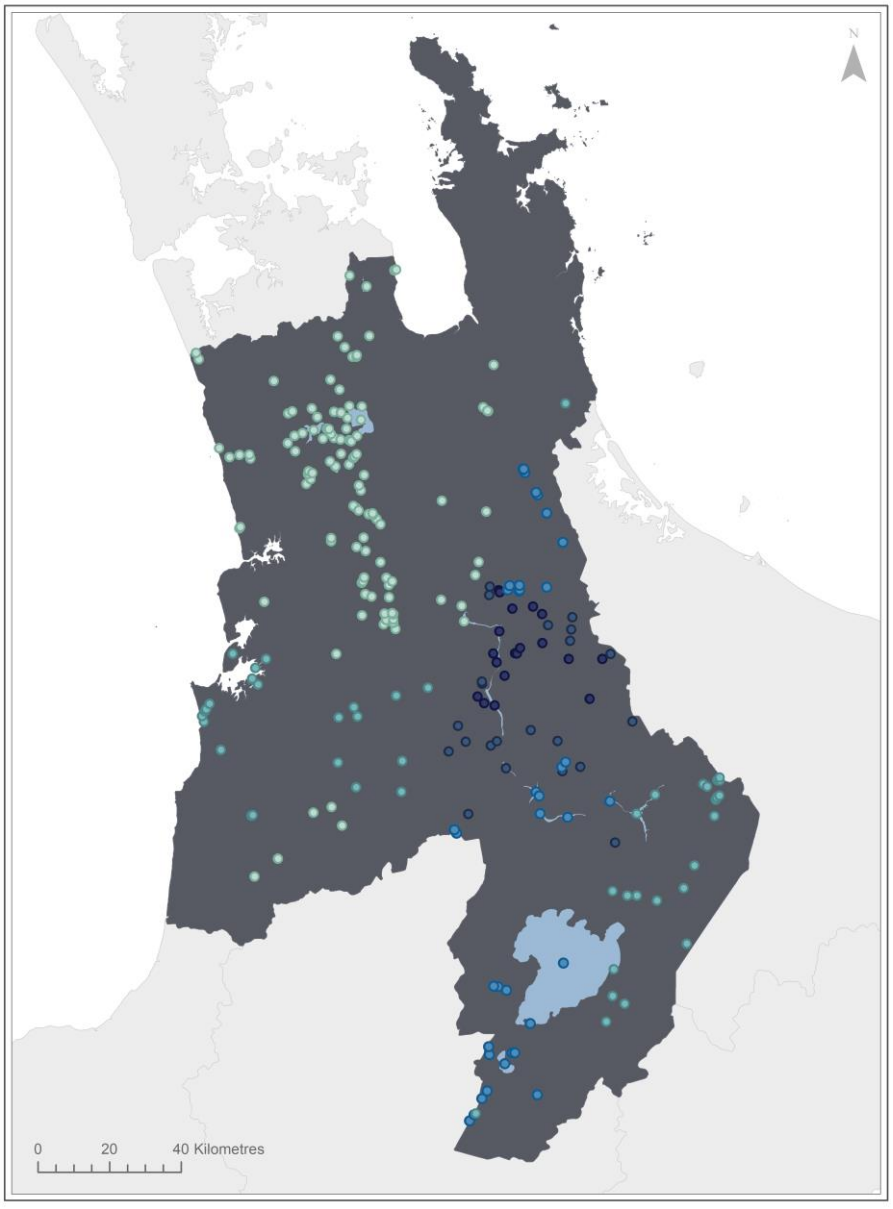

2017
ERI report number 87
Client report prepared for Waikato Regional Council by The University of Waikato, Environmental Research Institute

Moritz K. Lehmann, Lena A. Schallenberg and Mat Allan

Environmental Research Institute
University of Waikato, Private Bag 3105
Hamilton 3240, New Zealand

Environmental Research Institute
Te Pūtahi Rangahau Taiao
THE UNIVERSITY OF WAIKATO

THE UNIVERSITY OF WAIKATO
Te Whare Wānanga o Waikato

Reviewed by:

Ian Hawes

University of Waikato

Approved for Release by:

John Tyrrell

University of Waikato

Cover image: Locations of lakes in the Waikato Region. Colour coding indicates the average number of observations per year derived from the Landsat 8 archive.

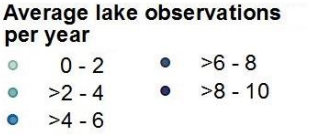

Executive Summary

The Waikato Regional Council (WRC) has statutory environmental monitoring requirements, including commitments arising from the National Policy Statement for Freshwater Management and State of the Environment reporting. Lakes, large rivers and estuaries pose a challenge for water quality monitoring programs due to their size, number and accessibility. To meet the increasing demand for more comprehensive monitoring to facilitate evidence-based regional policy making, cost-effective monitoring tools capable of capturing multiple attributes at various temporal and spatial scales are desirable.

Earth observation satellites currently collect complete imagery of New Zealand every 1 to 16 days and the data is freely available to download. Potentially, all water bodies which have at least a 90 by 90 m area of open water can be resolved from space and algorithms exist to convert the data to parameters related to water quality. This technology potentially provides an opportunity for supplementary monitoring of selected water quality-related variables at a greater frequency and spatial resolution and coverage than is currently available for the Waikato region's lakes, large rivers and estuaries. The University of Waikato was commissioned by the Waikato Regional Council to prepare this report to help WRC evaluate whether this opportunity is worthwhile pursuing through the implementation of a system for the routine monitoring of water quality using remote sensing.

This report summarises background information and reviews literature pertinent to the use of remote sensing for water quality monitoring. Water quality monitoring using satellite imagery is principally based on the measurement of the colour of water and the derivation of attributes through their respective contribution to the spectral light field. Attributes which can be derived include chlorophyll *a*, suspended sediments, coloured dissolved organic matter, Secchi depth and turbidity. Currently, Landsat-8, Sentinel-2a and Sentinel-3a are the most suitable satellite platforms to provide this data. Their data products are provided at sensor-specific resolutions, i.e., the sensor footprint (spatial resolution), number of wave bands (spectral resolution) and frequency of overpasses (temporal resolution). Table E1 summarises the properties of the most relevant remote

Table E1: Current and future satellite sensors feasible for use in inland water quality retrieval. The suitability of each sensor for the retrieval of individual constituents is suggested, along with the minimum water body size (Adapted from: Dekker & Hestir 2012).

Satellite	Spatial Resolution (m)	Repeat Cycle (days)	Spectral Bands (400-1000 nm)	Lifespan (years)	Water Quality Variables						Minimum water body size (ha)
					Chl *a*	TSS	PC	CDOM	SD	TURB	
Landsat 7	30	16	4	1999-2004+	🟡	🟢	🟡	🟢	🟢	🟢	1
Landsat 8	15	16	Pan*	2013-2023+							1
	30	16	5		🟢	🟢	🟡	🟢	🟢	🟢	
Sentinel-2 A&B	10	10 5 (with B)	4	2015-2023+	🟢	🟢	🟢	🟢	🟢	🟢	0.5
	20		4		🟢	🟢	🟢	🟢	🟢	🟢	
Sentinel-3 A&B	300	1-2 (with B)	21	A: 2016-2025+ B: 2017 - 2025	🟢	🟢	🟢	🟢	🟢	🟢	10

🟢 Highly Suitable 🟢 Suitable 🟡 Potential 🔴 Not Suitable

Chl *a*: Chlorophyll *a*, TSS: Total suspended solids, PC: Particulate carbon, CDOM: Coloured dissolved organic matter, SD: Secchi depth, TURB: Turbidity.

*Pan: one single band (panchromatic band 8, 500-680 nm)

sensing platforms and their suitability for water quality attribute detection. Improvements in relevant earth observations are anticipated as Sentinel-2b (launched 7 March 2017) becomes operational, Sentinel-3b is to be launched (scheduled for 2017) and a hyperspectral mission is being planned (HyspIRI anticipated launch in 2021).

This report also includes several regional case studies of lakes where remote sensing has been applied for the determination of water quality. These case studies provide quantitative insights into the accuracy of water quality algorithms and their applicability across the range of lakes of the Waikato region. Examples of remote sensing of water quality in rivers and estuaries come from the international scientific literature and often deal with larger systems which are easier to detect remotely than comparatively smaller Waikato waters. The case studies discussed in this report are summarised in Table E2.

Table E2: Summary of case studies discussed in this report.

Reference	Sensor	Parameter	Coefficient of determination (r^2)	Location	Water body Type
Allan (2008)	Landsat 7 ETM+	Log-Chl *a*	0.83 (*N* = 13, 0.8 - 136 µg L^{-1}) 0.91 (*N* = 16, 0.4 – 89.1 µg L^{-1})	Rotorua Lakes	Lakes
	Landsat 7 ETM+	Log-Chl *a*	0.84 (*N* = 6, 9 – 135 µg L^{-1})	Waikato Lakes	Lakes
	Landsat 7 ETM+	TSS	0.98 (*N* = 15, 0 – 350 mg L^{-1})		
Allan (2011)	Landsat 7 ETM+	Log-Chl *a*	0.80 (*N* = 33, 0.8 – 136 µg L^{-1})	Rotorua Lakes, Lake Taupo	Lakes
Hicks *et al.* (2013)		TSS	0.94 (*N* = 35, 0 – 962 mg L^{-1})	Waikato Lakes	Lakes
		Turbidity	0.92 (*N* = 36, 1.25 – 399 NTU)		
		Log-SD	0.67 (*N* = 32, 0.005 – 3.78 m)		
Allan (2014)	MODIS	Tripton*	0.73 (*N* = 9, 50 – 400 mg L^{-1})‡	Lake Ellesmere	Lake
			0.72 (*N* = 9, 50 – 400 mg L^{-1})‡		
Allan et al. (2015)	Landsat 7 ETM+	Chl *a*	0.68 (*N* = 87, 0.1 – 136 µg L^{-1})‡	Rotorua Lakes	Lakes
			0.58 (*N* = 87, 0.1 – 136 µg L^{-1})‡		
Zhao *et al.* (2011 & 2014)	Landsat 7 Panchromatic Band	Log-SD	0.64 (*N* = 51, 0.09 – 0.90 m)‡	Tributaries to Lake Taihu, China	Rivers
Schwarz *et al.* (2010)	MODIS, Landsat 7ETM+, SeaWiFS	Chl *a*, calcite	Not determined	Canterbury Rivers	Rivers
Olmanson *et al.* (2013)	Airborne hyperspectral sensors	Log-Chl *a*, Log-TSS Log-Turbidity	0.86 (*N* = 21, 8 – 380 µg L^{-1})‡‡ 0.84 (*N* = 21, 2 – 95 mg L^{-1})‡‡ 0.86(*N* = 21, 2 – 50 NTU)‡‡	Mississippi and Minnesota River	Rivers
Akbar *et al.* (2013)	Landsat 5 TM	CWQI categories** Turbidity classes	0.91 (*N* = 31, 2 – 4)	Bow River, Canada	Rivers

Reference	Sensor	Parameter	Coefficient of determination (r^2)	Location	Water body Type
Keith *et al.* (2014)	MERIS	Chl *a*	0.87 (N = 120, 1 – 122 µg L^{-1})‡	Neuse and Tar-Pamlico Estuaries, USA	Estuaries
Doxaran *et al.* (2009)	MODIS Terra MODIS Aqua	SPM	0.77 (N = 59, 10 – 2200 g m^{-3})‡ 0.82 (N = 59, 10 – 2200 g m^{-3})‡	Gironde Estuary, France	Estuary
Shen *et al.* (2010)	MERIS	Chl *a*	RMSE = 0.86 µg L^{-1} (spring, N = 57, 0.01 – 3 µg L^{-1}) RMSE = 2.87 µg L^{-1} (summer, N = 31, 1 – 31 µg L^{-1})	Yangtze Estuary, China	Estuary

Chl *a*: chlorophyll *a*, TSS: Total suspended solids, SD: Secchi depth, SPM: Suspended particulate matter, *N*: number of samples, RMSE: Root mean square error.
*Tripton includes sand, silt, clay and other inorganic material such as atmospheric dust as well as non-living organic matter
**Canadian Water Quality Index
‡Range of values read from graphs in the reference
‡‡Values shown are averages calculated from Table 2 in Olmanson *et al.* (2013)

In principle, a water body is suitable for remote sensing if the surface area is large enough to include water-only pixels and deep enough to preclude interference from bottom reflection. In practice, it also depends on the prevalence of clouds and the frequency of overpasses of the satellite. Almost all named lakes in the Waikato have been observed on average 25% of the time by Landsat 8, which equates to approximately six successful retrievals per lake, per year given its 16 day return time. The success rate appears to be largely due to cloud cover. Seasonality of visibility has not been assessed, but the limitations imposed by cloud cover suggest that Landsat 8 imagery may be best viewed as an adjunct to ongoing monitoring, by allowing selected variables to be monitored at more locations. Fifty-seven percent of the lakes (137) are also large enough to yield more than three pixels, potentially allowing spatial variability to be addressed.

A major limitation to observing rivers by remote sensing is the channel width relative to the resolution of the sensor. After the river banks are masked to reduce contamination of the signal by littoral effects, such as river bed reflectance and macrophytes, the visible image width is required to be at least one pixel, e.g., 10, 30 or 60 m. Only the Waikato River exceeds 30 m of width over much of its length and is therefore theoretically visible by Landsat sensors. The Waihou River also exceeds 30 m over some of its lower reach after buffering and both rivers exceed 60 m buffered width in some parts of their reach. The Waipa River is only visible with 10 m resolution sensors such as that of Sentinel-2 satellite. The lack of regional case studies means that this report cannot predict the accuracy of remotely sensed river water quality.

There are many estuaries in the Waikato region varying across a wide range of sizes. In addition to the constraints on visibility of lakes, estuaries are highly dynamic systems where tides and other coastal processes modify bathymetry, water depth and water clarity over a range of temporal and spatial scales. Visibility statistics for 23 of the larger (> 100 ha) estuaries show that on average 21% of Landsat overpasses yield data which may be used for water quality studies, equivalent to 5 times per year. The science of remote sensing of estuaries is less well developed than for lakes, and limitations to the quality of the data due to factors such as bottom reflectance and wave breaking must also be considered.

The hardware, software and human resources required to design and implement a system for the retrieval and processing of satellite data to generate water quality reports are considered. We note that:

- Remotely sensed data is freely available;

- Several free processing tools exist in the public domain;
- Some commercial software is already in use at WRC;
- No specialist hardware is needed; and
- The requirement for advanced technical expertise is easily outsourced.

We estimate that a single hardware system and 71 days of effort by a range of technical staff is sufficient to implement water quality monitoring by remote sensing, with 10 days of technical effort per month to maintain and operate thereafter.

The final chapter of this report synthesizes the technical information by way of a decision support framework, enabling managers to determine the feasibility of a remote sensing water quality monitoring system. This decision support framework is divided into three phases:

1. Initial scoping and investigation;
2. Planning; and
3. Implementation.

Each decision in the framework allows for compromises, i.e., by reconsidering the data requirements to improve feasibility, and suggests alternative monitoring methodologies to remote sensing**.** Finally, the framework prescribes a long-term review process for formal re-evaluation of the system, including whether it meets the operational goals and if it should be implemented. An example pathway of the decision support framework is presented.

Acknowledgements

This project was commissioned by the Waikato Regional Council and special thanks are due to Deniz Özkundakci and Michael Pingram for valuable discussions and input. The help of Glen Stichbury, Brendan Hicks, Julia King and David Hamilton during various stages of the project is greatly appreciated. Some analyses presented in this report were made possible through funding by MBIE Grant UOW 1503 (Enhancing the Health and Resilience of New Zealand Lakes).

Table of Contents

Introduction

The Waikato Regional Council (WRC) has statutory environmental monitoring requirements, including commitments arising from the National Policy Statement for Freshwater Management (NPS-FM, MfE 2015) and State of the Environment (SOE) reporting. Lakes, large rivers and estuaries pose a challenge for monitoring programs due to their size, number and accessibility. To meet an increasing demand for more comprehensive monitoring, for example, for evidence-based regional policy making, cost-effective tools that are capable of capturing multiple attributes at various temporal and spatial scales are desirable.

Remote sensing by satellite-borne sensors has the potential to address part of this challenge by autonomously collecting environmental data at synoptic space and time scales (Alikas *et al.* 2015). The University of Waikato was commissioned by the Waikato Regional Council to help WRC evaluate whether water quality monitoring using remote sensing is feasible.

The feasibility of using remote sensing for the routine monitoring of water quality of lakes, large rivers and estuaries from a scientific and technical stand point depends on the responses to two basic questions:

- What water-quality related parameters are amenable to remote sensing?
- Does remote sensing currently provide estimates of these water quality parameters to a satisfactory accuracy?
- If not, how much more research and development is required to allow retrieval to be sufficiently accurate to meet required standards
- Can satellites observe a sufficient number of water bodies often and regularly enough to be useful?
- Does the potential data return justify the cost of investment into remote sensing technology?

Decision making in this context is a sequential one, and in this report we focus on the technical issues related to the suitability of remote sensing to deliver data that will add to the monitoring programmes currently in place. We then provide guidance for the implementation of a system to use remote sensing for monitoring. It will furthermore discuss whether parameters derived from remote sensing can fulfil the requirements of overarching national regulations, such as the Resource Management Act (RMA) and National Policy Statement for Freshwater Management.

This report begins by summarising background information and reviewing literature pertinent to the use of remote sensing for water quality monitoring. It outlines the current satellite and sensor technologies, define the water quality parameters which are observable using remote sensing platforms and reviews which sensors are most suitable for the retrieval of individual parameters from lakes, rivers and estuaries at a regional scale. We also describe different algorithms used to estimate water quality parameters from satellite imagery in terms of their error and validation statistics. The review concludes with case studies of remote sensing applications to water quality parameters in lakes, rivers and estuaries both in New Zealand and internationally if no local applications exist, with particular attention given to studies using smaller water bodies similar to those in the Waikato region. These case studies illustrate the levels of accuracy remote sensing currently provides for estimates of water quality parameters. We note that our review is restricted to remote sensing products which are freely available. A number of commercial satellite services and companies offer operational water quality monitoring, but these are not considered here as their retrieval algorithms are often proprietary and not publicly documented and their data products are unlikely to be validated for New Zealand and the Waikato.

The section *Regional Context Analysis* presents the results of a spatial analysis on the size and shape of Waikato's lakes, rivers and estuaries to address the second question above regarding how many water bodies can be seen from space. It also reviews the current state of knowledge of optical variability in Waikato water bodies which is central to the performance of the retrieval algorithms.

The third section, *Implementation Pathway*, provides practical detail to help estimate the effort and cost associated with the implementation and operation of a system for water quality monitoring using freely available satellite data.

Review

This section describes the challenges of monitoring water quality at the regional level and outlines where remote sensing may provide opportunities to support monitoring programs. We present not a comprehensive literature review, but extend our previous work (e.g., Allan *et al.* 2015; Hicks *et al.* 2013) with new references and in-depth descriptions of pertinent details found by following the chains of citations and targeted literature searches using Google Scholar.

The Challenges of Water Quality Monitoring and the Remote Sensing Opportunity

The Waikato region contains 240 standing water bodies (lakes[1]) larger than 1 ha in surface area (FENZ geo-database, Leathwick 2010), approximately 1,800 km of rivers of order 5 or higher (M. Pingram, pers. comm.) and approximately 23 estuaries larger than 100 ha in surface area (H. Jones, pers. comm.). Conventional monitoring provides bimonthly, seasonal or annual sampling at best from a fraction of Waikato's surface water resources (Table 1). Sampling from such monitoring has limitations for detecting tends in water quality and important ecological processes occurring at weekly and monthly time scales. Remote sensing satellites have return periods of days to weeks and can potentially yield higher frequency observations.

Table 1: Summary of current water quality monitoring programs for lakes, large rivers and estuaries by the Waikato Regional Council.

Lakes	• Every two months from eight shallow lakes (going back over a decade); • Between 30 to 40 shallow lakes are sampled seasonally or annually; • Autonomous high-frequency monitoring instrumentation has been installed in four Waikato lakes (Ngaroto, Waahi, Whangape and Waikare). • No water quality information is available for 50% of the region's shallow lakes.
Large rivers	• Monthly monitoring of approximately 100 lotic systems spread across the region (10 sites on the main stem of the Waikato);
Estuaries	• Coastal water quality monitoring has focused on snapshot surveys of a number of estuaries (data is published on WRC website); • Coastal water quality monitoring programmes, including the installation of water quality monitoring buoys, are currently under development.

In contrast to conventional sampling methods, remote sensing offers views of the surface of water bodies theoretically at daily to weekly intervals and spatial resolutions superior to all but the most intense boat-based sampling grids, at comparatively small cost (Allan *et al.* 2015; Hicks *et al.* 2013). As a result, remote sensing technologies have been applied to a number of inland water quality studies across lakes, rivers and estuaries world-wide (see Section *Case Studies*). Continuous developments in satellite and sensor technologies and research into parameter retrieval algorithms are likely to increase the use of remote sensing methods for water quality monitoring (Dekker & Hestir 2012; Matthews 2011; Palmer *et al.* 2015).

The Fundamentals of Remote Sensing for Water Quality

Light travelling through a medium such as air or water can be absorbed, reflected and scattered, and the degree to which this happens depends on the optical properties of the transmitting medium (Figure 1)(Kirk 1994). Some parameters related to water quality have optical properties which change the nature of the underwater light field by scattering, absorption and reflection (Mobley

[1] While these standing water bodies may not be lakes by definition (pers. comm. D. Ozkundakci), the term "lake" is used in this report to for these water bodies for convenience.

1994). Satellites can measure the spectral composition of the light leaving the water providing an opportunity to back-calculate the concentrations of some water quality parameters (Seyhan & Dekker 1986).

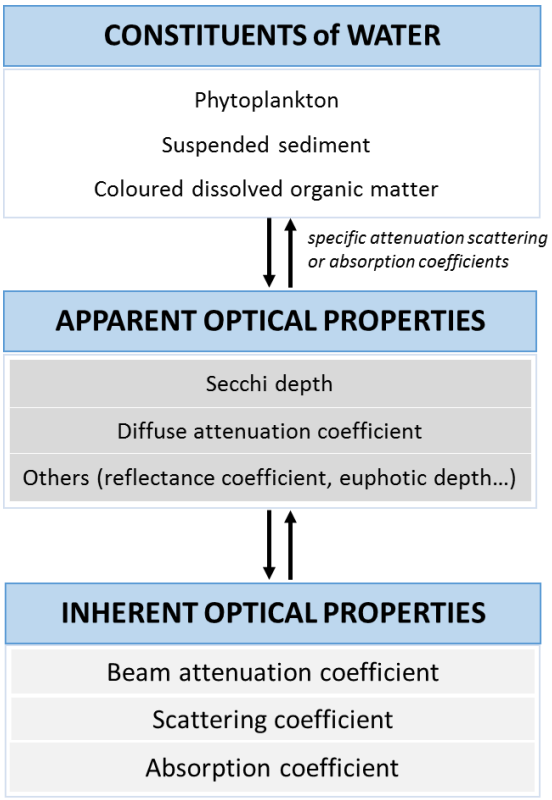

Figure 1: Relationship between constituents of water which attenuate light and various optical properties (After Vant & Davies-Colley 1984).

Several instances of absorption, reflection and scattering processes have to be taken into account when measuring light at altitude for the purpose of surface water assessment. First, light from the sun is both absorbed and scattered by the atmosphere, reaching the water surface as a mixture of direct sunlight and diffuse light scattered by the atmosphere (Olmanson *et al.* 2015). The water surface then reflects and refracts the downwelling irradiance, allowing a portion of light to penetrate the water column where it is further absorbed and scattered by water molecules and substances within the water (Kirk 1994) (Figure 2). Substances that alter the underwater light field are known as optically active constituents (OACs) and include the pigments of algal cells such as chlorophyll *a* (Chl *a*) and phycocyanin, suspended solids (both mineral and organic) and coloured dissolved organic matter (CDOM) which all scatter and absorb light at characteristic wavelengths (Dekker & Hestir 2012). Some of the light entering the water will be scattered and refracted such that it is directed upwards to leave the water with a spectral signature determined by the OACs of the water. Remote sensing platforms measure radiance reflectance, which is the ratio of water-leaving radiance over incoming solar irradiance. The normalization of upwelling radiance to downwelling irradiance accounts for variations in the intensity and spectral shape of the incoming solar radiation. It is important to note that all light related quantities are calculated across a range of wavelengths, the spectral band, which are specific to the design of the sensor.

The predominance of light at a particular wavelength is perceived by the human eye as colour. For example, chlorophyll *a* absorbs light throughout the visible wavelengths, except near 665 nm, which is the green part of the visible light spectrum; therefore, the 'greenness' of water can be related to the amount of chlorophyll *a*. Similarly, the 'brownness' and 'whiteness' of water can be related to

CDOM and suspended solids, respectively, but the difficulty lies in separating the interactions and overlaps between the spectral signatures of the OACs (Mobley 1994).

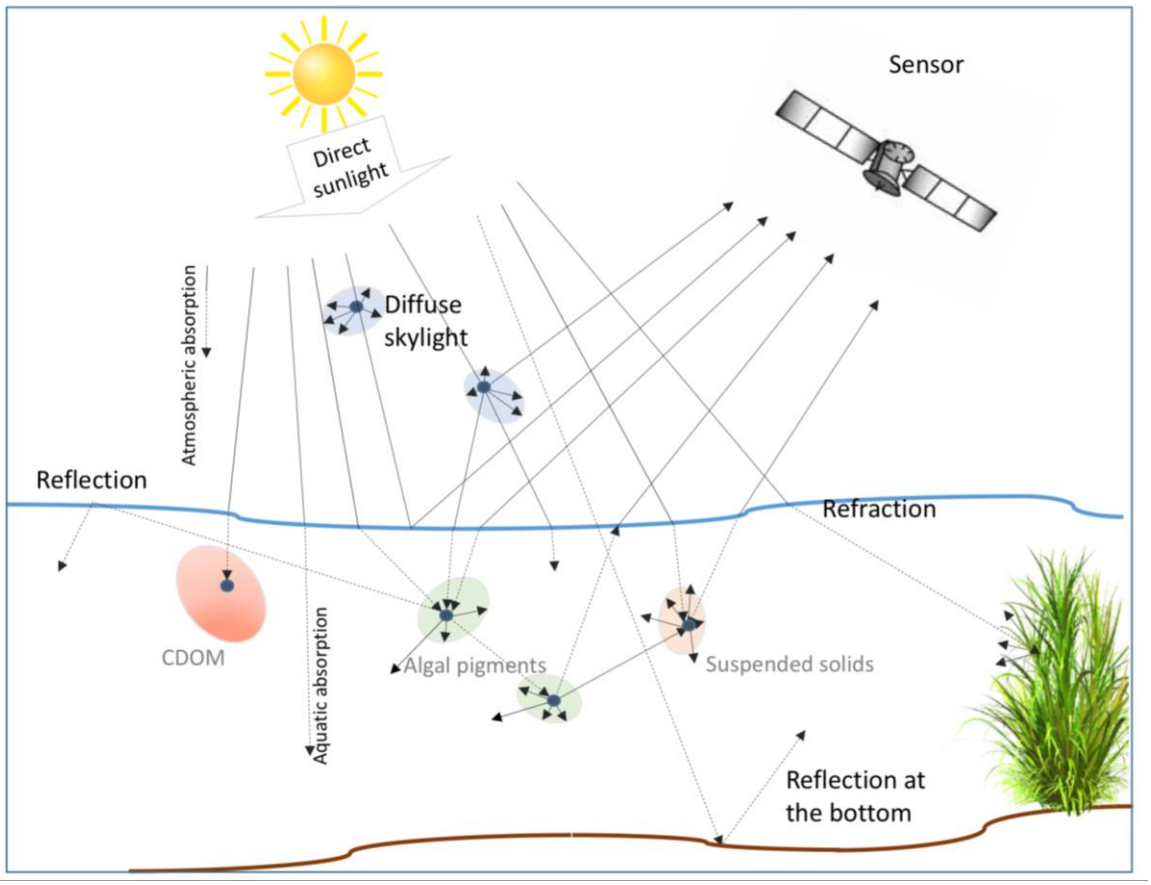

Figure 2: Light interactions through the atmosphere, water and substratum (After Dekker & Hestir, 2012).

The mixed spectral signatures received by the sensor are deconstructed using algorithms which relate the shape of the light spectrum to individual OACs. These algorithms can be developed in a variety of ways ranging from simple empirical relationships between *in situ* samples and radiance reflectance at certain wavelengths, to spectral additive models based on radiative transfer theory. Many algorithms have been developed and validated for individual sensors, however the majority of these were created specifically for ocean waters ('Case 1' waters) where the dominant OAC is chlorophyll *a* (Olmanson *et al.* 2015). Inland water bodies and estuaries are known as 'complex' or 'Case 2' waters where three or more constituents are normally present in a mixture (Matthews 2011). The complexity of Case 2 signatures lies in the fact that different constituents can have reflectance or absorption peaks in the same area of the spectrum, e.g. both chlorophyll *a* and total suspended solids (TSS) have a reflectance peak near 665 nm, making it difficult to distinguish one from the other. As a result, Case 1 algorithms do not produce accurate results in Case 2 waters and, moreover, no single Case 2 algorithm exists which works well in all Case 2 waters. A detailed review of algorithms is given in section *Retrieval Algorithms*.

Due to light extinction and scattering in the aquatic medium, most of the upwelling light comes from the surface layer of the water. Therefore, the depth to which the remotely sensed information is attainable depends on water clarity as it cannot resolve vertical variability in OACs.

The reflectance signature measured by an optical sensor contains information on the mixture of constituents from the surface water layer of the observed system. Such optical water quality information can add value to water quality analyses, as changes in optical water quality can

represent changes in primary productivity, temperature and biogeochemical processes as well as indicating trends such as eutrophication and sedimentation (Julian *et al.* 2013).

The Current State of Satellite Remote Sensing of Inland Water Quality Parameters

Remote sensing of water quality parameters is carried out using a sensor for electromagnetic radiation in the visible range of the spectrum (approximately 400 to 750 nm) mounted on earth orbiting satellites. Four main attributes of the sensor and their satellite platform determine the potential of remote sensing for monitoring water quality parameters: spatial resolution, spectral resolution, temporal resolution and swath size.

Spatial resolution refers to the pixel size of the image that is produced by a sensor, which ultimately determines the size of the feature that can be accurately mapped using remote sensing (Dekker & Hestir 2012). A greater number of pixels within a water body means that the spatial variability of water quality can be determined in finer detail and the water quality maps produced will have better resolution.

Spectral resolution involves the number of spectral bands that can be recorded by a sensor (Olmanson *et al.* 2015). A spectral band is a range within full spectrum of light over which a sensor responds with a signal. The response of a multispectral sensor typically spans ten to one hundred nanometres. The number of sensor bands and their width are important as the spectral signature of some water borne constituents can overlap and thus the more numerous and thinner the bands, the better the chances are for obtaining individual water quality parameters. Hyperspectral sensors employ imaging spectrometers which generally have hundreds to thousands of very narrow bands and are able to discern several OACs (Dornhofer & Oppelt 2016). For example, hyperspectral sensors have been successfully used to identify and quantify cyanobacteria using the pigment phycocyanin (Matthews 2011; Palmer *et al.* 2015) and sediment grain size composition from TSS (Dekker & Hestir 2012). Currently, satellites carry multispectral sensors which usually consist of up to 10 wave bands and many studies have successfully exploited their data to retrieve inland water quality parameters (Dornhofer & Oppelt 2016; Matthews 2011; Odermatt *et al.* 2012).

Temporal resolution is the frequency with which images of the same location are taken by a sensor (Matthews 2011). The temporal resolution of satellite sensor images depends on the specific satellite orbit which determines the return period of the satellite to the same location. Satellites used for earth observations have return periods ranging from one day to several weeks, with longer return periods meaning fewer images over a given duration. The return period and time of a satellite overpass is crucial when planning field work to collect corresponding *in situ* samples as these are required as near to the time of satellite overpass as possible. Whether *in-situ* samples can be usefully related to satellite observations depends on the time scale of variability in the environment, for example, most studies suggest that an offset be no more than a few days apart. Odermatt *et al.* (2010) found that images taken 5 days after *in situ* measurements were adequate for oligotrophic lakes, however estuary sites required sampling to be nearer the time of the satellite overpass.

The fourth sensor attribute important in determining sensor feasibility is swath size, defined as the extent of the sensor footprint on the ground. Many sensors sample a continuous track along the axis of satellite movement, so the swath size is the width of the sensor footprint perpendicular to the axis of movement. Swath size is an important property to consider in the design of routine monitoring applications for inland water bodies, because it determines how much of a region is covered in a single overpass. A complete image of a region may have to be composed of several overpasses which has implications when the objective is to compare simultaneous states of water bodies in the same region and also increases data processing requirements. Typically, sensors with larger swath sizes are more suited for monitoring at the regional scale, but there is the related disadvantage that greater spatial coverage comes at a lower spatial resolution, i.e., larger pixels.

Olmanson *et al.* (2015) suggest regional scale inland water quality monitoring requires freely available imagery with a spatial resolution of 5 to 50 m^2 at no less than weekly intervals and suitable spectral bands. To date no satellite sensor meets all these requirements. Current satellite platforms that are most suited to regional-scale water monitoring are those that provide the best balance between spatial, spectral and temporal resolution, swath size and cost. One of the challenges with satellite sensor platforms is their life expectancy and the fact that satellites can not be fixed easily if problems occur. For example, communication with the Envisat-1 satellite carrying the Medium Resolution Imaging Spectrometer (MERIS) was lost in April 2012, leaving a temporary gap in the capability to observe inland water bodies. In acknowledgement of this, two major agencies providing free satellite sensor imagery have established data continuity missions, releasing new satellites equipped with sensors that replace and improve older sensors as they are decommissioned. In 2013, NASA (United States National Aeronautics and Space Administration) released Landsat 8 to replace Landsat 5 and 7 and its enhanced spectral resolution was expected to reduce the retrieval error of Landsat 7 by around one-half (Roy *et al.* 2014). Similarly, the European Space Agency (ESA) has recently launched Sentinel-3a, which was designed to fill the gap left by the MERIS mission, matching the spatial resolution and improving on the spectral resolution with 6 additional spectral bands (Alikas *et al.* 2015; Palmer *et al.* 2015).

The continual development and improvement of sensors will allow the improvement of retrieval algorithms to new sensors as they become available (Augusto-Silva *et al.* 2014). For example, the Sentinel-2B satellite was launched on 7 March 2017 and Sentinel-3b is scheduled to launch in 2017. These platforms are the twins to the currently orbiting satellites, doubling the coverage of high-resolution optical imaging missions for the European Union Copernicus environmental monitoring system. To manage the transitions from previous to current and upcoming sensors, ESA formed the Global Lakes Sentinel Service (GLaSS), a group which focuses on the integration of the new Sentinel sensors into the current freshwater remote sensing environment. Studies produced by this group have suggested that the output from Sentinel-2 will be similar to, yet improve upon Landsat images, while Sentinel-3 output is expected to improve upon MERIS imagery (GLaSS 2015).

Currently the most ambitious project is the Hyperspectral Infrared Imager or HyspIRI satellite (Lee *et al.* 2015). This mission was recommended in the 2007 National Research Council Decadal Survey requested by NASA, NOAA, and USGS and is anticipated to collect hyperspectral imagery at 60 to 1000 m resolution over land and oceans. The launch is planned for 2021.

Characteristics of Current Satellite Sensors

The satellite sensors in orbit today cover a range of resolutions, return periods and spectral bands (Table 2). It is noted that the list includes the information to date, but may be incomplete or contain obsolete sensors at the time of reading due to the risks of space operations. For example, the highly successful MERIS sensor is not included in this list due to its recent decommissioning, however, its replacement Sentinel-3 Ocean and Land Colour Instrument (OLCI), are included.

Table 2: Current and future satellite sensors feasible for use in inland water quality retrieval. The suitability of each sensor for the retrieval of individual constituents is suggested, along with the minimum water body size. A plus (+) in the Lifespan column indicates that satellites often operate beyond their planned life span (Adapted from: Dekker & Hestir 2012).

Satellite (Operator)	Sensor	Spatial Resolution (m)	Repeat Cycle (days)	Spectral Bands (400-1000 nm)	Cost NZD (km^2)	Lifespan (years)	Water Quality Variables						Minimum water body size (ha)
							Chl *a*	TSS	PC	CDOM	SD	TURB	
Landsat 7 (NASA/USGS)	ETM+	30	16	4	Free	1999-2004+	Potential	Suitable	Potential	Suitable	Suitable	Suitable	1
Landsat 8 (NASA/USGS)	LDCM	15	16	Pan*	Free	2013-2023+							1
		30	16	5			Suitable	Suitable	Potential	Suitable	Suitable	Suitable	
Terra and Aqua (NASA)	MODIS	250	Daily	2	Free	1999-2008+	Not Suitable	Potential	Not Suitable	Not Suitable	Potential	Potential	10
		500	Daily	2			Not Suitable	Potential	Not Suitable	Potential	Potential	Potential	
		1000	Daily	9			Highly Suitable	Highly Suitable	Potential	Highly Suitable	Highly Suitable	Highly Suitable	
Suomi NPP (NASA/NOAA/ DoD)	VIIRS	750	0.5	7	Free	2011-2016	Suitable	Potential	Potential	Suitable	Suitable	Suitable	
Sentinel-2 A&B (ESA)	MSI	10	10 5 (with B)	4	Free	2015-2023+	Highly Suitable	Highly Suitable	Highly Suitable	Highly Suitable	Highly Suitable	Highly Suitable	0.5
		20		4			Highly Suitable	Highly Suitable	Highly Suitable	Highly Suitable	Highly Suitable	Highly Suitable	
Sentinel-3 A&B (ESA)	OLCI	300	1-2 (with B)	21	Free	A: 2016-2025+ B: 2017 - 2025	Highly Suitable	Highly Suitable	Highly Suitable	Highly Suitable	Highly Suitable	Highly Suitable	10

Highly Suitable Suitable Potential Not Suitable

*Pan: one single band (panchromatic band 8, 500-680 nm)

Acronyms: Chl *a*: Chlorophyll *a*, TSS: Total suspended solids, PC: Particulate carbon, CDOM: Coloured dissolved organic matter, SD: Secchi depth, TURB: Turbidity, NASA: National Aeronautics and Space Administration, USGS: United States Geological Survey, NOAA: National Oceanic and Atmospheric Administration, DoD: Department of Defense, ESA: European Space Agency

Figure 3 illustrates the current and future freely available satellite sensor bands and the spatial resolution of each. Sentinel-2 and Landsat 7 and 8 have the highest spatial resolution with pixel sizes ranging from 10 to 30 m, while MODIS (Moderate Resolution Imaging Spectroradiometer) has the lowest spatial resolution with pixels from 250-1000 m (Figure 3), allowing only for the retrieval of constituents from large water bodies.

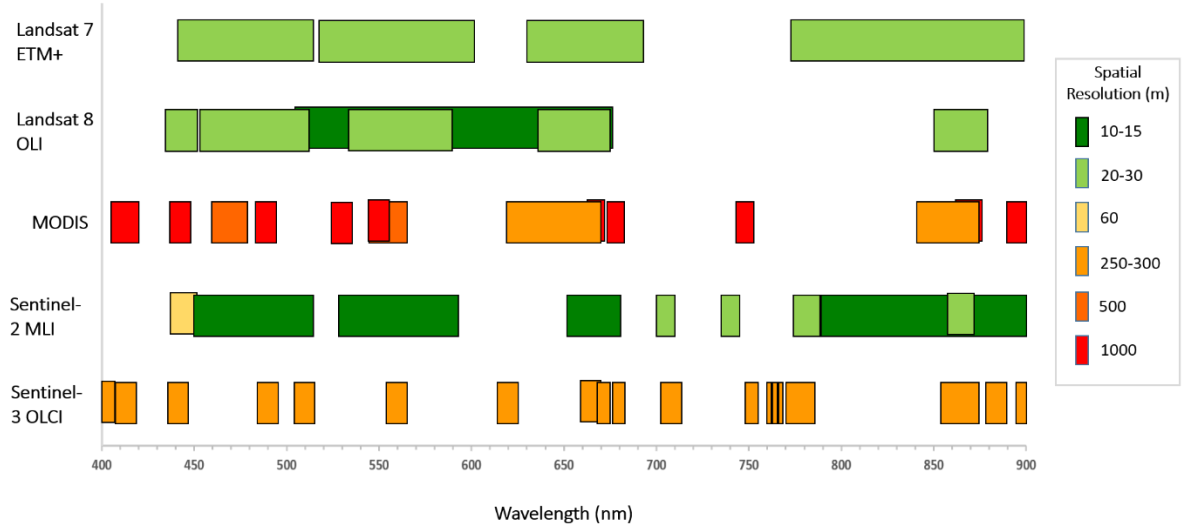

Figure 3. Existing and proposed satellite sensor platforms providing free imagery, illustrating the spatial and spectral resolution of each.

The spatial resolution of sensors has a direct influence on the size of the water body that can be accurately analysed, with high spatial resolution sensors able to remotely sense constituents from smaller water bodies such as rivers and small lakes. The minimum water body sizes detectable for major sensors have been determined in the literature and are summarised in Table 3 along with the calculated minimum water body size based on a relationship proposed by Dekker & Hestir (2012).

Table 3: Detectable water body size limits as determined in the literature along with the minimum water body area as calculated from four times pixel footprint as proposed by Dekker & Hestir (2012).

Sensor	Spatial resolution (m)	Minimum water body area	Reference	Calculated minimum water body area (ha)
Landsat 7 ETM+	30	Lakes: 4 ha	Olmanson *et al.* (2011 & 2015)	1.4
		River width: 65 m	Zhao *et al.* (2014)	
Landsat 8 OLI	30	1 ha	Roy *et al.* (2014)	1.4
MODIS	1000	1000 ha	Olmanson *et al.* (2011)	1600
	500	400 ha	Olmanson *et al.* (2011)	400
	250			100
Sentinel-2	10, 20, 60			0.64
Sentinel-3	300			144

The authors suggest that water body size should be at least 3 to 4 times the size of the pixel in order to obtain enough pure water pixels without signals from the surrounding banks and vegetation (Dekker & Hestir 2012). For example, a sensor with 30 m spatial resolution such as Landsat 7 and 8 could resolve a body of water of 120 by 120 m (1.4 ha). The Section *Regional Context Analysis* discusses the limitations of sensor footprint for the visibility of water bodies in the Waikato.

A study by Zhao *et al.* (2011) on the Xitiaoxi River in China found the minimum river width retrievable by a sensor with 30 m spatial resolution was between 65 and 98 m. In addition to river width, water depth also influences the retrieval of river spectral signatures, with the above study finding pixels within 17 m of the river shoreline were unusable due to adjacency effects (Zhao *et al.* 2014).

In summary, there is currently a trade-off between the spatial and spectral resolution of sensors, with Landsat sensors returning some of the highest spatial resolution at the expense of lower spectral resolution and broad spectral bands. The broad bands of Landsat sensors mean that there are smaller gaps in the spectrum and while the sensors can retrieve signatures across a wide range of wavelengths, individual constituents cannot be easily retrieved when co-occurring in a waterway. For example, the accurate and reliable retrieval of chlorophyll *a* estimates in complex waters using Landsat 7 has proven difficult (Allan *et al.* 2015), with MODIS images presenting similar challenges (Olmanson *et al.* 2011), however MODIS 1000 m resolution bands have sufficient spectral resolution to enable the application of semi-analytical algorithms which simultaneously estimate chlorophyll *a*, TSS and CDOM. MODIS and MERIS/Sentinel-3 have high temporal coverage, large swath widths and a greater number of spectral bands although the spatial resolution of these sensors is low and only applicable for large water bodies (Olmanson *et al.* 2011). Sentinel-2 currently has the best spatial and spectral resolution with a small pixel size of 10-20 m^2 allowing for the potential detection of water bodies as small as 0.64 ha using nine bands across the visible spectrum (Table 3, Figure 3).

Some investigators have attempted to circumvent the resolution trade-off by data-fusion techniques to merge images of high spectral resolution with images of high spatial resolution (Ashraf *et al.* 2008; Chang *et al.* 2015). The results of these analyses are impressive and should be considered to improve retrospective analyses. The requirements for such techniques for current purposes are arguably diminishing given the recent development of sensors with both high spatial and spectral resolution.

Other Sensor Platforms

Sensors akin to those mounted on satellites can also be used *in situ*, from the ground or on airborne platforms. Handheld and stationary sensors retrieve optical measurements from a water body at a small spatial scale (millimetres to metres) which can provide very detailed optical information for a particular site, but are inefficient to provide data outside the field of view. Tan *et al.* (2015) recommend using handheld spectrometers in conjunction with *in situ* sampling to accurately and conveniently measure the spectral signature of smaller rivers and streams. This would require field visits much like current monitoring regimes, though the empirical relationship found between these could be used to enhance algorithms developed for multispectral satellite or airborne sensors, which are limited by spectral resolution (Tan *et al.* 2015).

Airborne platforms are often optimal for monitoring small water bodies as they have high spatial resolution and can employ newer or larger hyperspectral sensors (Julian *et al.* 2013; Matthews 2011; Tan *et al.* 2015; Torgersen *et al.* 2001). In addition, the sensors are flown at low altitudes reducing the need for atmospheric correction when applying algorithms (Matthews 2011). Olmanson *et al.* (2013) found that airborne hyperspectral sensors could adequately predict water quality in large rivers, however the low-altitude flight paths again result in swath sizes too small for the complete capture of larger water bodies. Recurring flights are difficult to schedule for regular monitoring intervals, making it difficult to assess temporal trends. In addition, the large cost of both the sensors

and air time may exceed operational budgets for regional-scale routine monitoring purposes (Julian *et al.* 2013; Matthews 2011; Tan *et al.* 2015).

Observable Water Quality Constituents

Inland waters contain mixtures of these OACs resulting in a complex spectral shape composed of the contributions of individual constituents. Figure 4 shows how the spectral shape of pure water is modified by the addition of OACs as determined from a bio-optical model (Rudorff *et al.* 2006).

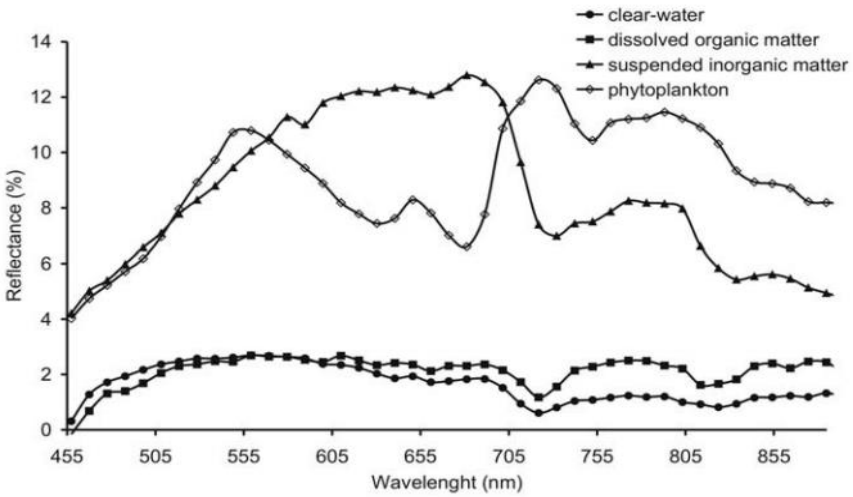

Figure 4: Modelled reflectance spectra of waters containing different optically active constituents (Source: Rudorff *et al.* 2006).

The result of the interaction of spectral absorption and scattering processes is shown in Figure 5 which shows a simplified eutrophic water reflectance spectrum, illustrating the peak reflectance (the peaks) and peak absorption wavelengths (the troughs) along with the regions of the spectrum often used to identify different constituents.

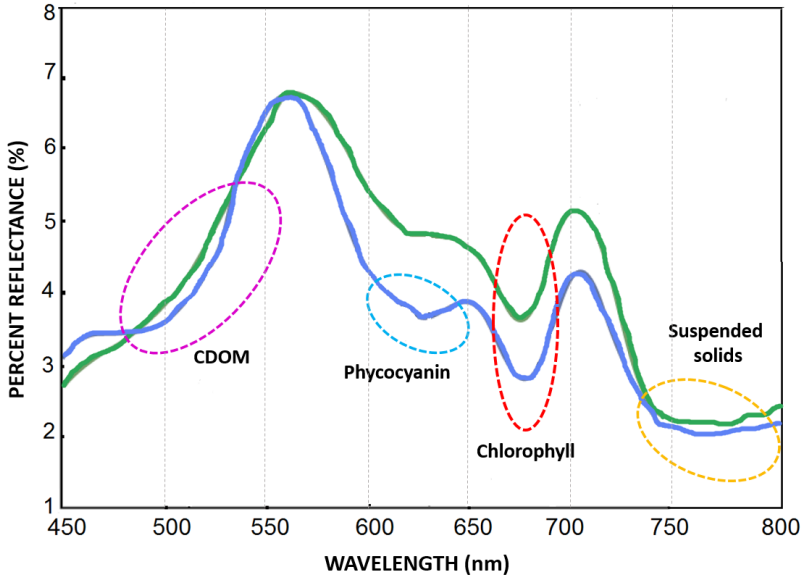

Figure 5: A simplified water reflectance signature for a eutrophic water body with circled areas indicating signature reflectance and absorption peaks often used to detect different water quality constituents (After Schalles & Yacobi 2000).

Figure 6 shows where regions affected by individual OACs lie along the spectrum of visible light. The goal of a remote sensor is to measure light intensity at as many of those spectral regions as possible

and it can be seen in Figure 6 how the current range of sensors achieves this. One challenge is the overlap in the constituent peaks (vertical bands in Figure 6), such as those of TSS and Chl *a* at 700 nm, which leads to difficulties in deciphering individual contributions to measured reflectance at that wavelength (Gitelson *et al.* 2008; Olmanson *et al.* 2015).

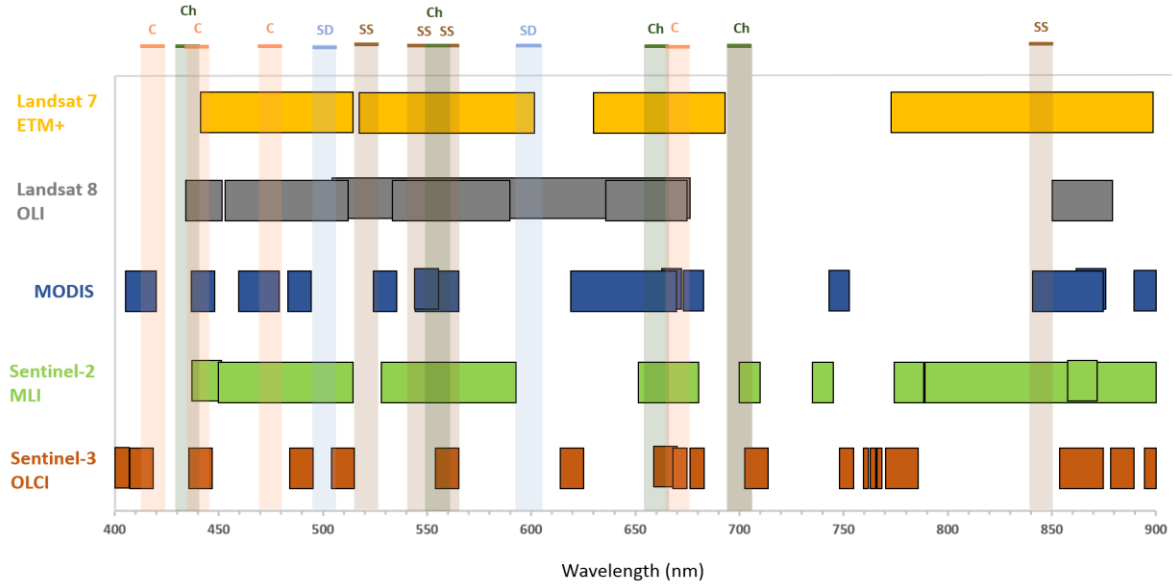

Figure 6: Current and future satellite sensor systems showing the wavebands (coloured horizontal bands) of each along with major signature peaks commonly used to isolate individual constituents (vertical bars). C: CDOM, Ch: chlorophyll *a*, SD: Secchi depth and SS: TSS.

The suitability of existing and future sensors for the retrieval of individual water quality parameters based on the spectral capabilities of each sensor is summarised in Table 2, adapted from Dekker & Hestir (2012). The Sentinel series appears best suited for the retrieval of all inland water quality parameters while Landsat 7 and 8 are suitable for most parameters. Landsat 7 and 8 and Sentinel-2 have the highest spatial resolution, allowing water bodies larger than 1 ha to be studied. The following sections describe issues related to the retrieval of individual water quality components.

Chlorophyll *a* and Phycocyanin

The photosynthetic pigment chlorophyll *a* found in algae and the accessory pigment phycocyanin found in cyanobacteria are indicative of phytoplankton and cyanobacterial biomass, respectively (Dekker & Hestir 2012). High concentrations of chlorophyll *a* can signify nuisance algal blooms, high nutrient levels and increased trophic status while high phycocyanin concentrations can indicate the presence of often harmful or toxic cyanobacterial blooms (Dekker & Hestir 2012). Chlorophyll *a* concentrations <30 µg L^{-1} have been successfully retrieved using a strong absorbance trough at 440 nm, while chlorophyll *a* concentrations >30 µg L^{-1} have been retrieved using both a peak at 560 nm and the ratio of the absorbance trough near 660 nm with the reflectance peak at 700 nm (Figure 6) (Allan, 2008; Matthews, 2011; Odermatt *et al.* 2012; Olmanson *et al.* 2013). Inclusion of the peak at 700 nm has proven highly successful in a number of studies on lakes, rivers and estuaries (r^2 > 0.8) as CDOM absorption in this region is minimal, aiding in the distinction between these two co-occurring constituents (Matthews 2011; Olmanson *et al.* 2013). It should be noted that the exact location and width of these spectral peaks and troughs differ depending on the species of phytoplankton present as well as their physiological state (Allan 2014) which may add an error to the retrieval of chlorophyll concentration from reflectance.

Phycocyanin has a strong absorption peak at 620 nm, often detectable by sensors with narrow bands. This spectral region falls within a gap in Landsat sensor wavebands (Matthews 2011; Olmanson *et al.* 2015), however, successful retrieval estimates have been obtained using MERIS

imagery. Simis *et al.* (2005) and Gomez *et al.* (2011) both found close relationships of phycocyanin (r^2 = 0.94 – 0.97) using MERIS imagery to both *in situ* samples and fluorometry measurements, respectively.

Coloured Dissolved Organic Matter (CDOM)

CDOM is comprised of coloured humic and fulvic acids which originate from the breakdown of both allochthonous and autochthonous organic matter; it is also known as yellow-substance, gelbstoff or gilvin, and is often visible in water as brownish or tea-like colouration (Matthews 2011; Vant 2015). As such, CDOM concentrations can be indicative of the organic matter and aquatic carbon content of water (Dekker & Hestir, 2012) as well as potentially providing an indication of dissolved organic carbon (DOC) concentration, although these correlations require further development (Brezonik *et al.* 2015). CDOM is often a major constituent in peat lakes (Allan 2008; Davies-Colley & Vant 1987) and it is the main light absorbing constituent in many rivers under normal flow conditions, with concentrations increasing after storm events which flush humics from the catchment (Julian *et al.* 2013). Due to the strong absorbance characteristics of CDOM, it is often difficult to derive (Dornhofer & Oppelt 2016), however many studies have used the strong absorption peak at 440 nm or the ratio of both sensitive bands below 600 nm and normalisation bands above 600 nm to retrieve CDOM estimates (Matthews 2011; Odermatt *et al.* 2012) (Figure 6).

Total Suspended Solids (TSS)

Total suspended solids (TSS) include all particles suspended in water which do not pass through a 0.2 µm filter. According to this definition TSS is constituted of a wide variety of material, such as mineral or inorganic particles, detritus, phytoplankton cells and animal matter. Especially in shallow lakes, TSS can include considerable amounts of detritus and inorganic mineral particles resuspended from the bottom. While its detailed optical characteristics depend on the absorption and scattering properties of the various constituents (Vant 2015), scattering by the suspended mineral fraction causes a reflection peak between 510 – 550 nm and in the infrared part (above 700 nm) of the spectrum (Allan 2008). The reflectance peak between 510 and 550 nm is successfully used to derive TSS when these are below 30 mg m^{-3}, but at higher TSS concentrations, reflectance above 800 nm is used due to superimposition by the optical properties of chlorophyll *a* at 550 nm (Olmanson *et al.* 2013).

Often in the technical literature, variables related to TSS are defined and used in remote sensing applications, e.g., suspended sediment, suspended particles, suspended matter or non-volatile suspended solids. This makes it difficult to compare and contrast TSS-related results in detail. In this review, several operational definitions for TSS-related variables may be reported.

Turbidity

Turbidity is a measure of water clarity related to light absorbed and scattered by all OACs. Turbidity is a useful measure of light availability under water and is therefore related to many ecosystem processes (Dekker & Hestir 2012). Due to the strong influence of suspended solids on water clarity, reflectance at 700 nm is most often used to derive turbidity from remotely sensed signals (Figure 6) (Hicks *et al.* 2013).

Secchi Depth

Secchi depth (SD) is a measure of water clarity in the vertical direction. Like turbidity, it is a function of scattering and absorption caused by all OACs. It has been successfully correlated to OACs, especially to chlorophyll *a* concentrations in the open ocean and due to its relationship with water clarity it can be related to the depth of the euphotic zone, i.e. the depth to which net positive rates of photosynthesis occur. Remote sensing has been shown to produce very good estimates of Secchi depth in several studies, most often using the ratio of peaks at 500 nm and 610 nm (Figure 6) (Allan 2008; Hicks *et al.* 2013; Olmanson *et al.* 2015; Zhao *et al.* 2011; Zhao *et al.* 2014).

Retrieval of Water Quality Constituents

The main steps required in obtaining estimates of water body constituents from remote sensing imagery are (summarised from Dekker & Hestir 2012):

1. Accessing the raw satellite data;
2. Pre-processing of the raw data including the conversion of raw Top of Atmosphere (TOA) volts into TOA radiance data and correcting for atmospheric effects;
3. Water body identification and isolation of water-only pixels; and
4. Algorithm application and the retrieval of water quality information.

Currently, the remote sensing satellite imagery used is freely available. The first step involves the acquisition of this satellite imagery which can usually be downloaded from the website of the operator or from their file service. The pre-processing step can range from simple to complex depending on the corrections applied to the image. TOA reflectance signatures are a result of the many optical effects created by atmospheric aerosols and clouds, in fact up to 90% of satellite measured irradiance can be a result of atmospheric scattering and absorption (e.g., Allan *et al.* 2015). As such, the majority of studies employ atmospheric correction methods and cloud cover assessments that aim to remove atmospheric effects, resulting in water-leaving radiance or water-leaving reflectance. Satellite data at the processing level used for studies of water quality is already georectified with information on the quality of the georectification relative to control points provided in the meta data.

The most common atmospheric correction methods are either image-based or radiative-transfer-theory-based. Image-based correction methods rely solely on the information provided in the satellite image and involve the use of either dark or light pixels as an estimate of path irradiance which is then subtracted from the TOA reflectance resulting in the water-leaving radiance (Allan *et al.* 2011). Alternatively, methods based on radiative transfer theory are often preferred due to their flexibility in being able to model atmospheric complexities over inland waters such as changes in elevation and adjacency effects (Allan *et al.* 2015; Campbell *et al.* 2011). Radiative transfer methods, such as the model "Second Simulation of a Satellite Signal in the Solar Spectrum" (the 6sv model of Vermote *et al.* 1997) requires an accurate record of the atmospheric conditions present during satellite image capture. Such information can be difficult to obtain and may have to be estimated, although more recent satellite sensors such as MODIS now collect concurrent atmospheric data which can be used for correction (Allan 2014). While radiative transfer modelling aims for a more accurate correction, numerous atmospheric parameters are often estimated from literature values, which can create considerable uncertainty in the result (Allan *et al.* 2011). Some studies found that non-atmospherically corrected empirical methods produced similar if not more accurate results than atmospherically corrected semi-analytical algorithms in Minnesota lakes (e.g., Olmanson *et al.* 2011). This suggests that it is possible to get atmospheric correction wrong with detrimental effects for the parameter retrieval.

Cloud cover determination is an important step in constituent retrieval and cloud masks are often applied to remove pixels disguised or contaminated by cloud (Olmanson *et al.* 2008; Allan 2014). Cloud detection methods can be automated as successfully demonstrated by Hicks *et al.* (2013) and Allan (2014). To improve these assessments, newer sensors include bands specifically positioned for cloud detection such as the new Short Wave Near-Infra Red (SWNIR) band on Landsat 8 (Roy *et al.* 2014) and two SWNIR bands on Sentinel-2 (Olmanson *et al.* 2015).

Step three involves the removal of all non-water pixels and those contaminated by light reflected from the bottom or stray light from the surrounding land. This is usually a done by first masking terrestrial pixels from the image and, second, analysing the data to detect spectral signatures typical for scattering from the bottom or edges.

The fourth step is arguably the most important in the retrieval of water quality constituents and subsequently has received the most attention. Given the optical complexity and heterogeneity of inland waters, rigorous algorithm development and testing is required to find suitable algorithms for a range of sites, conditions and constituent concentrations. To date, no operational algorithm exists that is generally applicable to complex inland waters (Palmer *et al.* 2015; Politi *et al.* 2015), unlike open ocean algorithms, which are operational and widely applicable.

Retrieval Algorithms

Retrieval algorithms are used to estimate the concentration of a water quality parameter from the spectral water-leaving radiance detected by a sensor. Commonly used algorithms generally fit into two categories, empirical or semi-analytical (IOCCG 2006; Olmanson *et al.* 2015). Empirical algorithms describe the statistical relationships between spectral band reflectance and *in situ* water quality samples. They can be viewed as a black box approach which requires little understanding of radiative transfer. The semi-analytical approach, on the other hand, aims to use radiative transfer theory to estimate parameter concentrations based on spectral absorption and scattering by OACs. Figure 7 illustrates the fundamental difference between empirical and semi-analytical algorithms.

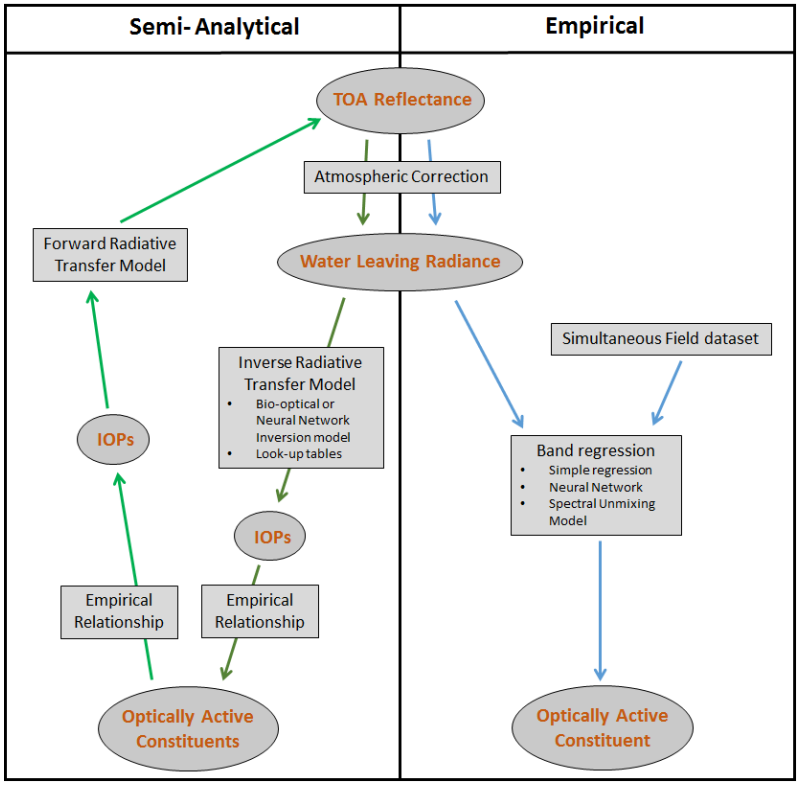

Figure 7: Generalised flow chart of common constituent retrieval methods, from satellite image (top) to constituent concentration (bottom) including empirical algorithm methods (blue paths) and semi-analytical methods involving radiative transfer (green paths). IOP: Inherent optical properties, TOA: Top of atmosphere.

The major difference between the types of algorithms for end users is the scale of possible application. Empirical algorithms are generally applicable only to the water body and the specific sensor for which they were created, while semi-analytical algorithms should be more generally applicable to a range of water bodies and concentrations (Allan *et al.* 2015).

The next two sections provide a comprehensive review of recent advances in the application of both types of algorithms. In addition, tables in *Appendix A: Retrieval Algorithms* list algorithms that have been developed for and applied to the retrieval of water quality constituents for inland waters.

Empirical Algorithms

Empirical algorithms require *in situ* data on each water quality variable in order to determine a statistical relationship between the reflectance of spectral bands and the concentration of constituents at the time of image capture (Dornhofer & Oppelt 2016; Olmanson *et al.* 2015). The resulting algorithm returns a site and time specific estimate of a single constituent, calibrated with *in situ* data points that can then be applied to each pixel in the image (Matthews 2011). These methods most commonly utilise one of three different approaches, empirical band regressions, spectral unmixing models and semi-empirical neural network models (Dornhofer & Oppelt 2016).

Empirical band regression uses either atmospherically corrected water-leaving radiance or raw satellite TOA reflectance regressed with *in situ* data. A successful example for this kind of algorithm is the estimation of Secchi depth (SD, m) from Landsat imagery (Kloiber *et al.* 2002). It uses the ratio of reflectance in Landsat bands 1 and 3 in the linear equation:

$$\text{Ln(SD)} = a(\text{TM1/TM3}) + b(\text{TM1}) + c$$

where TM1 and TM3 are the mean band reflectance values of pixels within a given distance of measured *in situ* locations (Zhao *et al.* 2011) and *a*, *b*, and *c* are constants estimated by regression. This algorithm has been highly successful in many complex waters, particularly the 10,000 lakes region of Minnesota (r^2 = 0.71 – 0.96 for 280 samples ranging from 0.1 to 9.8 m) as reported by Olmanson *et al.* (2011). Generally, algorithms incorporating three bands have the highest accuracy in more complex waters (Lyu *et al.* 2015).

Spectral unmixing models are particularly useful in optically complex waters where OACs co-occur and their constituent signatures overlap, for example the spectral signatures of CDOM, TSS and chlorophyll *a* share peaks near 440 nm, 560 nm, 660 nm and 700 nm, respectively, rendering the simple band regression problematic. The method is a multivariate regression technique in which the known spectra of pure OACs (e.g., chlorophyll, CDOM, TSS) are combined such that their sum reproduces the observed spectrum (Allan 2008; Tyler *et al.* 2006; Zhang *et al.* 2014). Zhang *et al.* (2014) used a four endmember spectral decomposition model to retrieve chlorophyll *a* concentrations in Lake Taihu, a shallow, eutrophic lake in China. Tyler *et al.* (2006) carried out a retrospective analysis of chlorophyll *a* concentrations in Lake Balaton, a large shallow lake in Europe using a spectral mixing model which was significantly correlated with *in situ* chlorophyll *a* samples above 10 µg l^{-1} (r^2 = 0.95, 12 samples). Allan (2008) applied a linear spectral unmixing model to Landsat images of the Waikato region in order to obtain chlorophyll *a* estimates. Given the optical complexity of many Waikato lakes, a spectral unmixing approach was chosen and applied to Landsat 7 Enhanced Thematic Mapper Plus (ETM+) images (see *Case Studies*, below).

Another approach uses a neural network model to determine which satellite bands are most strongly correlated with the retrieved water-leaving radiance before applying a band regression (Dornhofer & Oppelt 2016). Matthews (2011) found that this approach improves the strength of the correlation, and if applied to atmospherically corrected data, can reduce errors associated with atmospheric scattering. Due to the additional neural network step, Matthews (2011) termed this approach semi-empirical.

While often correlating well with *in situ* data, the major disadvantage of using empirical methods is that these are strictly only valid within the ranges of data used to build the models. The further the algorithm is applied across time or space, the greater the chance to encounter atmospheric and water-related conditions outside the initial range leading to errors associated with the predictions (Allan 2008; Matthews 2011). Specifically, these models have been found to be unreliable in water bodies with particularly high or low concentrations of constituents, suggesting that non-linear relationships exist at the extremes (Chang *et al.* 2015). Further, empirical algorithms lack the ability to retrieve more than one parameter and are often unable to discriminate between covariant

constituents (Matthews 2011). These disadvantages have attributed to a shift in focus towards the development of analytical and semi-analytical algorithms (Chang *et al.* 2015).

Semi-Analytical Algorithms

Analytical algorithms use purely theoretical methods to estimate constituents while semi-analytical methods strike a balance between the use of physical theory and the inclusion of *in situ* data (Olmanson *et al.* 2015). A major advantage for analytical and semi-analytical algorithms as compared with empirical algorithms is their ability to retrieve multiple constituents simultaneously using one algorithm (Matthews 2011). Semi-analytical algorithms are based on fundamental optical principles and often forward or inverse models to approximate the equation of radiative transfer. Forward models predict the spectral signature of water-leaving radiance based on the water column constituents and benthic reflectance, and inverse models predicting the concentration of OACs based on the waters spectral reflectance (Matthews 2011; Dekker & Hestir 2012). Semi-analytical methods require knowledge of the specific optical properties of the water being studied, including inherent optical properties (IOPs) or apparent optical properties (AOPs) as well as *in situ* measurements for calibration and validation. IOPs, most importantly scattering and absorption, are properties of the water medium and independent of the surrounding light field (Dekker & Hestir 2012). These coefficients include scattering and absorption contributions from phytoplankton, CDOM, non-algal particles and pure water. AOPs, e.g., reflectance, on the other hand, depend on the IOPs and the characteristics of the underwater light field (Wang *et al.* 2016).

Look-up tables are often used to speed up computation times within semi-analytical algorithms, in which water-leaving radiance spectra with known IOPs and constituent concentrations are compared to the water-leaving radiance and optical properties of the studied water body until a match is found and the constituent concentration is assumed to be similar (Dornhofer & Oppelt 2016).

Alternatively and more intensively, bio-optical models can be used to determine the relationship between the AOPs, IOPs of a constituent and the water-leaving radiance by focusing on the physical processes responsible for the relationship between remotely sensed irradiance and *in situ* constituent concentrations (Allan *et al.* 2015). Forward bio-optical models can be used to estimate the subsurface reflectance ($r_{rs}(\lambda)$,where λ is wavelength) of the water using IOPs relevant from that water body (Dekker *et al.* 2001). A commonly used forward bio-optical model is (Gordon *et al.* 1988):

$$r_{rs}(\lambda) = g_0 u(\lambda) + g_1 [u(\lambda)]^2$$

The values g_0 and g_1 are constants that depend on the anisotropy of the downwelling light field and scattering. $u(\lambda)$ is a function of the total backscattering coefficient (b_b, m^{-1}) and the total absorption coefficient (a, m^{-1}):

$$u(\lambda) = \frac{b_b(\lambda)}{a(\lambda) + b_b(\lambda)}$$

Inverse models can then be used to relate the r_{rs} with the satellite sensor signature to infer the IOPs present and estimate concentrations of waterborne constituents. The MERIS Case 2 bio-optical algorithm for chlorophyll *a* has been successfully applied to MERIS imagery of the Neuse and Pamlico Estuaries in the USA, a comparison with *in situ* data returning an r^2 of 0.84 (Keith 2014). Allan *et al.* (2015) used a simplified semi-analytical model to estimate chlorophyll *a* concentrations in the Rotorua lakes utilising IOPs measured from Dutch lakes due to a lack of relevant local data. The model returned an r^2 of 0.58, performing more poorly than an empirical regression with the same data, but there is potential for an improvement in retrieval of chlorophyll *a* concentration assuming that local IOP data can be collected.

Semi-analytical algorithms can be time consuming and costly to develop, although many satellite sensor organisations now supply companion algorithms developed for use specifically with particular sensors. For example, NASA provides free data processing software for MODIS (SeaWiFS Data Analysis System (SeaDAS)) as well as offering specific algorithms, but the local application of these to coastal waters in Canterbury were not overly successful (Schwarz *et al.* 2010). Similarly, the ESA offers a MERIS Case-2 bio-optical algorithm that has been applied to inland waters with limited success (Matthews *et al.* 2010; Odermatt *et al.* 2010). However, Keith *et al.* (2014) retrieved successful chlorophyll *a* estimates from estuaries in the United States using the algorithm (r^2 = 0.84 - 0.87). The transferability of semi-analytical algorithms between among sensors that share similar waveband locations and widths is another potential way to reduce the time and cost of algorithm development. Augusto-Silva *et al.* (2014) applied three bio-optical algorithms originally developed for MERIS imagery to simulated output expected from the Sentinel-3 sensor found two of the three algorithms were successfully transferrable.

The main disadvantages associated with semi-analytical algorithms include the larger data requirements, the sensitivity to errors arising from atmospheric correction and the error accrued from the estimation of IOPs (Matthews 2011). Allan (2014) identified the need for local IOP data in order to successfully develop regional bio-optical models, avoiding the uncertainty in using literature values and non-local data. A number of researchers address the errors associated with IOP estimates by measuring site specific IOPs and conduct bio-optical modelling. More details on bio-optical sampling can be found in Belzile *et al.* (2014), Gallegos *et al.* (2008) and Wang *et al.* (2016). However, bio-optical variability over time and between water bodies can result in poor performance when semi-analytical algorithms are used to extrapolate beyond the observational data set (Politi *et al.* 2015). This means that no single bio-optical algorithm is likely to be applicable to all water bodies in a region or to neighbouring water bodies of different trophic levels. The high initial cost associated with the development of an algorithm is another disadvantage in addition to modelling errors. This is in part due to the collection and analysis of *in situ* samples for calibration, although there is expected to be little cost associated with the ongoing use of a validated algorithm and further *in situ* measurements should not be required (Dekker & Hestir 2012).

There has been much discussion in the literature regarding the applicability and feasibility of empirical compared with semi-analytical algorithms for the retrieval of inland water quality parameters. All algorithms that fall within these categories have individual disadvantages, for example empirical algorithms lack wider applicability (Odermatt *et al.* 2012), while bio-optical algorithms may not be applicable to all lake types and trophic levels (Politi *et al.* 2015; Lyu *et al.* 2015). Olmanson *et al.* (2011) suggest that semi-analytical methods are not feasible for regional scale monitoring due to the lack of IOP data available for most water bodies and the difficulty associated with developing models applicable to a range of lakes and trophic levels. In contrast, Dekker & Hestir (2012) conclude that semi-analytical algorithms based on optical principles are most appropriate for large-scale water quality monitoring programmes as they are easily automated, can be applied or adapted to historical and future imagery and provide confidence and error estimates. Given the lack of consensus regarding algorithm applicability, the decision of what algorithms to use in a potential monitoring system for Waikato waters should be informed by a targeted and applied study.

Case Studies

This section summarizes pertinent applications of remote sensing for water quality parameters in lakes, rivers and estuaries, respectively. Where possible, case studies from the work of our group are summarised, because of their regional applicability. Other examples resulted from sources found during the background research for this section or from Google searches using the terms [lakes/rivers/estuaries] and “water quality” and “remote sensing”. It is recommended that a more targeted literature is carried out if and when a decision has been made to further pursue water

quality monitoring by remote sensing. For quick reference, all case studies are listed in Table 4 along with summary information on the sensor, parameter and fit statistic of the study. The coefficient of determination (r^2) from the linear regression of *in situ* versus remotely sensed observations is the most reported metric for the fit of the satellite-retrieved parameters versus in-situ measurements.

Table 4: List of case studies discussed in this report.

Reference	Sensor	Parameter	Algorithm type	Coefficient of determination (r^2)	Location	Water body Type
Allan (2008)	Landsat 7 ETM+	Log-Chl *a*	Regression using Band 1/Band 3 ratio	0.83 (*N* = 13, 0.8 - 136 µg L^{-1}) 0.91 (*N* = 16, 0.4 – 89.1 µg L^{-1})	Rotorua Lakes	Lakes
	Landsat 7 ETM+	Log-Chl *a*	Regression using Band 1, 2 and 3 spectral unmixing model	0.84 (*N* = 6, 9 – 135 µg L^{-1})	Waikato Lakes	Lakes
	Landsat 7 ETM+	TSS	Regression - Band 3	0.98 (*N* = 15, 0 – 350 mg L^{-1})		
Allan (2011)	Landsat 7 ETM+	Log-Chl *a*	Regression – Band 1/Band 3 ratio	0.80 (*N* = 33, 0.8 – 136 µg L^{-1})	Rotorua Lakes, Lake Taupo	Lakes
Hicks *et al.* (2013)	Landsat 7 ETM+	TSS	Regression - Band 4	0.94 (*N* = 35, 0 – 962 mg L^{-1})	Waikato Lakes	Lakes
		Turbidity	Regression - Band 4	0.92 (*N* = 36, 1.25 – 399 NTU)		
		Log-SD	Regression – Band 1/Band 3 ratio	0.67 (*N* = 32, 0.005 – 3.78 m)		
Allan (2014)	MODIS	Tripton*	Regression - Band 1	0.73 (*N* = 9, 50 – 400 mg L^{-1})‡	Lake Ellesmere	Lake
			Bio-optical modelling	0.72 (*N* = 9, 50 – 400 mg L^{-1})‡		
Allan et al. (2015)	Landsat 7 ETM+	Chl *a*	Symbolic regression	0.68 (*N* = 87, 0.1 – 136 µg L^{-1})‡	Rotorua Lakes	Lake
			Bio-optical modelling	0.58 (*N* = 87, 0.1 – 136 µg L^{-1})‡		
Zhao *et al.* (2011 & 2014)	Landsat 7 Panchromatic Band	Log-SD	Regression, Panchromatic band	0.64 (*N* = 51, 0.09 – 0.90 m)‡	Tributaries to Lake Taihu, China	Rivers
Schwarz *et al.* (2010)	MODIS, Landsat 7 ETM+, SeaWiFS	Chl *a*, calcite	Semi-analytical MODIS algorithm	Not determined	Canterbury Rivers	Rivers

Reference	Sensor	Parameter	Algorithm type	Coefficient of determination (r^2)	Location	Water body Type
Olmanson *et al.* (2013)	Airborne hyperspectral sensors	Log-Chl *a*, Log-TSS Log-Turbidity	Regression against narrow wave bands and wave-band ratios	0.86 (*N* = 21, 8 – 830 µg L^{-1})‡‡ 0.84 (*N* = 21, 2 – 95 mg L^{-1})‡‡ 0.86 (*N* = 21, 2 – 50 NTU)‡‡	Mississippi and Minnesota River	Rivers
Akbar *et al.* (2013)	Landsat 5 TM	CWQI categories** Turbidity classes	Regression against wave bands and wave-band ratios	0.91 (*N* = 31, 2 – 4)	Bow River, Canada	Rivers
Keith (2014)	MERIS	Chl *a*	Bio-optical modelling	0.87 (*N* = 120, 1 – 122 µg L^{-1})‡	Neuse and Tar-Pamlico Estuaries, USA	Estuaries
Doxaran *et al.* (2009)	MODIS Terra MODIS Aqua	SPM	Regression – Band 1/Band 2 ratio	0.77 (*N* = 59, 10 – 2200 g m^{-3})‡ 0.82 (*N* = 59, 10 – 2200 g m^{-3})‡	Gironde Estuary, France	Estuary
Shen *et al.* (2010)	MERIS	Chl *a*	Synthetic Chlorophyll Index (SCI)	RMSE = 0.86 µg L^{-1} (spring, *N* = 57, 0.01 – 3 µg L^{-1}) RMSE = 2.87 µg L^{-1} (summer, *N* = 31, 1 – 31 µg L^{-1})	Yangtze Estuary, China	Estuary

TSS: Total suspended solids, SD: Secchi depth, SPM: Suspended particulate matter, *N*: number of samples, RMSE: Root mean square error

*Tripton includes sand, silt, clay and other inorganic material such as atmospheric dust as well as non-living organic matter

**Canadian Water Quality Index

‡Range of values read from graphs in the reference

‡‡Values shown are averages calculated from Table 2 in Olmanson *et al.* (2013)

Lakes

Rotorua and Waikato Lakes

Allan (2008) looked at chlorophyll *a* and Secchi depth in the Rotorua lakes along with TSS and chlorophyll *a* in the Waikato lakes using Landsat 7 ETM+ imagery from 2002. In 12 Rotorua lakes, a simple ratio (Band 1 / Band 3) regression was applied to log-transformed chlorophyll concentrations. This simple method is possible, because chlorophyll *a* is often the dominant colour producing constituent (Scholes 2009). In shallow Waikato lakes, which often contain high concentrations of CDOM, TSS and chlorophyll *a* concurrently, a linear spectral unmixing model was applied to retrieve log-transformed chlorophyll *a* concentrations.

The B1/B3 ratio was the best method for log-chlorophyll *a* estimation in the Rotorua lakes (r^2 = 0.82 – 0.91, Figure 8), although the equations are lake specific and use regional atmospheric factors and as such are not expected to perform as well in other lakes or images from different times. The timing of image capture can be particularly important in systems such as Lake Rotorua, as blooms can congregate at the surface during stratification but can also dispersed quickly by, for example, an afternoon wind.

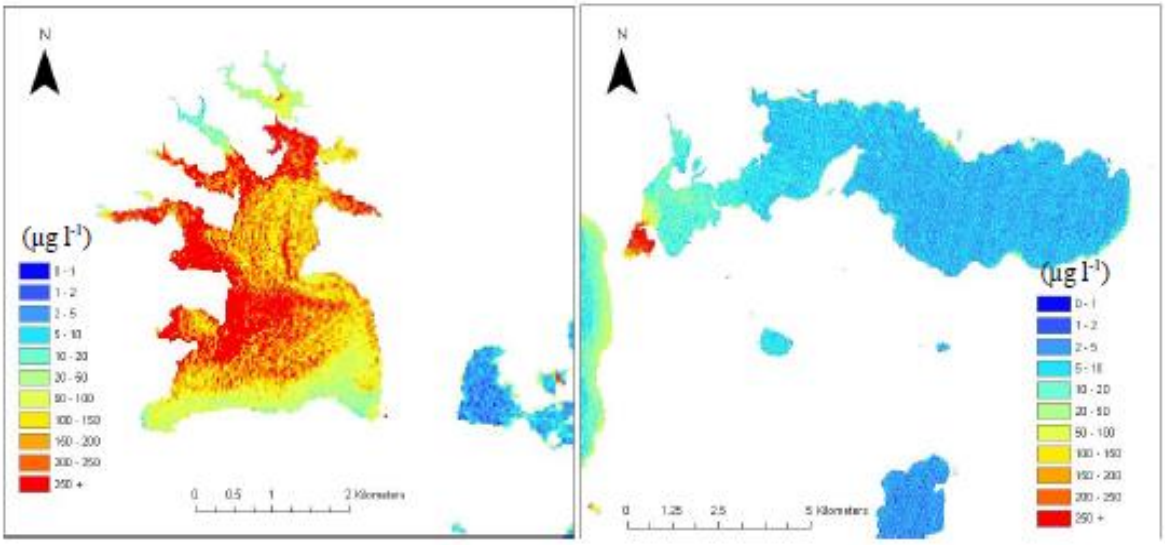

Figure 8: Lake Rotoehu (left) and Rotoiti (right) chlorophyll *a* concentrations estimated from a Landsat image taken on 6 January 2001 using the band ratio regression equation: Ln Chl *a* = 14.141-5.0568 (B1/B3), r^2 = 0.91 (Source: Allan 2008).

Six of the over 40 Waikato Lakes between 0.01 to 34.4 km^2 were sampled for TSS and chlorophyll *a* in 2000 and 2002, coinciding with Landsat7 ETM+ overpasses. TSS concentrations were then retrieved using a simple Band 3 regression (TSS = 0.0388 + 0.0008 B3, r^2 = 0.98) while chlorophyll *a* was retrieved using a linear spectral unmixing model (Chl *a* = 5.7298 + 2.527 · (Chl *a* endmember percentage), r^2 = 0.84) (Figure 9). The results show high spatial variability of TSS and chlorophyll *a* in the studied lakes which suggests that current, monthly *in situ* monitoring samples are unlikely to be representative of entire water bodies. The results further show that peat lakes often exhibited high chlorophyll *a* and lower TSS concentrations whereas riverine lakes had both higher TSS and chlorophyll *a* concentrations.

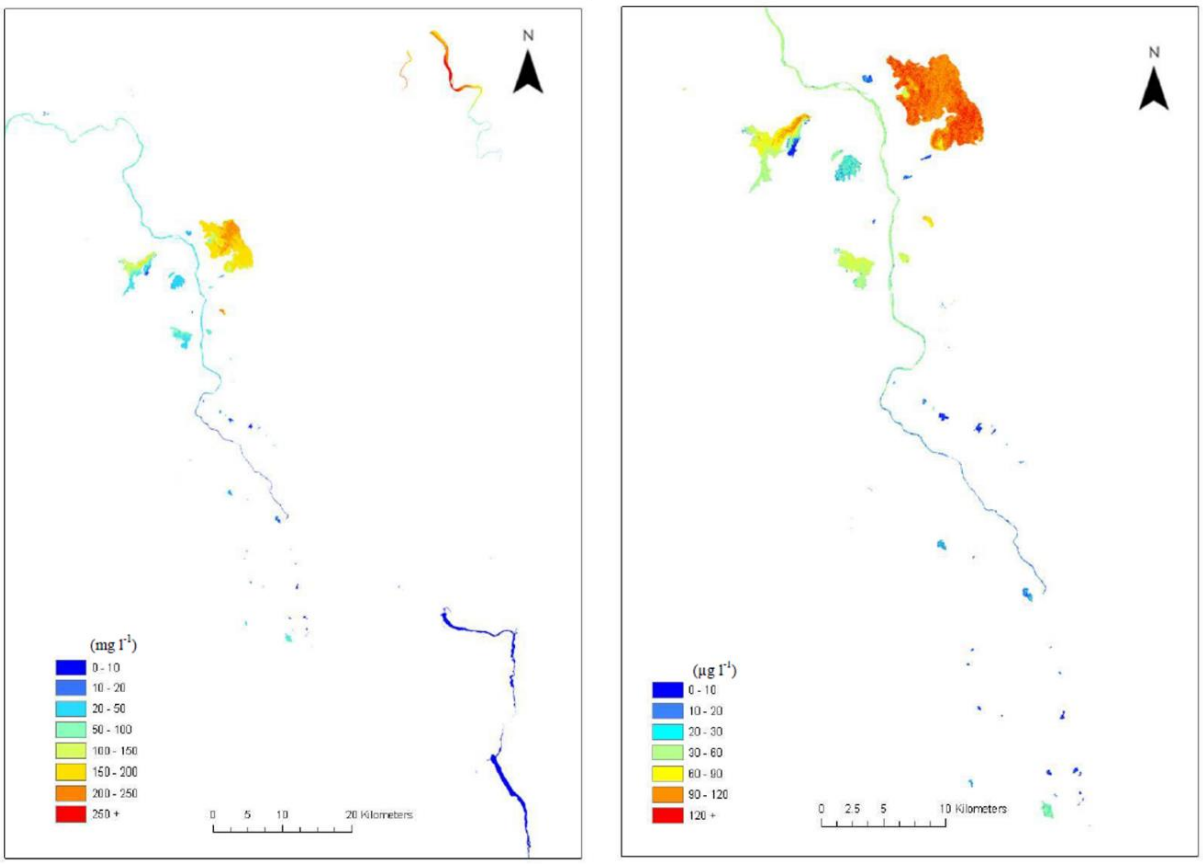

Figure 9: Landsat 7 ETM+ estimated TSS concentrations (left) and chlorophyll *a* concentrations (right) on the 28th August, 2002 (Source: Allan, 2008).

Rotorua Lakes and Lake Taupo

Allan *et al.* (2011) derived simple empirical relationships between remote sensing reflectances of Landsat 7 ETM+ wavebands and chlorophyll *a*, Secchi depth and turbidity measured *in situ* in 12 lakes in the Bay of Plenty region and Lake Taupo (Waikato region). *In situ* samples from regular monitoring programmes were chosen which fell within two days of two satellite overpasses (24 January 2002 and 23 October 2002) and satellite pixels closest to the sampling locations were used.

The approach of the study was to compare the goodness of fit of *in situ* water-quality parameters with reflectances at the satellite wavebands (and also commonly used band ratios) and to test the sensitivity of the relationships to two types of atmospheric correction. The authors found that all *in situ* variables could be related to one of the remotely sensed spectral bands using one of two atmospheric correction methods (Pearson correlation coefficients, between $r = 0.84$ and $r = 0.98$). The scatter plot in Figure 10 shows that log-chlorophyll *a* concentrations can be derived using band 3 reflectance and data pooled from all lakes and both image-capture dates. This relationship appears to hold over three orders of magnitude of chlorophyll concentration.

The results suggest that remote sensing may be used to observe lake water quality parameters at the regional scale across a wide range of trophic states simultaneously. One of the caveats of this study is that there was no single best retrieval algorithm for each variable, but the optimal method varied unpredictably depending on the date of the satellite overpass. This suggests that there is significant temporal variability in the dominant OACs affecting which retrieval algorithm to use and that further ground truthing is needed.

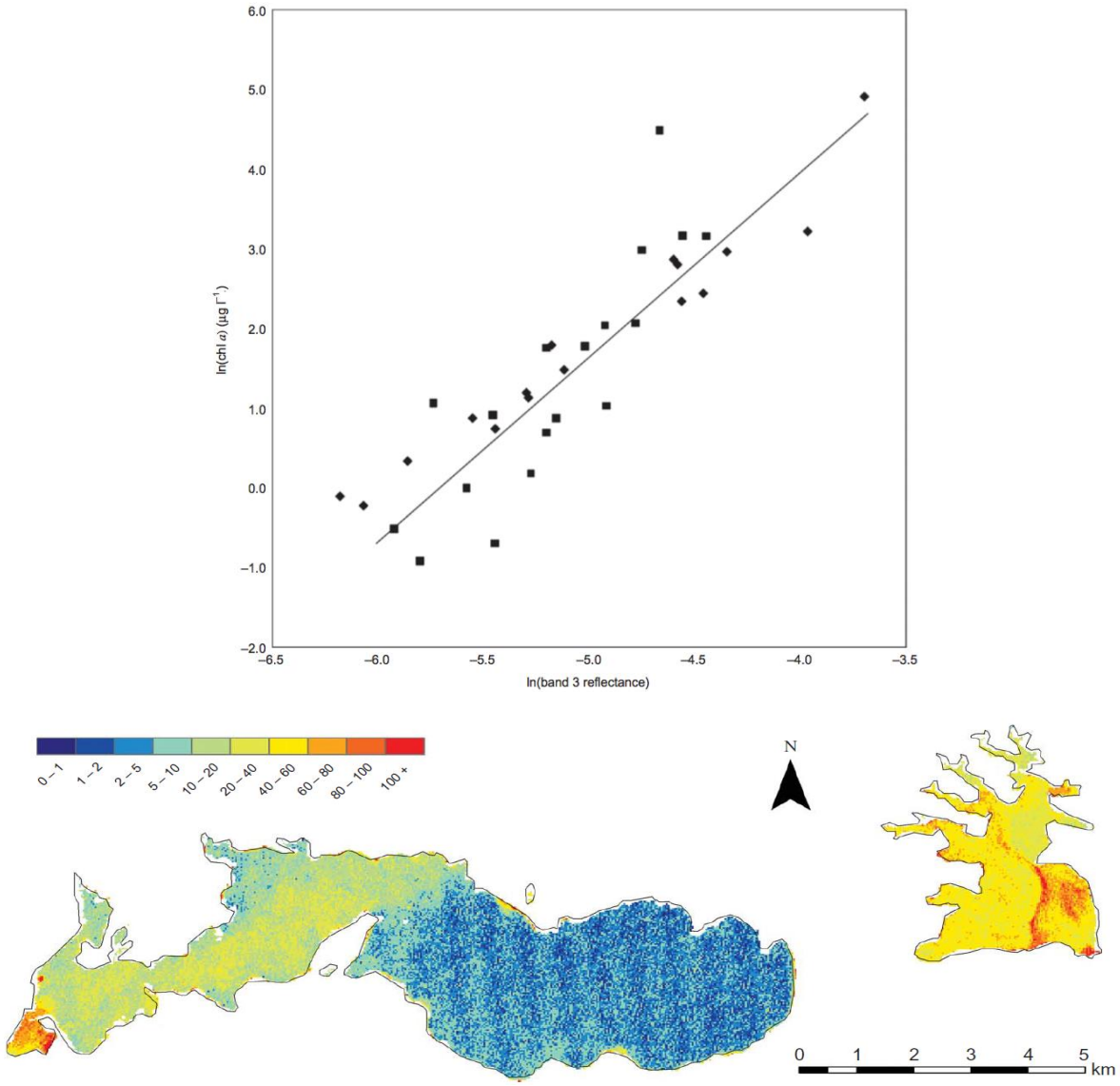

Figure 10: Top: The empirical retrieval algorithm recommended by Allan *et al.* (2011) is a linear regression of ln(chl *a*) concentration against ln(band 3 reflectance) using 6sv atmospheric correction, r^2= 0.795. Bottom: Chlorophyll *a* concentrations (µg L^{-1}) estimated for Lake Rotoiti (left) and Lake Rotoehu (bottom right) by Landsat 7 ETM+ for 24 January 2002 using the regression shown in the scatterplot above. (Source: Allan *et al.* 2011).

Waikato Lakes

Hicks *et al.* (2013) used Landsat 7 ETM+ imagery to predict TSS, Secchi depth and turbidity in 34 Waikato lakes (including Lakes Waikare, Whangape, Waahi, Rotomanuka, Gin, Rotopiko, Rotokauri, Ngaroto, Maratoto, and Hakanoa) over a 10-year period (2000 – 2009). The authors developed regression relationships between *in situ* measurements and spectral reflectance over multiple lakes to find an overall relationship specific to the Waikato region that can be applied to local unmonitored lakes lacking in-situ data. Reflectance intensity in Band 4 from Landsat images at the locations of *in situ* samples were regressed against measured TSS in mg L^{-1} (r^2 = 0.94), turbidity in nephlometric turbidity units (NTU; r^2 = 0.92) and measured Secchi depth (r^2 = 0.67). These empirical relationships (Table 5) were then used to hindcast water clarity predictions for the images without *in situ* measurements. Secchi depth was the most poorly predicted variable, probably because of the interference of CDOM and suspended sediment (e.g., Allan 2008).

Table 5: Water clarity relationships between *in situ* measured variables and band reflectance from Landsat 7 ETM+ images for 12 sample sites in 10 shallow lakes in the Waikato region calculated by least squares regression (Source: Hicks *et al*. 2013).

Water clarity variable	*N*	Equation	r^2	RMSE	P
Total suspended solids in mg L^{-1} (TSS)	35	TSS = –52.817 + 1449.4 * B4	0.939	21.3	<0.001
Turbidity in NTU (TURB)	36	TURB = –63.717 + 1587.8 * B4	0.924	25.9	<0.001
Secchi depth in m (SD)	32	Ln(SD) = –2.0298 + 2.7517 * Ln(B1:B3) – 0.6022 * Ln(B1)	0.670	0.33	0.016

Imagery pre-processing including atmospheric correction and cloud detection and masking was automated and applied to 53 images over 10 years. The results showed clear spatial variation within lakes which would have been missed in spot samples (Figure 11). For example, the three *in situ* sampling points in Lake Waikare shown in the 9 Sep 2001 image (Figure 11b) did not sample the suspended sediment plume at the southern end of the lake that appears to have originated from flood waters of the Matahuru Stream (see Hicks *et al.* 2013 for more detail). These results suggest that in-lake spatial variability in TSS in large Waikato lakes should be taken into account when examining whole-lake values. The root mean square error for TSS was 21.3 mg L^{-1} (RMSE, Table 5), which suggests that the equation is less accurate for low values than for high values. However, most values for shallow Waikato lakes were above the RMSE, showing the utility of this relationship for unmonitored lakes. The validity of applying the relationships in Table 5 to unmonitored lakes and to images without *in situ* data can be assessed by examining the ranges of the data used in the regressions. All of the lake and yearly means and the vast majority of the individual data points fell within the range of the observations (Table 6 and Appendix in Hicks *et al.* 2013), suggesting that the procedure is robust.

Table 6: Statistics of the data used in the regression relationships in Table 5 (Source: B. Hicks, pers. comm.).

	SD (m)	TSS (mg L^{-1})	Turbidity (NTU)
N	32	35	36
Minimum	0.05	2.0	1.3
1st quartile	0.25	5.9	3.9
Median	0.68	20.0	11.9
Mean	0.77	58.1	56.7
3rd quartile	1.16	67.5	68.1
Maximum	3.04	344.0	399.0

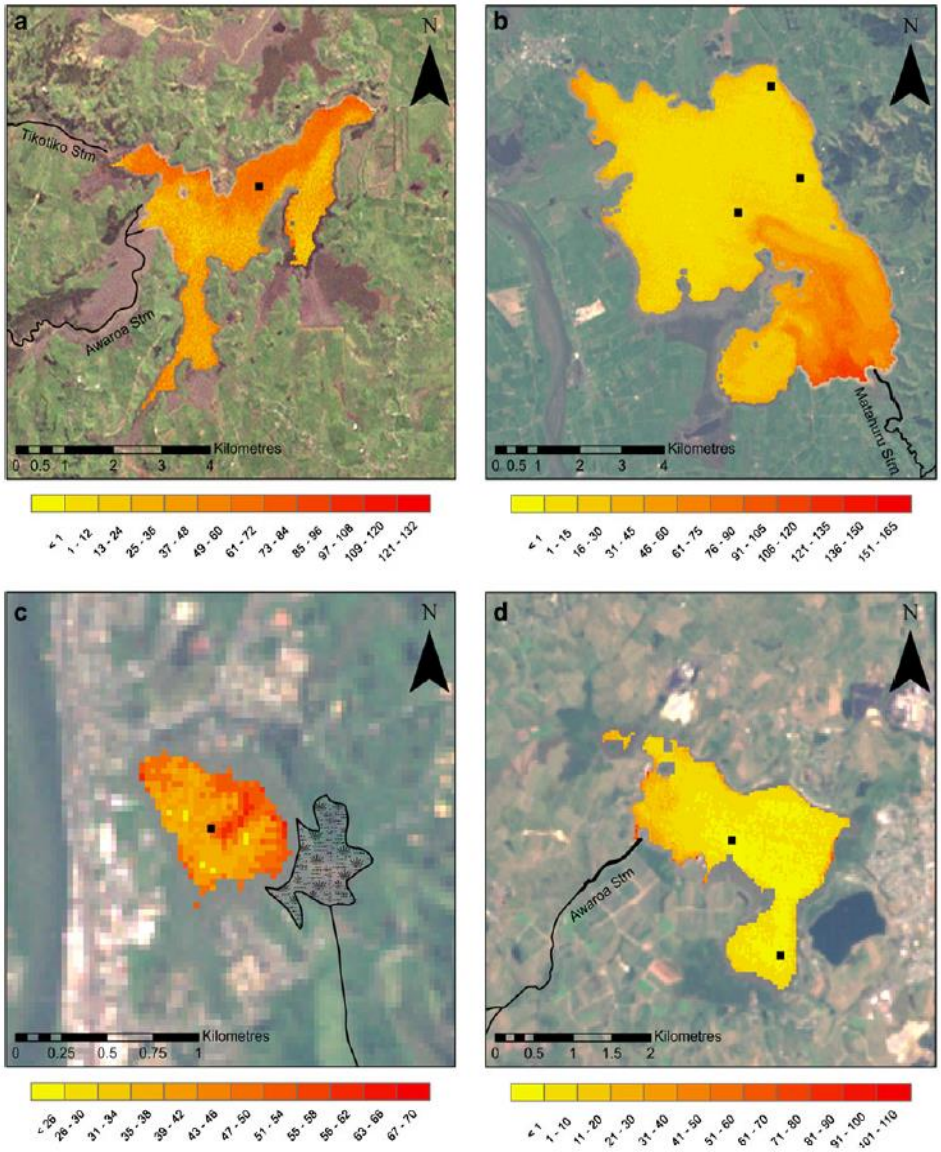

Figure 11: Estimated TSS (mg L^{-1}) for Lakes Whangape (a), Waikare (b), Hakanoa (c) and Waahi (d) showing spatial variability in concentrations. Black dots indicate *in situ* sampling sites and black lines indicate major lake inflows (Source: Hicks *et al.* 2013).

Lake Ellesmere

Allan (2014) used MODIS band 1 reflectance to estimate suspended particles concentrations in Lake Ellesmere, a large shallow turbid coastal lagoon (Figure 12). Semi-analytical and empirical algorithms were derived to determine spatial and temporal variations in suspended particles in the lake. Both model algorithms predicted suspended particles similarly (normalised RMSE[2] of 18 %), but the semi-analytical model had the advantage of being applicable to different satellite sensors, spatial locations, and suspended particles concentration ranges. When compared to literature values of error in TSS estimation, this error is of a similar magnitude (e.g., 18 and 22 % for MODIS Terra and Aqua 250 m resolution data respectively, in extremely turbid Gironde estuary, France (Doxaran *et al.* 2009). In semi-analytical models the values g_0 and g_1 (see section *Semi-Analytical Algorithms*) are sometimes treated as empirical constants that depend on the anisotropy of the downwelling light field and scattering within the water and the values found were similar to those reported for other highly turbid waters. This finding suggests that the semi-analytical model to estimate suspended

[2] Normalised RMSE is the root mean square error relative to the range of the observations: normalised RMSE = RMSE/(max-min); multiplication by 100 yields percent values.

particles can be applied over the existing archive and future images of the MODIS sensor for the purposes of environmental monitoring.

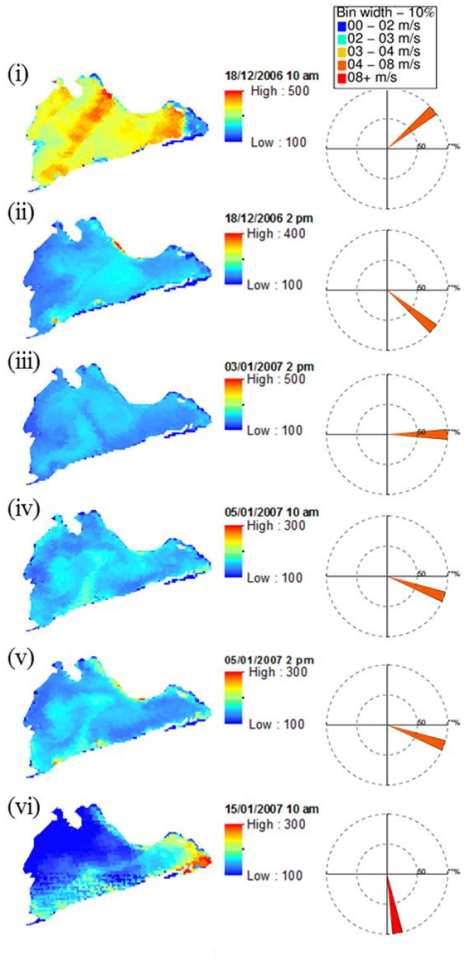

Figure 12: MODIS estimated suspended mineral concentrations (mg L^{-1}) (left) alongside 3D model simulated concentrations (right), showing average hourly wind speed and direction (Source: Allan 2014).

The bio-optical and empirical algorithms used to estimate suspended particles in Lake Ellesmere are directly applicable to Waikato lakes, as the turbid ones may also show variation of g_0 and g_1. However, the number of lakes of sufficient size to be effectively remotely sensed using the 250 m pixel size of MODIS will be limited to large lakes such as Lake Taupo, Lake Waikare and Lake Whangape. In addition, the values of g_0 and g_1 used in Lake Ellesmere would need to be tested for applicability to Waikato lakes and potentially modified. In an ideal situation, inherent optical properties of Waikato lakes derived from field and lab samples would be used to parameterise the bio-optical model. Alternatively, parameters of the bio optical model could be iteratively fitted to minimise errors between *in situ* and bio-optical model estimated TSS.

Rotorua Lakes

Allan (2014) also analysed Landsat 7 ETM+ imagery for the retrieval of chlorophyll *a* concentrations in the Rotorua Lakes. The author used forward and inverse bio-optical modelling in addition to symbolic regression to compare estimates of chlorophyll *a* using different algorithms. The forward bio-optical model was used to estimate spectral reflectance signatures across varying concentrations of chlorophyll *a* which were then used in an inverse model to determine the constituent concentrations based on the modelled and retrieved reflectance signatures (Figure 13). Ideally, the spectral signatures should be determined by bio-optical measurements in the study lakes (see sections *The Fundamentals of Remote Sensing for Water Quality* and *Semi-Analytical Algorithms*),

but in the absence of this information, literature values had to be used. The symbolic regression (r^2 = 0.68; Figure 14) outperformed the bio-optical model (r^2 = 0.58; not shown), though the scatter of points about the regression line attests to a limited ability to accurately model observed chlorophyll *a* using generic algorithms.

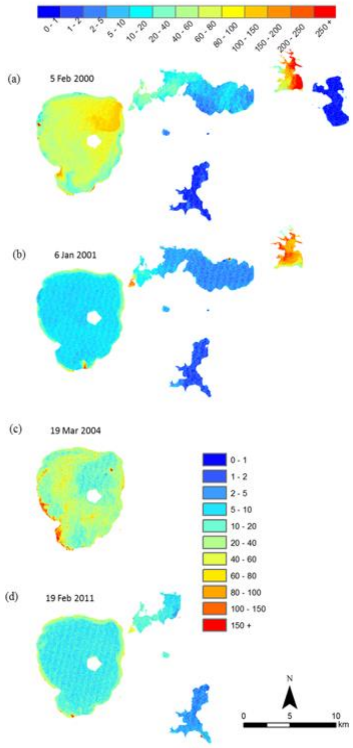

Figure 13: Spatial variability of chlorophyll *a* concentrations (µg L^{-1}) estimated using a symbolic regression algorithm for the north-western Rotorua Lakes (Source: Allan 2014).

Allan *et al.* 2015 went further to developed customised algorithms for chlorophyll *a* retrieval, improved atmospheric correction and automated processing workflows to derive chlorophyll *a* concentration across a wide range of trophic levels in the Rotorua lakes (Figure 14).

Five different semi-analytical and empirical models were derived in order to estimate chlorophyll *a* concentrations within 137 Landsat 7 ETM+ images between 1999 to 2013. Atmospheric correction applied radiative transfer modelling, with atmospheric conditions prescribed from MODIS Terra and Atmospheric Infrared Sounder (AIRS) data. The best-performing semi-analytical and empirical equations resulted in similar levels of variation explained (r^2 =0.68) and RMSE = 10.69 µg L^{-1}, respectively between observed and estimated chlorophyll *a*. However, the symbolic regression algorithm had higher r^2 at chlorophyll *a* concentrations less than 5 µg L^{-1} (r^2 0.35 as opposed to 0.15 using the semi-analytical algorithm). Symbolic regression uses evolutionary computational algorithms to search a space of mathematical expressions while minimising the r^2 and RMSE values.

The New Zealand-specific studies described above show that the remote sensing of TSS and chlorophyll *a* concentration is possible using broadband sensors. There is, however, a large potential for error in estimated chlorophyll *a* using currently available algorithms, most likely due to independently varying concentrations of CDOM or suspended particles. Bio-optical algorithms may reduce errors by allowing simultaneous estimation of CDOM absorption, suspended particulates and chlorophyll *a*. However, the Landsat series of satellite sensors possess spectrally broad bands which do not allow for a stable inversion with a bio-optical model. For the Waikato lakes Landsat images, the application of linear spectral unmixing could provide a potential solution to errors, and this area

of research needs exploration to determine if the estimation of chlorophyll *a* concentrations within turbid Waikato lakes is feasible.

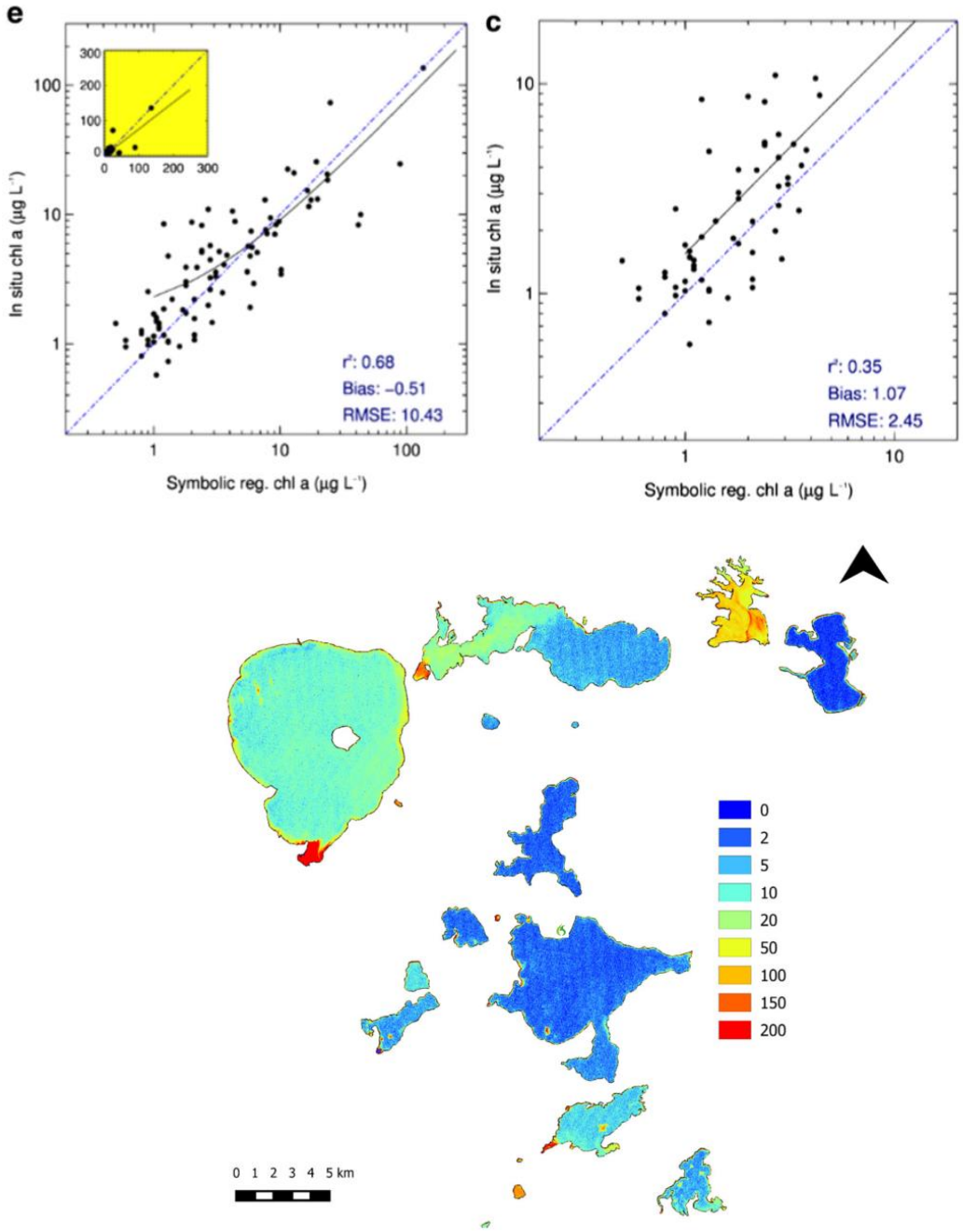

Figure 14: Top: In situ versus remotely sensed chlorophyll *a* from the best-performing algorithm in Allan *et al.* 2015 used symbolic regression analysis; the right plot shows a version of the algorithm calibrated for chlorophyll values below 5 µg l^{-1}. Bottom: Chlorophyll *a* (µg l^{-1}) derived from the symbolic regression model on 24 January 2002 (Source: Allan *et al.* 2015).

Rivers

Tributaries to Lake Taihu, China

Zhao *et al.* (2011) used Landsat 7 ETM+ imagery to estimate water clarity in Lake Taihu and surrounding rivers. Thirteen rivers in total were analysed, with average widths over stretches of individual rivers ranging from 37 – 173 m and lengths between 8 – 61 km. Given the spatial resolution of Landsat ETM+ multispectral bands is too low for the study of many rivers, the authors

determined the feasibility of using the 15 m resolution Panchromatic band in place of the common ETM+ bands for the retrieval of Secchi depth. The panchromatic band was found to capture 93% of the variation in Secchi depth and was subsequently used in this study. The panchromatic brightness, when regressed with *in situ* river samples returned an r^2 of 0.64, similar to the panchromatic band estimation within Lake Taihu (r^2 = 0.68), however, both relationships explained less variability than the common Band1/Band3 ratio regression which returned an r^2 of 0.77 in the lake.

Given the relatively low r^2 (0.64) returned using the panchromatic band, Zhao *et al.* (2014) again focused on Landsat ETM+ imagery to determine the minimum river width retrievable using the common multispectral bands. Rivers were found to be heavily contaminated by adjacency effects from banks and river beds, however the authors suggested water pixels were useable when greater than 17 m from the shoreline which resulted in a minimum river width of 65-98 m for the 30 m resolution Landsat imagery.

This study demonstrates that due to its higher spatial resolution (15 m), the panchromatic band of Landsat 7 ETM+ can be used to estimate Secchi depth in narrower rivers compared to methods using the spectral bands (at 30 m resolution), but at the cost of lower accuracy.

Canterbury Rivers and Lake Ellesmere

Schwarz *et al.* (2010) tracked TSS plumes from ten rivers and from Lake Ellesmere into the Canterbury Bight using MODIS, Landsat ETM+ and SeaWiFS imagery. The authors used algorithms implemented in NASA's processing software (SeaDAS) without local calibration. Of the eight optical products and constituents tested, only the algorithms for chlorophyll *a* retrieval and calcite concentration were robust enough in the near-shore environments. Therefore, freshwater and sediment plumes were tracked using true colour, chlorophyll *a* concentration, and calcite concentration products only (Figure 15).

Figure 15: Section of Figure A24 from Schwarz *et al.* (2010) showing sediment plumes visible in a Landsat true colour image from 26 September 2008 (Source: Schwarz *et al.* 2010).

Water quality characteristics in the Mississippi River and its tributaries

Olmanson *et al*. (2012) used hyperspectral imagery from aircraft-borne sensors and calibration data from ground sampling to detect spectral characteristics of optically complex waters and relate these to chlorophyll, suspended sediments and turbidity of major rivers in Minnesota, USA (Figure 16). Data from three airborne surveys and corresponding in-situ samples are reported and Table 4 lists the average fit statistics, number of samples and total range from all three surveys.

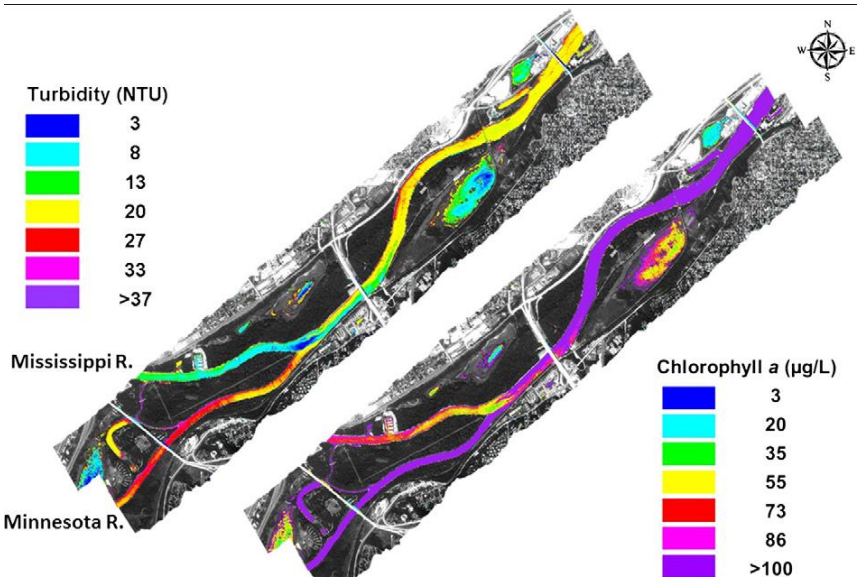

Figure 16: Maps of turbidity and chlorophyll *a* levels near confluence of Minnesota River and Mississippi River, August 30, 2007 (Source: Olmanson *et al.* 2012).

High spectral resolution data potentially allows better retrieval of water quality parameters because spectral signatures of optically active constituents can be isolated. For the simple regressions reported in Olmanson *et al.* (2012), the fit statistics are comparable to those obtained from satellite sensors and the authors conclude that only a few key spectral bands are needed to capture key characteristics of water quality. Combined with high spatial resolution a multispectral airborne system can be a tool for routine monitoring, which is likely to become more cost effective with advances in drone technology.

Remote sensing based model for water quality Bow River, Alberta, Canada

Akbar *et al.* (2013) used the Landsat 5 Thematic Mapper (TM) dataset from 2006 to 2010 to develop empirical models for the Canadian Water Quality Index (CWQI) and turbidity. The CWQI is a metric ranging from 1 to 100 and is calculated using the observed rate of exceedance of water quality objectives for any number of water quality parameters (17 in this case). For this analysis, the monthly CWQI binned into five categories (1 - excellent, 2 - good, 3 - fair, 4 - marginal and 5 - poor) and these categories were regressed against 26 alternate combinations of four spectral band from Landsat 5 TM. The best predictor of CWQI categories was a simple linear model of the red spectral band (r^2 = 0.91, N = 31, Figure 17, left). An example map of predicted CWQI categories along 14 km of the Bow River is shown in Figure 17 (right).

While the statistical model described here may be criticised for its limited range of the response variable, the approach of remote prediction of a composite index should be of interest to regulatory agencies working with similarly processed environmental data. Furthermore, this case study demonstrates that the Landsat 5 TM dataset is a useful archive for retrospective analysis. This satellite was launched in 1984 and has the same spectral and spatial characteristics as Landsat 8.

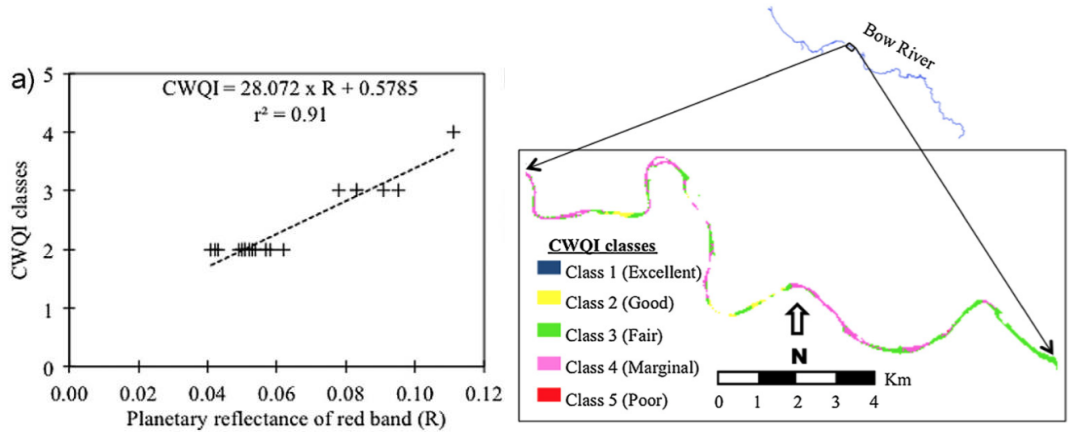

Figure 17. Left: Linear relationship between CWQI categories and the red band of Landsat 5 TM. Right: An example of CWQI classes along a 14 km portion of the Bow River obtained by application of the best empirical model on a Landsat 5 TM image dated 21 June 2007 (Source: Akbar *et al.* 2013).

Estuaries

Regulatory Monitoring of North Carolina Estuaries

Keith *et al.* (2014) used MERIS images to determine how often and to what extent water quality in the Neuse and Pamlico Estuaries, North Carolina USA, exceeded the chlorophyll *a* guideline set by the North Carolina Management Commission of 40 µg L^{-1} (Figure 18, right panel). The authors first used the semi-analytical MERIS case 2 coastal water algorithm to predict chlorophyll *a*. These predicted values were then fit against field measurements of chlorophyll *a* collected within one day of the satellite overpass to produce a locally calibrated chlorophyll *a* estimate which predicted chlorophyll in the estuaries with an r^2 = 0.87 (Figure 18, left panel).

This study demonstrates the successful use of an existing algorithm in conjunction with a local calibration in a regulatory context. However, the Neuse and Pamlico Estuaries are part of the second largest estuarine system in the United States (52,000 km^2). The size and depth of the American estuaries justify the use of a coastal water algorithm and a sensor with 300 m resolution and therefore, the transfer of this methodology to the Waikato has to be carefully considered.

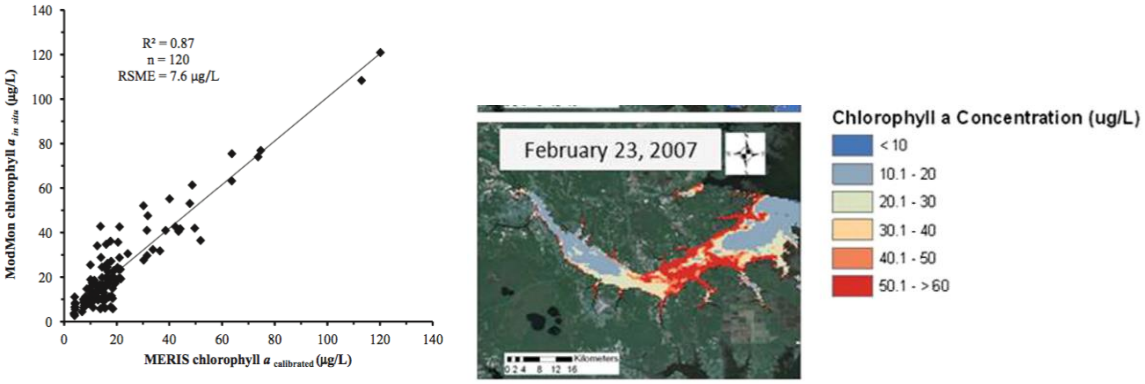

Figure 18: Left: Relationship between calibrated MERIS chlorophyll *a* and observations from within one day of the satellite overpass. Right: Estimated chlorophyll *a* concentration in the Pamlico Estuary, USA, showing breaches of the 40 µg L^{-1} guideline from January to May, 2007 (Source: Keith *et al.* 2014).

Gironde Estuary, France

Doxaran *et al.* (2009) looked at the dynamics of the turbidity maximum zone (TMZ) in the Gironde Estuary using field and satellite data to give complimentary information at different spatial and

temporal scales. The transport of suspended solids becomes complex and unpredictable in estuaries where tidal influence can increase the residence time of freshwater and fine sediments in the TMZ. To study the movement of the TMZ, the authors used four fixed platforms with turbidity sensors and used MODIS 250 m resolution images, captured twice daily. An algorithm for suspended particulate matter (SPM), which had been developed using 204 simultaneous field hyperspectral reflectance spectra along with *in situ* measurements taken over 10 years, was applied to MODIS Band 1 (620-670 nm) and Band 2 (841-876 nm). The resulting regression with *in situ* SMP was successful (r^2 = 0.77 – 0.82) and satellite data corroborated field data, showing the movement of the turbidity maximum zone in the estuary (Figure 19). The authors were then able to determine the conditions within which sediments are exported to the ocean and delineate seasonal cycles of surface TSS.

This study highlights the combination of observations from *in situ* instrument platforms and satellites with daily return periods to generate a large calibration data set and the potential for almost real time monitoring of large systems.

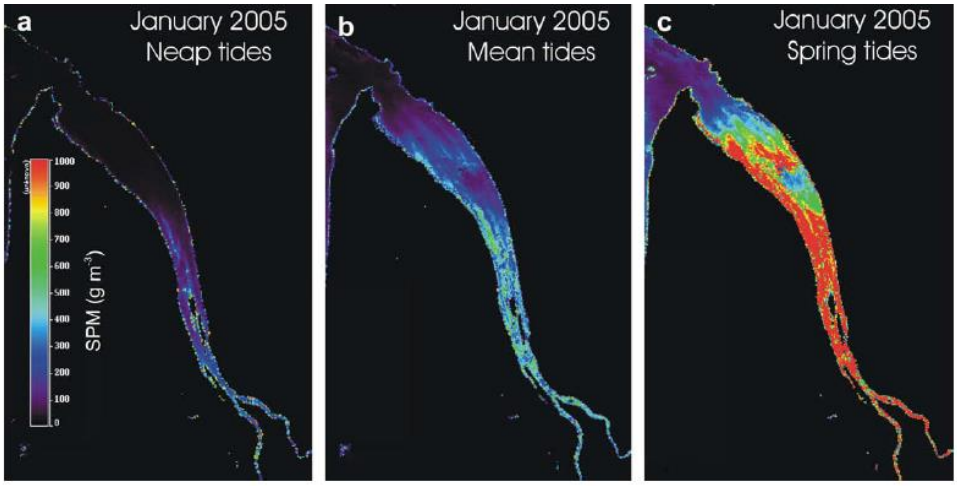

Figure 19: Estimated suspended particulate matter concentrations (g m^{-3}) in the Gironde Estuary during neap, mean and spring tides in January 2005, retrieved using MODIS imagery and a suspended particulate matter algorithm developed for the site (Source: Doxaran *et al.* 2009).

Yangtze Estuary, China

Shen *et al.* (2010) developed a Synthetic Chlorophyll Index algorithm (SCI) for estuaries due to the tendency of existing algorithms to over or underestimate chlorophyll *a* in high TSS waters such as estuaries. The SCI algorithm maintains a quadratic instead of linear relationship with measured chlorophyll *a* concentrations and can be used in waters with a range of TSS concentrations including those with more than 100 mg L^{-1}. The authors applied the algorithm to MERIS images of the Changjiang/Yangtze Estuary from 2008 (Figure 20) and found that the new SCI algorithm (RMSE = 0.4 – 3.1 µg L^{-1}) improved estimation of chlorophyll *a* compared with the commonly used fluorescence line height algorithm (RMSE = 5 – 10 µg L^{-1}).

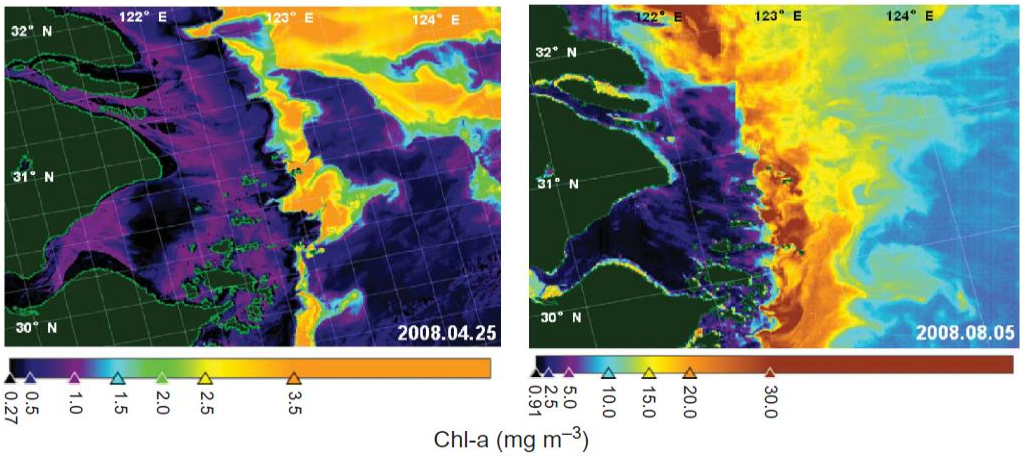

Figure 20: Chlorophyll *a* concentration estimated using an SCI algorithm applied to a MERIS image of the Yangtze Estuary, China on 8 August, 2008. Note that mg m^{-3} is equivalent to µg L^{-1} (Source: Shen *et al.* 2010).

Regional Context Analysis

This section provides information of the extent to which lakes, rivers and estuaries of the Waikato region are visible by the remote sensing satellites that are considered in this study. In principle, a water body is suitable for remote sensing if the surface area is large enough to include water-only pixels and deep enough to preclude interference from bottom reflection. In practice, this visibility then depends on the size and shape of the water body, the characteristics of its bathymetry and water clarity. Furthermore, a consideration for large features may be whether they lie in the same path or whether the entire water body can only be mapped in consecutive overpasses (Figure 21). Finally, visibility depends on the occurrence of clouds and the frequency of overpasses of the satellite.

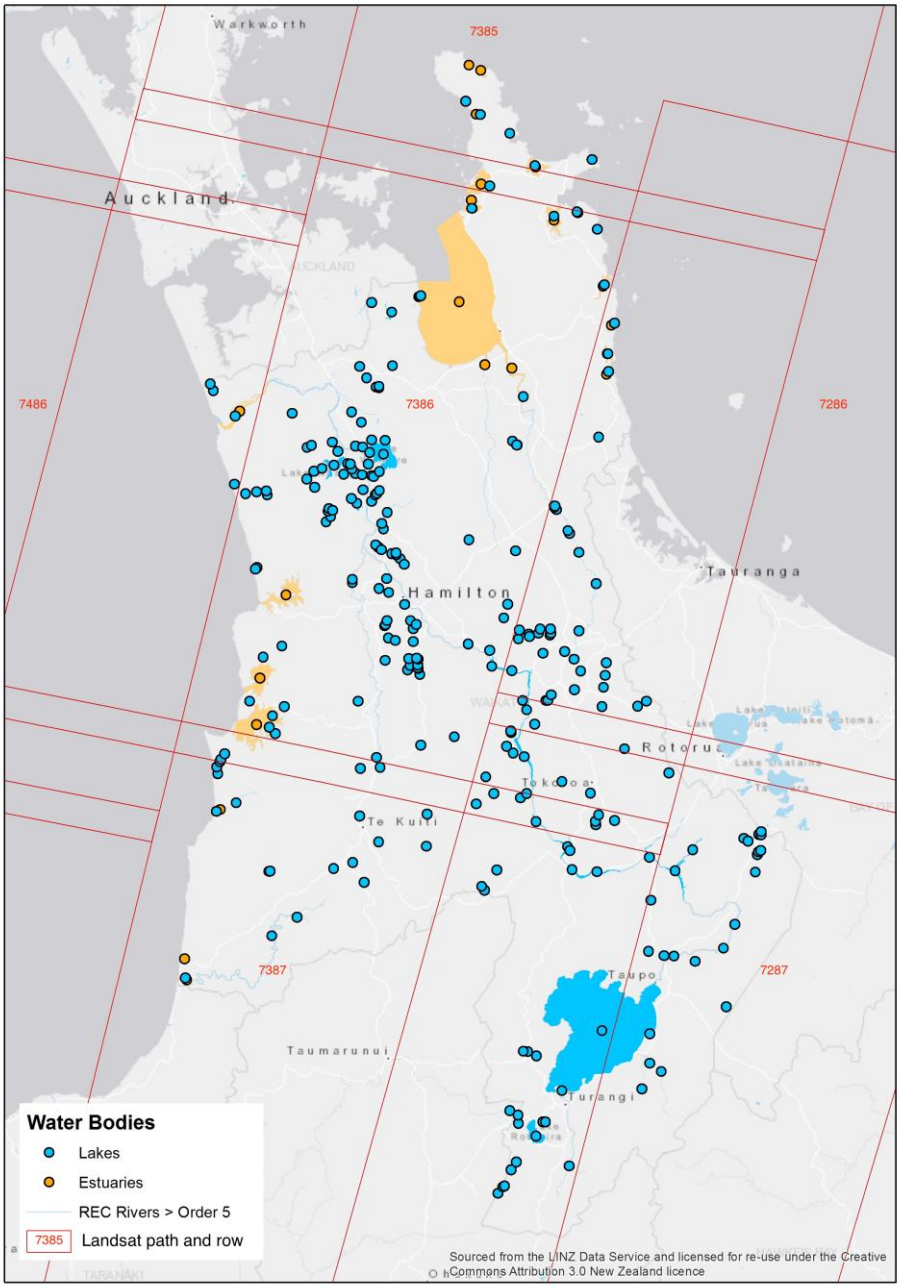

Figure 21: Lakes greater than 1 ha, rivers and estuaries in the Waikato region. The red lines oriented northeast to southwest delineate the swath of the Landsat sensor path. Each path swath is divided into rows so that each scene can be identified by a four digit path-row number (red numbers).

The ability to develop and evaluate algorithms to retrieve water quality parameters depends on our knowledge of how the optically active constituents vary in lakes, rivers and estuaries. Ideally, a suite of *in situ* optical measurements in combination with measurements of chlorophyll, suspended sediment and coloured dissolved organic matter are required to determine optical water types. The last part of this section, *Optically Active Constituents in Waikato Waters*, reviews the relevant information currently available.

Lakes

There are 240 water bodies greater than 1 ha classified as lakes in the Waikato region (Figure 21, see Appendix B for full list) according to the Freshwater Ecosystems geo-database (FENZ geo-database, Leathwick 2010). Effectively, visible size is reduced by extending the shoreline inwards by the width of a satellite pixel (e.g., 10 m, 30 m or 60 m respectively, depending on satellite resolution) to avoid contamination of the upwelling radiance by signals from the shoreline and the bottom. The number of lakes with a masked area greater than 1 ha reduces to 238, 180 and 83 for masks of 10 m, 30 m or 60 m, respectively. Figure 22 shows how the number of observable lakes lessens as satellite resolution decreases.

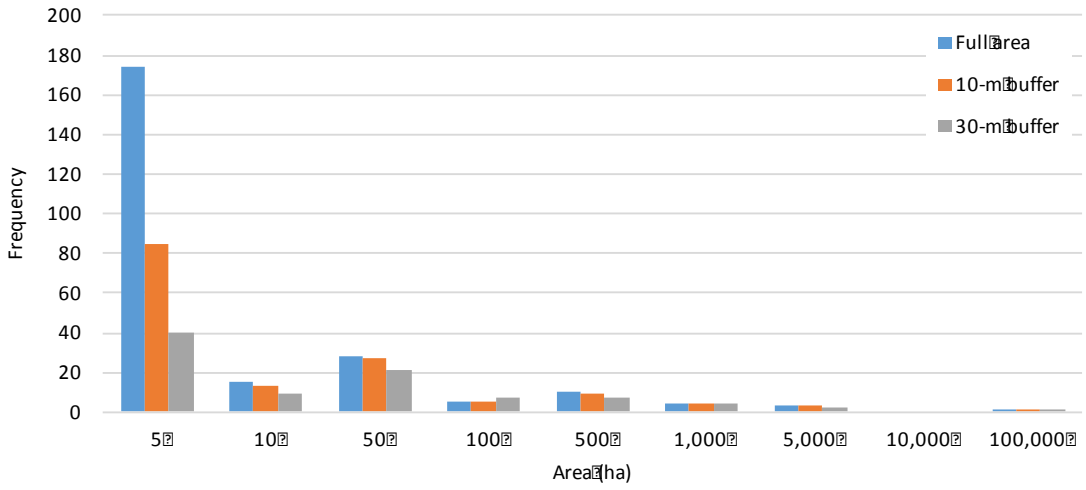

Figure 22: Frequency histogram of Waikato lakes within bins of surface areas (blue bars). Orange and grey bars show the number of lakes in corresponding surface area bins after subtraction of buffered shorelines corresponding to 10 m and 30 m pixel size, respectively. The numbers on the x-axis are upper bin bounds; the first bin includes lakes between 1 and 5 ha.

A second visibility consideration is the shape of the lake. In long narrow water bodies the topographical area may be larger than 1 ha, but the effective open water area may be small and difficult to observe at coarser sensor resolutions.

Specific insight into lake visibility can be gained by determining the extent to which Waikato lakes have previously been surveyed by satellites. For this analysis, the archives of Landsat 7 (between July 1999 and December 2012) and Landsat 8 (from January 2013 to December 2015) were used in the following procedure:

1. The complete catalogue of images during the time spans given above was manually pre-screened to exclude images of full or almost full cloud cover to reduce processing requirements;
2. The shoreline of all lakes greater than 1 ha were masked with a 30-m wide inside buffer;
3. Masks were applied to retain only water pixels;
4. The number of water-only pixels per lake in any given image was counted and summary statistics were computed over all images.

The summary statistics for named Waikato lakes are shown in Table 7 and data for all Waikato lakes is provided in Appendix B. Table 7 provides insight into the following empirical properties of each lake:

- The maximum number of pixels observed show the observable lake size specific to the sensor used, i.e., 30 m in this case;
- The total number of successful retrievals (images with at least one pixel in a given lake due to partly or entirely cloud-free skies) indicates the number of observations over the last 16 years and 3 months; and
- The average number of retrievals per year provides an estimate of the expected number of images per year for each lake from Landsat 7 or 8, respectively (both satellites have the same orbit and ground resolution).
- A shape parameter to address the degree of lake elongation, the isoperimetric quotient[3] (*Q*),

The average annual number of retrievals provides an estimate of the number of times data from any of the Waikato lakes larger than 1 ha may be observed using a Landsat sensor. Combining Landsat 7 and 8 in this analysis is possible, because these missions have been designed to provide long-term continuous earth observations and therefore have almost identical sensor and orbit specifications. This analysis shows that the named lakes have been observed on average six times per year with at least one pixel. 57% of all lakes (137) are also large enough to yield more than three pixels. Having more pixels per lake reduces the sampling error for whole-lake average values and offers the possibility that spatial variability can be studied. Elongated lake shape did not emerge as a negative correlate of retrievals or success rate, rather there was a tendency for retrieval success to decrease with increasing "roundness". Furthermore, the average annual retrieval is only weakly explained by increasing lake size (r^2 = 0.25) which suggests that cloud cover dominates the visibility statistic rather than lake-specific properties. That suggests that the successful retrievals are unlikely distributed evenly over the year and that most observations can be expected during seasons with less cloud cover.

Table 7: Named lakes greater than 1 ha in the Waikato region with characteristics relevant for remote sensing. The lakes are sorted by surface area. The maximum number of pixels observed shows the observable lake size specific to the sensor used, i.e., 30 m in this case. The total number of successful retrievals (images with at least one pixel in a given lake) indicates the number of observations over the last 16 years. The number of average annual retrievals is the number of partly or entirely cloud free images of the lake divided by the number of years of Landsat 7 and 8 operations (16.25 years at the time of this analysis). The full list of lakes is provided in Appendix B.

Name	Area (ha)	Isoperimetric quotient	30-m buffered area (ha)	Max. number of pixels	Number of successful retrievals	Average annual retrievals
Lake Taupo (Taupomoana)	61,334.9	0.25	60,813.8	674976	101	6.2
Lake Waikare	3,438.7	0.24	3,312.0	36766	127	7.8
Lake Rotoaira	1,567.8	0.41	1,502.8	16672	97	6.0
Lake Whangape	1,078.9	0.15	990.9	10771	127	7.8
Lake Ohakuri	940.2	0.02	714.0	8022	104	6.4
Lake Arapuni	828.2	0.06	700.4	7766	221	13.6

[3] An isoperimetric quotient is essentially a measure of how round a feature is in comparison to a circle, with a value of 1.0 being a perfect circle, and is given by ratio of its area (*A*) and that of the circle having the same perimeter (*L*), calculated as $Q = (4\pi A)/L^2$.

Name	Area (ha)	Isoperimetric quotient	30-m buffered area (ha)	Max. number of pixels	Number of successful retrievals	Average annual retrievals
Lake Karapiro	770.3	0.02	559.8	6296	221	13.6
Lake Whakamaru	539.0	0.05	434.6	4886	112	6.9
Lake Waahi	444.7	0.26	401.9	4453	117	7.2
Lake Maraetai	400.6	0.05	308.4	3480	205	12.6
Lake Rotongaro	283.9	0.41	256.3	2878	120	7.4
Lake Taharoa	216.5	0.31	189.6	2144	109	6.7
Lake Atiamuri	203.5	0.03	125.0	1417	214	13.2
Lake Otamangakau	156.4	0.07	112.3	1276	94	5.8
Mangatangi Reservoir	154.5	0.03	86.6	1046	108	6.6
Upper Mangatawhiri Reservoir	123.9	0.09	89.6	1023	108	6.6
Lake Waipapa	116.6	0.09	77.7	900	204	12.6
Lake Kuratau	103.1	0.24	81.8	863	94	5.8
Lake Ngaroto	91.8	0.46	77.0	865	114	7.0
Lake Rotopounamu	85.1	0.73	73.9	830	90	5.5
Lake Rotokawa	65.5	0.78	56.1	630	87	5.4
Lake Hakanoa	56.4	0.63	46.9	530	107	6.6
Lake Rotoroa	52.0	0.48	41.3	467	113	7.0
Lake Kimihia	48.8	0.51	38.7	427	115	7.1
Lake Aratiatia	45.1	0.09	21.3	255	90	5.5
Lake Kopuera	44.9	0.58	35.9	408	106	6.5
Lake Rotongaroiti	44.5	0.34	33.7	389	111	6.8
Lake Rotokauri	38.0	0.52	29.3	340	104	6.4
Lake Rotongaio	34.2	0.51	25.8	295	93	5.7
Upper Tama	31.4	0.59	24.0	276	75	4.6
Lake Areare	30.4	0.50	22.5	259	107	6.6
Lake D	27.2	0.36	18.4	210	112	6.9
Lake Rotoroa	22.6	0.43	15.5	181	98	6.0
Lake Hinemaiaia	21.8	0.29	13.0	107	90	5.5
Lake Ngapouri	21.3	0.52	15.0	173	88	5.4
Lower Tama	21.1	0.92	16.3	187	79	4.9
Lake Harihari	18.4	0.18	8.5	104	107	6.6
Lake Maraetai	18.0	0.09	5.5	62	88	5.4
Lake Maratoto	17.9	0.49	11.7	135	112	6.9
Blue Lake	17.2	0.94	12.9	148	63	3.9
Lake Ohinewai	17.1	0.59	11.7	135	98	6.0
Lake Numiti	15.8	0.54	10.6	121	97	6.0
Lake Hotoananga	15.6	0.87	11.4	119	100	6.2
Lake Rotokawau	14.8	0.41	8.7	105	107	6.6
Lake Mangakaware	14.6	0.32	8.0	90	111	6.8
Lake Rotomanuka	13.6	0.74	9.4	104	108	6.6
Lake Parangi	12.0	0.26	5.4	67	98	6.0
Lake Ruatuna	11.8	0.63	7.6	89	112	6.9
Lake B	9.7	0.57	5.7	68	104	6.4

Name	Area (ha)	Isoperimetric quotient	30-m buffered area (ha)	Max. number of pixels	Number of successful retrievals	Average annual retrievals
Lake Ngahewa	8.4	0.53	4.5	54	81	5.0
Lake Mangahia	7.9	0.52	4.3	47	99	6.1
Lake Moananui	7.9	0.19	2.1	24	166	10.2
Lake Okowhao	7.5	0.57	4.1	49	98	6.0
Lake Ngakoro	7.0	0.47	3.2	37	70	4.3
Lake Rotongata	6.1	0.46	2.5	29	172	10.6
Lake Puketi	5.9	0.64	3.0	36	91	5.6
Lake Koromatua	4.9	0.76	2.5	29	91	5.6
Lake Otamatearoa	4.9	0.86	2.6	28	90	5.5
Lake Pataka	4.8	0.68	2.4	30	89	5.5
Lake Orotu	4.7	0.31	1.4	18	74	4.6
Lake Cameron	4.7	0.60	2.0	22	102	6.3
Lake Pikopiko	4.7	0.67	2.2	27	97	6.0
Lake Serpentine N	4.6	0.84	2.4	29	107	6.6
Lake te ku utu	4.6	0.66	2.1	24	96	5.9
Hamareha Lakes	4.4	0.39	1.3	16	28	1.7
Lake Serpentine W	4.3	0.15	0.4	8	101	6.2
Pukuriri Lagoon	3.6	0.69	1.5	20	28	1.7
Lake Whangioterangi (Echo Lake)	3.6	0.32	0.5	6	70	4.3
Lake Okoroire	3.5	0.32	0.7	8	62	3.8
Horseshoe Lake	3.4	0.46	1.0	14	70	4.3
Lake Ngarotoiti	3.3	0.51	0.9	12	97	6.0
Lake Tutaeinanga	3.1	0.51	1.0	11	87	5.4
Lake E	3.1	0.39	0.7	9	96	5.9
Lake A	2.8	0.94	1.3	17	87	5.4
Lake Rotokura	2.7	0.78	1.0	14	42	2.6
Rotowhero (Green Lake)	2.6	0.69	0.9	11	77	4.7
Lake Rototapu	2.0	0.90	0.7	8	93	5.7
Lake C	1.6	0.38	0.0	1	91	5.6
Lake Serpentine E	1.4	0.67	0.2	3	97	6.0
Lake Waiwhata	1.3	0.53	0.1	1	78	4.8
Ngakoro	1.3	0.70	0.2	2	17	1.0
Lake Rotokotuku	1.2	0.93	0.3	4	10	0.6
Lake Rotopataka	1.1	0.36	0.0	*	*	*
Beggs Pool	1.1	0.30	0.0	*	*	*

*No retrievals available for these lakes due to their small size.

Rivers

The natural limitation to observing rivers by remote sensing is the narrow width relative to the resolution of the sensor. After river banks are masked to reduce contamination of the signal by land, bottom and macrophytes, width still has to be at least one pixel, e.g., 10, 30 or 60 m, to be visible. A spatial analysis of rivers in the Waikato region shows that after masking both shores with a 10 m buffer, only the Waikato River exceeds 30 m of width over much of its length and is therefore

theoretically visible by Landsat sensors (Figure 23). The Waihou River also exceeds 30 m over some of its reach (after buffering) and both rivers exceed 60-m buffered width in some part of their reach. The Waipa River is only visible with 10 m resolution sensors such as those of Sentinel-2 satellite. At this stage, the poor visibility of rivers to extant satellite observing systems suggests that the feasibility of monitoring, other than for specific questions regarding these few large rivers, is low.

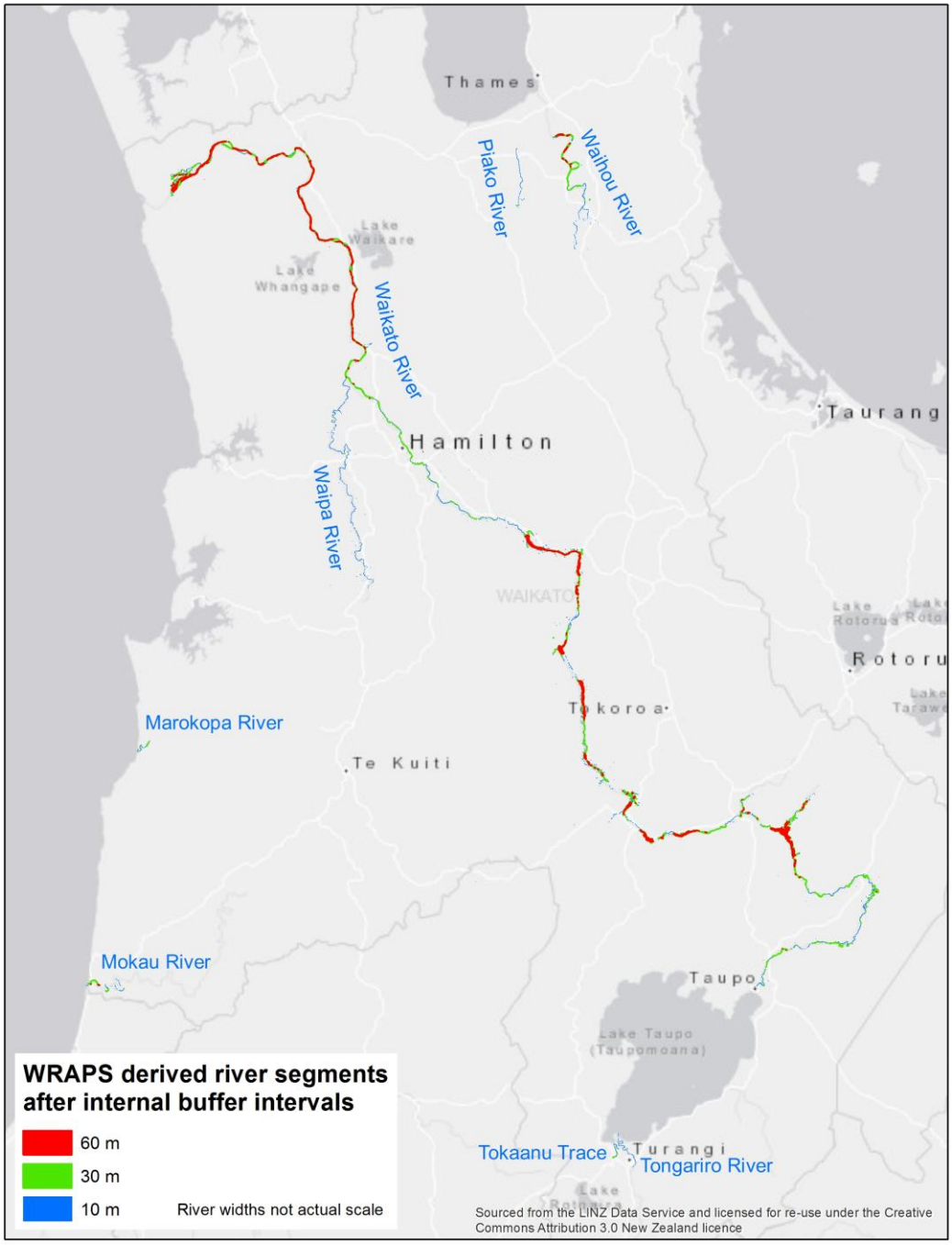

Figure 23: Rivers whose width exceeds 60, 30 and 10 m after masking the shoreline with the 10 m buffer. Rivers were delineated from water pixels found in 2012 Waikato Regional Aerial Photography Service (WRAPS) imagery; pixels were classified as water using the Normalised Difference Water Index (NDWI) according to (NDWI > - 0.009) & (B4 < 70) where NDWI = (B2 - B4) / (B2 + B4). B2 is the green band and B4 the infrared band.

Estuaries

Remote sensing of water quality parameters in estuaries poses challenges in addition to the previously discussed constraints on visibility due to size and shape. Estuaries are highly dynamic systems where tides and other coastal processes modify bathymetry, water depth and water clarity over a range of time and space scales. For example, many estuaries run almost dry during low tide, limiting the chances of successful image retrieval. The air photo of the Waikato river estuary (left panel in Figure 24) illustrates the complicated bathymetry and coastline. The right panel in Figure 24 shows a Landsat 8 scene processed for total suspended solids (TSS); the apparent high TSS concentration at the mouth of the estuary is likely an artefact of waves breaking in that region, and issue that appears only to have been addressed by development of site-specific empirical algorithms (Teodoro *et al.* 2004).

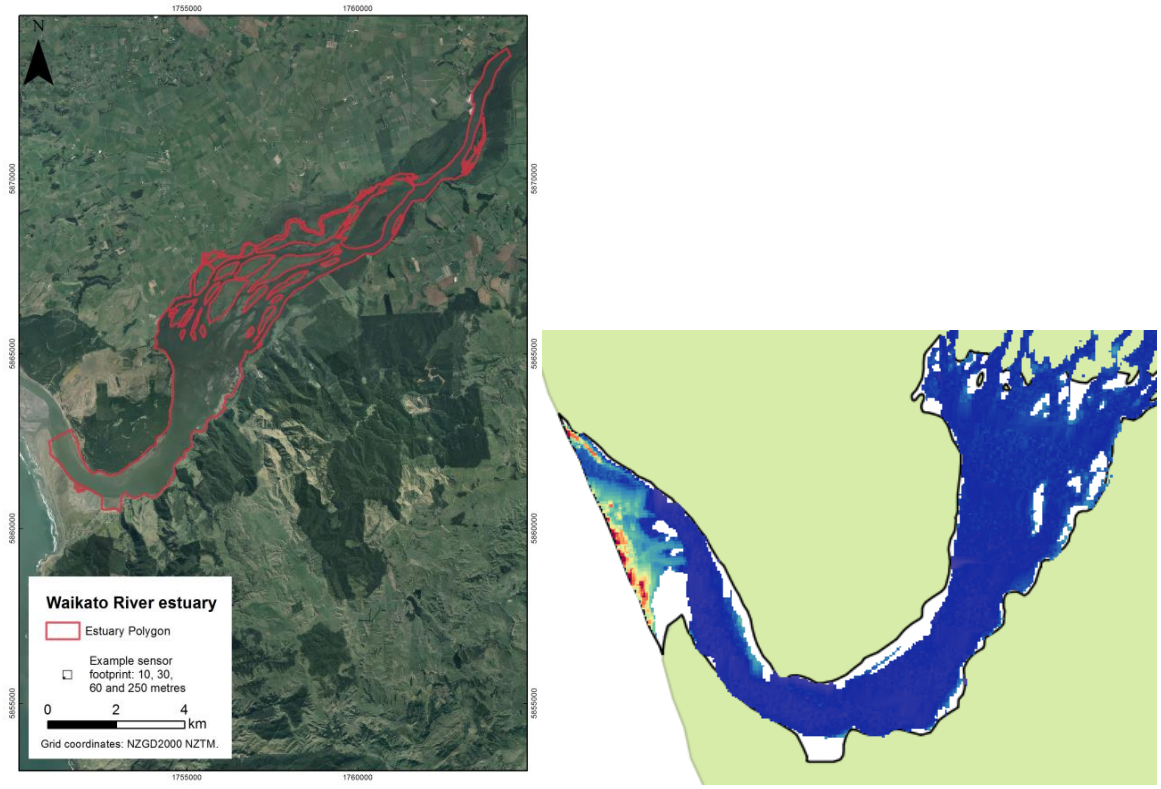

Figure 24: Waikato River estuary. Left: Red line is derived from the Land Cover Database (LCDB) estuary shape by applying an inside buffer of 30 m (red line); background air photo from WRAPS 2012. Right: Landsat 8 scene from 29 September 2014 processed for total suspended solids.

A preliminary assessment of estuary size with respect to satellite resolution was carried out for 23 Waikato estuaries for which shape files were provided by WRC (H. Jones, pers. comm. 5th September 2016). Estuary boundaries were masked with an inside buffer of 30 m (the pixel size of Landsat) to reduce the number of pixels which include a signal from land. The buffered surface area is listed in Table 8. An air photo of each of the estuaries with its buffered boundary is shown in Appendix C (see also Figure 24) to provide a visual impression of their size and shape relative to satellite footprints. In addition, Landsat 7 and 8 images between 1999 and 2015 for ten estuaries for which imagery had been retrieved previously (M. Allen, unpublished data) were processed for visibility statistics (Table 8). Cloud and land detection algorithms were applied to the estuary areas allowing a count of water pixels. The number of images where water could be seen out of 401 satellite overpasses provides a success rate indicative of the visibility of the estuary from space taking into account cloud cover and tides. On average over the ten estuaries, water was visible in 21% of overpasses providing data which can potentially be used to derive water quality parameters.

Table 8: Estuaries of the Waikato region and their size after subtraction of a 30 m shoreline buffer. The number of average annual retrievals is the number of partly or entirely cloud free images of the estuary divided by the number of years of Landsat 7 and 8 operations (16.25 years at the time of this analysis); this estimate is provided where available.

Name	Area after 30 m shoreline buffer (ha)	Max. number of pixels	Number of successful retrievals	Average annual retrievals
Aotea Harbour	3,016.1			
Awakino River estuary	3.7			
Colville Bay	422.7	1224	12	0.74
Coromandel Harbour	2,432.7			
Firth of Thames	55,404.2			
Kawhia Harbour	6,268.7			
Manaia Harbour	571.0	2611	103	6.34
Marokopa River estuary	26.7			
Mokau River estuary	55.2			
Otahu Estuary	57.2	389	107	6.58
Piako River estuary	89.1			
Port Charles	452.0			
Purangi Estuary	91.5	592	104	6.40
Stony Bay	104.2			
Tairua Harbour	510.3	5027	112	6.89
Te Kouma Harbour	239.2			
Waihou River estuary	793.8			
Waikato River estuary	1,479.0	12539	125	7.69
Whaingaroa (Raglan) Harbour	2,778.3			
Whangamata Harbour	375.6	3313	111	6.83
Whangapoua Harbour	1,184.9	10550	113	6.95
Wharekawa Harbour	161.4	853	108	6.65
Whitianga Harbour	1,319.5	8554	115	7.08

Optically Active Constituents in Waikato Waters

Constituents of water quality and optical properties of water are linked by optical principles: optically active constituents (OAC) determine the inherent optical properties, which in turn determine apparent optical properties, such as remote sensing reflectance (Figure 1). Attempts to back-calculate OACs from remote sensing reflectance are constrained because many combinations of phytoplankton, suspended matter and coloured dissolved organic matter can lead to the same absorption, scattering and beam attenuation signatures. In lakes, these combinations vary widely and independently of one another and to improve the retrieval algorithms, it is necessary to measure this variability in as many lakes as possible to derive patterns on a regional or temporal basis.

There are few bio-optical observations from lakes, rivers and estuaries in New Zealand and existing work has mainly been carried out in Waikato waters. Vant and Davies-Colley (1984) report inherent optical properties, apparent optical properties and ancillary measurements from one-off sampling of 27 New Zealand lakes, eight of which were in the Waikato region (Rotongaro, Lake D, Hakanoa,

Waahi, Rotoroa, Ngaroto, Rotomanuka and Karapiro). While this early survey provides only spectrally averaged estimates of scattering, absorption and beam attenuation, it illustrates well the central problem of freshwater remote sensing: the respective contributions of chlorophyll *a*, suspended solids and coloured dissolved organic matter are extremely variable, especially in the Waikato lakes (Figure 25). Later, Davies-Colley and Vant (1987) found that coloured dissolved organic matter ranged over a factor of 50, almost the entire reported range. Lake Rotokakihi had the lowest value resembling clear ocean waters and Lake D was highly coloured.

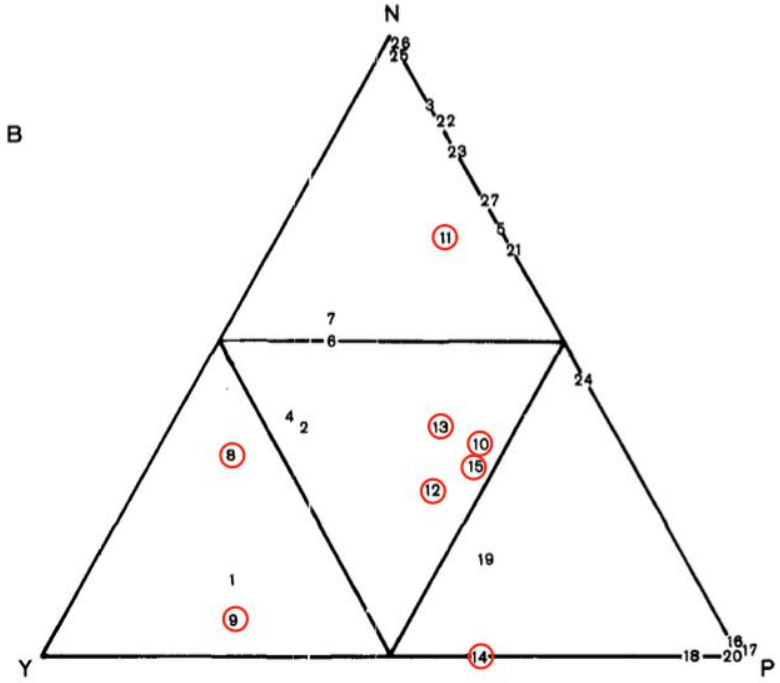

Figure 25: Contributions of chlorophyll *a* (P), non-volatile suspended solids (N) and coloured dissolved organic matter (Y) to the average absorption coefficient for 27 New Zealand lakes (numbers). Waikato lakes (8 to 15, circled) are Rotongaro, Lake D, Hakanoa, Waahi, Rotoroa, Ngaroto, Rotomanuka and Karapiro, respectively. Adapted from Vant and Davies-Colley (1984).

The work of Belzile *et al.* (2004) in Lake Taupo provides a good example for a modern bio-optical survey, with measurements of spectral absorption coefficients and diffuse attenuation coefficients along with ancillary measurements. As expected from a clear, deep, oligotrophic lake, variability in optical properties is relatively low and coloured dissolved organic matter, phytoplankton and non-algal particles play relatively equal roles in determining water transparency and colour. Therefore, all three components must be taken into account in order to understand and predict the water colour of this lake (Figure 26). This existing work would assist the development and parameterisation of enhanced remote sensing retrieval algorithms.

Optical studies of Waikato rivers and estuaries comparable to that of Belzile *et al.* (2004) could not be found. Vant (2015) summarises the data collected in the Waikato and Waipa Rivers by NIWA and the Waikato Regional Council between 2005 and 2014. On average, over 10 years, phytoplankton and attenuation by non-algal particles contributed most to the overall absorption and beam attenuation in both rivers in about equal parts. The contribution by coloured dissolved organic matter was found to be low (between 2-8%). The values for absorption, scattering and beam transmission reported by Vant (2015) are not spectrally resolved and the information is not sufficient for designing retrieval algorithms. However, this study suggests that retrieval algorithms may be simpler for rivers than for lakes, because of the limited importance of coloured dissolved organic matter.

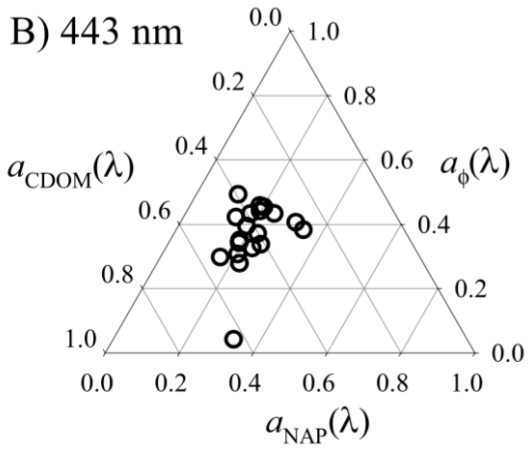

Figure 26: The absorption budget at 443 nm (blue light) from 19 stations in Lake Taupo shows that the "blueness" of Lake Taupo has little within-lake variability and is equally affected by phytoplankton, non-algal particles and CDOM (Source: Belzile *et al.* 2004).

Further published optical data for lakes, rivers and any data for estuaries in New Zealand could not be found within the time frame of work on this report. Additional data may be available in Howard-Williams and Vincent (1984) and Schwarz (1996) and from other investigators, e.g. Matt Pinkerton, (NIWA Wellington).

Implementation Pathway

The design, planning and implementation of a system for the retrieval and processing of satellite data to generate water quality reports requires specific hardware, software and personnel resources. This section provides details of the tools available for building such a system. We present choices for different tools to accomplish certain tasks in the workflow and estimate the technical skills needed to use them. Finally, the effort to build, run and maintain a processing system is estimated to allow cost-benefit analysis and resource planning.

The final design of a system for remote sensing of water quality parameters depends on the objectives to be addressed by remote sensing. To help define these objectives in a way meaningful for the system requirements, the following questions should be answered quantitatively:

1. How many sites are to be monitored?
2. What is the desired spatial and temporal resolution?
3. What parameters should be monitored?
4. What is the desired level of automation?
5. How much data should be backed up?

A decision framework to deal with these questions is presented in the concluding chapter of this report (*Synthesis and Conclusion*).

Processing Work Flow

The work flow which generates water quality parameter estimates from remote sensing is broken down into the following steps (for details see section *Retrieval of Water Quality Constituents*):

1. Downloading of satellite data;
2. Data processing:
    a. Atmospheric correction;
    b. Extraction of data for relevant water bodies, including removal of edge pixels;
    c. Removal of cloudy pixels;
    d. Application of parameter retrieval algorithms; and
3. Generation of results tables, plots and maps.

Multiple tools are available for each step in the process and the choice for a specific set of these depends on the data source, i.e., the sensor, and the desired level of automation, efficiency and user friendliness. We present details here on a selection of tools which we recommend for consideration for a routine monitoring system. These tools are most commonly used by the remote sensing community, supported by the providers of satellite data, mostly free of charge or are industry standards for the tasks to be accomplished. We have not been able to find any descriptions of operational systems for the monitoring of inland or estuarine water quality parameters using remote sensing. Therefore, the work flows in this section have been developed based on our experience. The flow chart in Figure 27 illustrates our recommended tools (tool acronyms are explained in the text below) and their dependencies on each other and on the satellite sensor. We note that the tools are not mutually exclusive and it is likely that several approaches will be tested and used during the development and operation of the monitoring system.

Processing satellite imagery is a technical task which requires the handling and management of large data sets and experience in spatial analysis. While one-off remote sensing studies of water quality can be performed by point-and-click navigation of software based on graphical user interfaces, efficient routine monitoring will require automation using scripting languages. We categorise the

skill required for each task into one of three levels: basic, intermediate or advanced, and use a simple graphical gauge to visualize it. The skill levels are defined as follows.

Basic: Interact with a graphical user interface following prescribed instructions to access and process data.

Intermediate: Utilise pre-written computer scripts or batch commands to automate the processes of accessing and analysing data. Basic scripting experience required to ensure processes function smoothly (such as changing directory paths or schedule code execution).

Advanced: Fully comprehend computer scripts to maintain and modify automated processes as required (e.g. modify the access to data downloads, implementation of updated algorithms).

Note that some tools can be applied at more than one skill level. For example, an intermediate user is assumed to have the skills necessary to use existing Python scripts and adapt them to the local environment, but authoring scripts and extending their functionality requires an advanced skill level. Furthermore, we consider only the application of established image processing techniques and algorithms here, thus, the skill-level requirement assigned to technology options relate to operational skills only and not research and development.

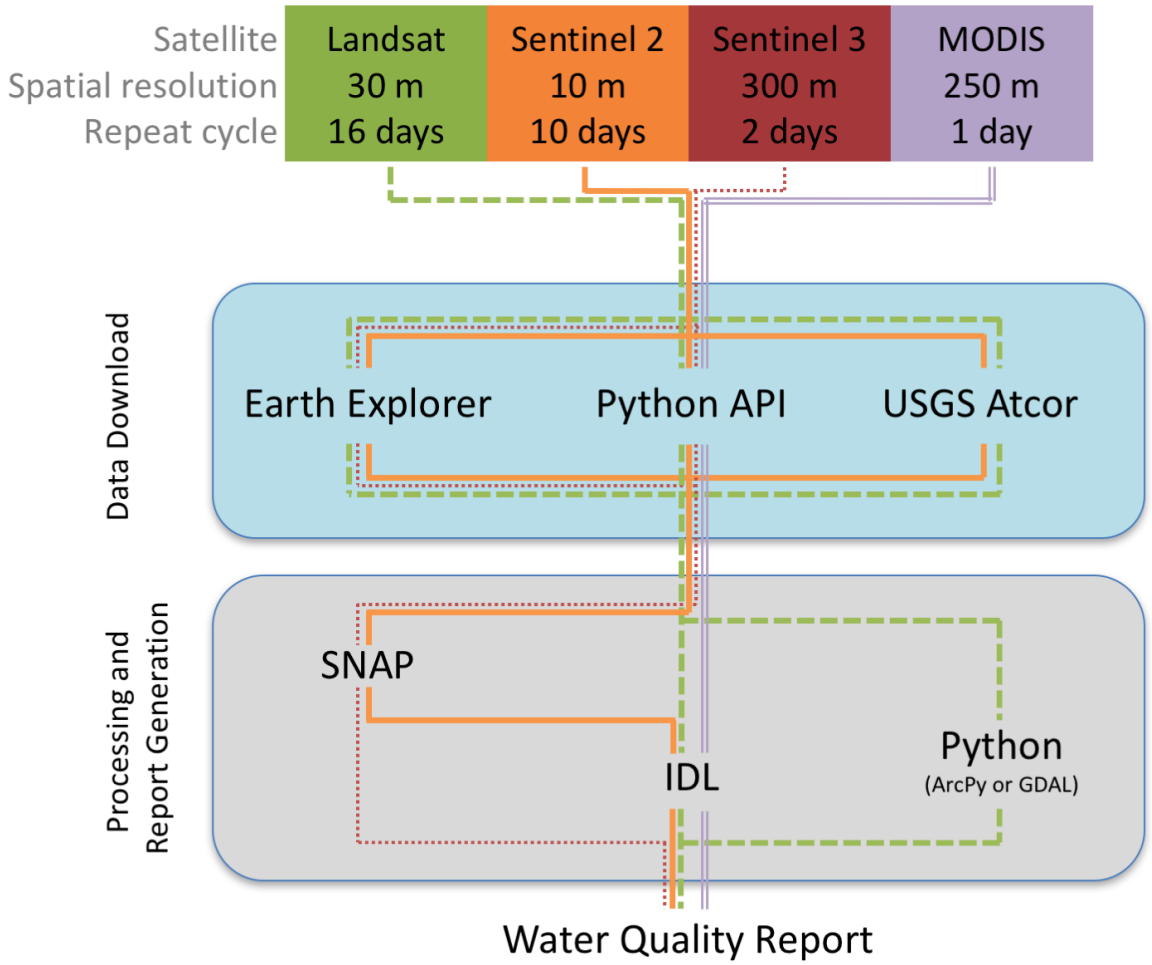

Figure 27: Chart illustrating the interdependencies of tools available for the work flow from downloading remote sensing data to generating water quality reports. Each tool is defined in the text of this section. Acronyms are defined in the text.

Download Options

Landsat, Sentinel-2 and MODIS data are currently freely available to download using web based user interfaces. These have been designed for manual ordering and downloading of on-demand single or bulk lots of images. Existing script libraries are available to automate downloading of Landsat, Sentinel-2 and MODIS images and others are in development.

Earth Explorer: The Earth Explorer web browser interface (http://earthexplorer.usgs.gov/) is an easy to use graphical user interface for manually selecting Landsat and Sentinel-2 imagery. After selection, single or multiple images can be ordered and are available for download within a day using the United States Geological Survey (USGS) Bulk Download Application. While manual selection takes time, it can decrease the data volume to transfer and process through cloud detection routines. Free registration is currently required to download data.

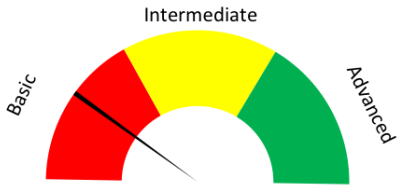

Python API: The data archives of the satellites discussed here have Application Programming Interfaces (APIs) which allow automated downloading using computer scripting languages such as Python together with file transfer protocols. Existing Python libraries[4] can be utilised to run automated schedules for pre-screening and downloading of imagery.

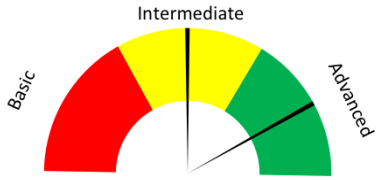

USGS Atcor: The USGS provides atmospherically corrected data (Atcor). Using Atcor data greatly reduces the processing and computation time. The data has to be ordered manually through the Earth Resource Observation and Science Centre Science Processing Architecture On Demand Interface[5]. Bulk downloading is currently available from this service via the ESPA Bulk Downloader[6] which is executable using Python and a web API is in development that will enable the automation of ordering and downloading of data.

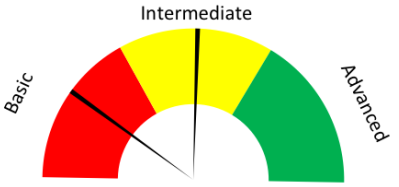

Processing Options

Image processing generally involves a number of distinct tasks described in the section *Retrieval of Water Quality Constituents*. These tasks can be accomplished manually on an image-by-image basis or they can be automated using a scripting language. The software tools recommended for processing are listed below and which one is chosen depends on the satellite sensor (see Figure 27) and the desired level of automation.

SNAP: SNAP (Sentinel Application Platform) is an open source common architecture which applies Sentinel toolboxes[7]. Using SNAP, Sentinel-2 images can be georectified, and atmospherically corrected. SNAP is an easy-to-use graphical user interface, suitable for users new to remote sensing.

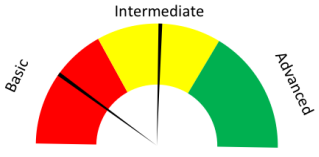

[4] https://pypi.python.org/pypi/sentinelsat
[5] http://espa.cr.usgs.gov/index/
[6] ESPA is the USGS Earth Resources Observation and Science (EROS) Center Science Processing Architecture available at https://github.com/USGS-EROS/espa-bulk-downloader
[7] http://step.esa.int/main/toolboxes/snap/

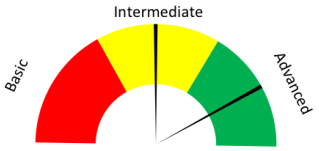

SNAP automation: SNAP includes a Graph Processing Framework (GPF): for creating user-defined processing chains, which allows automation of image processing such as atmospheric correction.

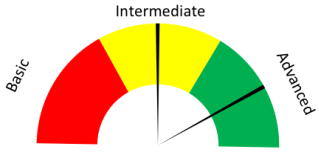

ENVI IDL (Alog): ENVIE is a graphical-user-interface-based image processing environment commonly used in professional and research environments to work with data such as images from remote sensing, astronomy and atmospheric physics. The IDL (Interactive Data Language) programming language allows extension and automation of ENVIE image processing tasks. Note that this is commercial software with a large user base and library of remote sensing scripts.

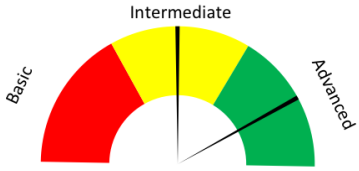

Python: Python is a widely used open source high level programming language that is becoming the programing environment of choice for geospatial analysis. ArcPy is a Python site package allowing the automation of ArcMap functionality. GDAL (Geospatial Data Abstraction Library) is a translator library for raster and vector geospatial data formats and can be integrated into many programing languages (like Python) to enable powerful geospatial processing capability. The open-source distribution and operating-system independence makes Python a very flexible tool for use in the remote sensing and geospatial processing.

Computer System Requirements

The ability to download and process satellite imagery at the regional scale is within the capability of a moderately powerful workstation running a Microsoft Windows or Linux system. Specifications of a computer system which we believe can handle Waikato's water bodies and processing options discussed here are provided in Table 9.

Table 9: Recommended specifications of a computer system for the processing of existing data and continuous monitoring.

Recommended Specifications
CPU: 3.00GHz Multi-core processor System: 64-bit OS RAM: 32 GB Hard Drive: 12 TB

Backup and Data Retaining Options

Retaining and backing up data requires a choice of storage hardware or cloud-based backup providers. Three data types are generated during the processing of remote sensing imagery for which a storage decision has to be made: raw imagery, processed imagery and result reports. Table 10 provides details on each data type and expected storage capacity.

Table 10: Data types and their approximate storage requirements for the size of the current image archive.

Data Type	Detail	Storage requirement*
Raw imagery	● Landsat - GeoTIFF format ● Sentinel - Standard Archive Format for Europe (SAFE) ● Radiances ● Atmospherically corrected (Landsat only) ● Landsat swath 185 km ● Sentinel swath 290 km	Landsat archive 1 TB MERIS 5 TB Sentinel-2a 6+ GB**
Processed imagery	● GeoTIFF format ● Products including temperature, chl *a*, TSS ● Whole region and masked to water bodies	Landsat 2 TB MERIS 5 TB Sentinel-2a 1 TB**
Result reports	● Derived water quality maps and tables ● Time series updates, e.g. in FWENZ for lake sites	500 GB

*Depending on the sensor as specified.
**Each 100-by-100 km Sentinel-2a tile is 600 MB. There are fewer than 10 relatively clear images for the northern Waikato tile from the time frame November 2015 to February 2017; these already take up 5 GB; archiving of future imagery will require considerable storage requirement.

Level of Effort

This section presents an estimate of the effort required to set up, run and maintain a system for the routine monitoring of water quality parameters based on our current experience. The process is divided into a number of high-level tasks and the effort is split between four types of technical staff as defined by the skill level given above. The effort is in units of days and in days per month for routine monitoring. We assumed the use of Landsat 7 and 8 platforms and processing using the lower skill-level tools. The effort is an order-of-magnitude estimate and the actual effort is expected to be between half and double of the number listed.

Ten tasks have been identified to design and build a system capable of conducting routine monitoring of water quality, to train technical staff and to process the existing archive of Landsat 7 and 8 imagery (Table 11). Our order-of magnitude estimate of the effort is 71 days, 54% of which would be allocated to the work of staff with intermediate and basic skill levels together, and 36% to someone with advanced ability and understanding. The remaining 10% are allocated to decision making, planning and quality control by relevant managers.

Table 11: Effort estimate in units of days for setting up a system for the processing of remote sensing data to retrieve water quality parameters. This estimate also includes the processing of the existing archive of Landsat imagery.

System setup and archive processing	Effort requirement in days			
	Manager	Advanced staff	Intermediate staff	Basic staff
System design decisions	3	3		
Hardware purchase and setup		1	3	
Software purchase and installation		3	1	
Workflow design and scripting*	1	10	2	
Training	2	5	5	5
Download of existing archive				2
GIS data quality control				2
Processing of archive		2	2	10
Quality control and validation	1	1		
Reporting of existing archive**	0.5	0.5	1	5
Sum	7.5	25.5	14	24

*including trouble shooting
**Generation of maps, result tables and time series, not including validation

The effort of routine monitoring is estimated as 10 days per month (Table 12). Staff of basic skill level should be able to perform most of the routine work in about 4 days per month (about 40% of the effort). Intermediate- and advanced-level staff together are estimated to require 4.5 days per month (45% of the effort) to maintain and the system, quality control and keep up to date with technology developments. Managerial involvement is estimated at 1.5 days per month.

Table 12: Effort estimate in units of days per month for carrying out water quality monitoring using remote sensing.

Routine monitoring	Effort requirement in days per month			
	Manager	Advanced staff	Intermediate staff	Basic staff
Ongoing data download and processing			1	3
Quality control	0.5	1		
Script maintenance and trouble shooting		1	0.5	
Technology updates	1	0.5	0.5	1
Sum	1.5	2.5	2	4

Summary

The design, planning and construction of a system for the retrieval and processing of satellite data to generate water quality reports requires dedicated hardware, software and personnel resources. This section provided details on each of these components to help managers to make informed decisions regarding the pursuit of this technology and help with detailed system design. It specifically

demonstrates that from a technical standpoint, once a decision to proceed is taken, remote sensing of parameters related to water quality offers few technical barriers because:

- Remote sensing data are provided for free;
- Several free processing tools exist in the public domain;
- Some commercial software is already in use at WRC;
- No specialist hardware is needed; and
- The requirement for advanced technical expertise is easily outsourced, if necessary.

In summary, a single hardware system and 71 days of effort by a range of staff is estimated to be sufficient to implement water quality monitoring by remote sensing and 10 days per month to operate and maintain it.

Synthesis and Conclusion

Earth observation satellites collect complete imagery of New Zealand every 2 – 16 days and the data are freely available to download. Potentially, all water bodies which have at least a 90 by 90 m area of open water can be resolved from space and algorithms exist to convert the satellite data to parameters related to water quality. This technology provides an opportunity for supplementary water quality monitoring at a greater frequency, and covering a greater number of locations, than is currently available for the Waikato region's lakes, large rivers and estuaries. This report was prepared to help WRC evaluate whether this opportunity is worthwhile pursuing through the implementation of a system for the routine monitoring of water quality using remote sensing. This chapter relates the technical information of this report into a decision framework to help managers make this evaluation.

The decision framework (Figure 28) is divided into three phases:

1. Initial scoping and investigation;
2. Planning; and
3. Implementation.

Each decision in the framework allows for compromises, e.g., by reconsidering the data requirements to improve feasibility, and suggests consideration of alternative monitoring methodologies to remote sensing, if necessary**.** Finally, the framework prescribes a long-term review process for formal re-evaluation of whether the system meets its operational goals should it be implemented.

The following paragraphs describe an example pathway through the decision framework. It is designed to illustrate how the information in this report can be used to inform the decision framework. It is not a detailed case study and should not form the basis of any conclusive decisions.

The initial scoping and investigation phase of the decision framework deals with the definition of the objective of the system in terms of parameters and regional domain. For example, the objective might be to contribute to the grading of Waikato lakes in terms of National Objective Framework (NOF) bands which requires the reporting of annual median values of water quality attributes. Remote sensing can provide water quality parameters of lakes, so the decision flow may proceed to "Determine data requirements". These data requirements may initially appear as follows:

- NOF attributes currently include total phosphorus, total nitrogen and chlorophyll *a*;
- All lakes larger than 1 ha should be monitored; and
- The NOF recommends sampling at monthly intervals (Burns *et al.* 2000; MfE 2015) for the calculation of annual median values.

The Landsat family of satellites provides an 18-year archive of remote sensing data, in addition to a large library of publications and mature data retrieval processes. Therefore, it may be desirable to use Landsat 8 for this routine monitoring objective. Matching the data requirements with the capability of Landsat 8 is addressed in the next step "Determine if available images and algorithms can meet the requirements of the question" and this report provides the following insights, in order of the bullet points above:

- Chlorophyll *a* is the only current NOF parameter which can be derived from remotely sensed data (see section *Observable Water Quality Constituents*); TN and TP cannot be derived from satellite observations;

- The accuracy of chlorophyll retrieval by Landsat 8 relative to *in situ* measurements has an r^2 = 0.68 (Table 4, Allan *et al.* 2015), a likely 95% prediction error of ±50%;
- Remote observations pertain to surface water concentrations only, but in many locations multiple pixels per lake allow spatial resolution;
- Landsat can observe open-water areas larger than 90 by 90 m (0.8 ha) (see section *Characteristics of Current Satellite Sensors*); and
- On average, Waikato's named lakes are observed six times per year (see section *Regional Context Analysis*). Note that
    - These images are unlikely to be evenly distributed throughout the year; and
    - Image frequency may be increased by using MODIS imagery for larger lakes and, in the future, by using upcoming satellite missions, such as Sentinel-2b.

If the above data characteristics are considered adequate, the planning stage may be entered and a system designed. System design includes decisions on workflows for downloading and processing the data, hardware and software choices and the level of automation, as discussed in section *Implementation Pathway*. The system design process will reveal the requirement for skills, personnel, software, hardware and algorithms. If these requirements can be met by existing resources or are within the available budget, the system may then enter the implementation stage. The section *Level of Effort* provides an order-of-magnitude estimate of the personnel resources required to build and operate a monitoring system.

Implementing the monitoring system and its operation should be dealt with according to process-control practices at the Waikato Regional Council. The framework allows for regression to the *Resource requirement* stage should the process control reveal shortcomings.

Conclusion

Remote sensing has the potential to gather water quality information for all water bodies large enough to be seen from space. However, the opportunities offered by this technology vary due to the visibility of water bodies and compounding influences that complicate the remote sensing signal. Currently, the science and methodology is more advanced for the observation of lakes than for rivers and estuaries, with a number of case studies of the region's lakes published. However, these studies also highlight the need to adapt remote sensing water quality algorithms to the region's lakes using *in situ* observations if high accuracy is to be achieved.

In large rivers, morphological constraints such as narrow widths and shallow water complicate the application of water quality algorithms. However, the operational principles for water quality retrieval in rivers are identical to those of lakes and in some cases, the optical signature may be more straightforward due to the predominance of single water quality attributes. There is potential to observe water quality in the Waikato and Waihou rivers using Landsat 8 and the Waipa and Piako rivers with higher-resolution satellites, e.g., Sentinel-2. Unfortunately, the lack of regional case studies means that this report can not predict the accuracy and yield of remotely sensed river water quality.

For estuaries, morphological constraints such as narrowness and shallow water also apply and are further complicated by marine forcing. Estimates of the visibility of the Waikato region's estuaries from space suggest remote sensing of water quality can only be applied to large estuaries and that the data yield is reduced by observations during low tide.

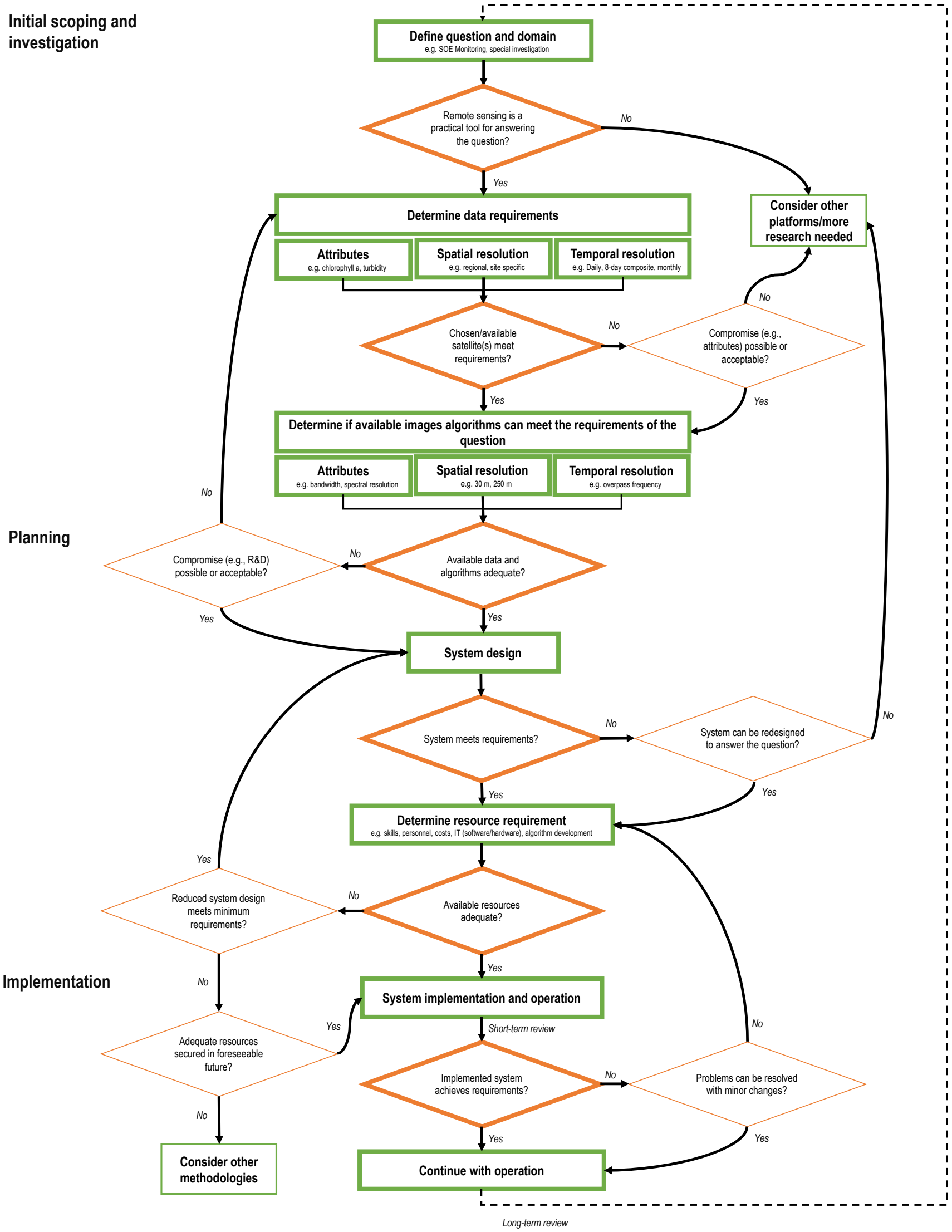

Figure 28: Decision framework with relates the technical information of this report to a management process to evaluate the feasibility of using remote sensing for water quality monitoring.

References

Alikas, K., Kangro, K., Randoja, R., Philipson, P., Asukull, E., Pisek, J., & Reinart, A. (2015). Satellite-based products for monitoring optically complex inland waters in support of EU Water Framework Directive. *International Journal of Remote Sensing, 36*(17), 4446-4468.

Allan, M. G. (2008). *Remote Sensing of Water Quality in Rotorua and Waikato Lakes.* MSc thesis, University of Waikato, Hamilton, New Zealand.

Allan, M. G. (2014). *Remote sensing, numerical modelling and ground truthing for analysis of lake water quality and temperature.* PhD thesis, University of Waikato, Hamilton, New Zealand.

Allan, M. G., Hamilton, D. P., Hicks, B., & Brabyn, L. (2015). Empirical and semi-analytical chlorophyll *a* algorithms for multi-temporal monitoring of New Zealand lakes using Landsat. *Environmental Monitoring and Assessment, 187*(6), 364.

Allan, M. G., Hamilton, D. P., Hicks, B. J., & Brabyn, L. (2011). Landsat remote sensing of chlorophyll *a* concentrations in central North Island lakes of New Zealand. *International Journal of Remote Sensing, 32*(7), 2037-2055.

Ashraf, S., Brabyn, L., & Hicks, B. (2008). *Evaluating remote sensing data classification techniques for mapping freshwater habitats: Trial application in the Tongariro River delta, Lake Taupo.* CBER Contract Report 87. Centre for Biodiversity and Ecology Research, University of Waikato, Hamilton, New Zealand. 33p.

Augusto-Silva, P. B., Ogashawara, I., Barbosa, C. C. F., de Carvalho, L. A. S., Jorge, D. S. F., Fornari, C. I., & Stech, J. L. (2014). Analysis of MERIS reflectance algorithms for estimating chlorophyll *a* concentration in a Brazilian reservoir. *Remote Sensing, 6*(12), 11689-11707.

Belzile, C., Vincent, W. F., Howard-Williams, C., Hawes, I., James, M. R., Kumagai, M., & Roesler, C. S. (2004). Relationships between spectral optical properties and optically active substances in a clear oligotrophic lake. *Water Resources Research, 40*(12).

Brezonik, P. L., Olmanson, L. G., Finlay, J. C., & Bauer, M. E. (2015). Factors affecting the measurement of CDOM by remote sensing of optically complex inland waters. *Remote Sensing of Environment, 157*, 199-215.

Burns, N., Bryers, G., & Bowman, E. (2000). *Protocol for Monitoring Trophic Levels of New Zealand Lakes and Reservoirs.* Ministry for the Environment, Wellington.

Campbell, G., Phinn, S. R., Dekker, A. G., & Brando, V. E. (2011). Remote sensing of water quality in an Australian tropical freshwater impoundment using matrix inversion and MERIS images. *Remote Sensing of Environment, 115*(9), 2402-2414.

Chang, N. B., Imen, S., & Vannah, B. (2015). Remote sensing for monitoring surface water quality status and ecosystem state in relation to the nutrient cycle: A 40-year perspective. *Critical Reviews in Environmental Science and Technology, 45*(2), 101-166.

Davies-Colley, R. J., & Vant, W. N. (1987). Absorption of light by yellow substance in fresh-water lakes. *Limnology and Oceanography, 32*(2), 416-425.

Dekker, A. G., & Hestir, E. L. (2012). *Evaluating the Feasibility of Systematic Inland Water Quality Monitoring with Satellite Remote Sensing.* CSIRO: Water for a Healthy Country National Research Flagship.

Dekker, A. G., Vos, R. J., & Peters, S. W. M. (2001). Comparison of remote sensing data, model results and in situ data for total suspended matter (TSM) in the southern Frisian lakes. *Science of the Total Environment, 268*(1-3), 197-214.

Dornhofer, K., & Oppelt, N. (2016). Remote sensing for lake research and monitoring - Recent advances. *Ecological Indicators, 64*, 105-122.

Doxaran, D., Froidefond, J. M., Castaing, P., & Babin, M. (2009). Dynamics of the turbidity maximum zone in a macrotidal estuary (the Gironde, France): Observations from field and MODIS satellite data. *Estuarine Coastal and Shelf Science, 81*(3), 321-332.

Gallegos, C. L., Davies-Colley, R. J., & Gall, M. (2008). Optical closure in lakes with contrasting extremes of reflectance. *Limnology and Oceanography, 53*(5), 2021-2034.

Gitelson, A. A., Dall'Olmo, G., Moses, W., Rundquist, D. C., Barrow, T., Fisher, T. R., Gurlin, D., & Holz, J. (2008). A simple semi-analytical model for remote estimation of chlorophyll *a* in turbid waters: Validation. *Remote Sensing of Environment, 112*(9), 3582-3593.

GLaSS. (2015). *Shallow lakes with low transparency due to resuspension.* Global Lakes Sentinel Services. http://www.glass-project.eu/downloads.

Gomez, J. A. D., Alonso, C. A., & Garcia, A. A. (2011). Remote sensing as a tool for monitoring water quality parameters for Mediterranean Lakes of European Union water framework directive (WFD) and as a system of surveillance of cyanobacterial harmful algae blooms (SCyanoHABs). *Environmental Monitoring and Assessment, 181*(1-4), 317-334.

Gordon, H. R., Brown, O. B., Evans, R. H., Brown, J. W., Smith, R. C., Baker, K. S., & Clark, D. K. (1988). A semianalytic radiance model of ocean color. *Journal of Geophysical Research-Atmospheres, 93*(D9), 10909-10924.

Hicks, B. J., Stichbury, G. A., Brabyn, L. K., Allan, M. G., & Ashraf, S. (2013). Hindcasting water clarity from Landsat satellite images of unmonitored shallow lakes in the Waikato region, New Zealand. *Environmental Monitoring and Assessment, 185*(9), 7245-7261.

Howard-Williams, C., & Vincent, W. F. (1984). Optical properties of New Zealand lakes 1. Attenuation, scattering, and a comparison between downwelling and scalar irradiances. *Archiv Fur Hydrobiologie, 99*(3), 318-330.

IOCCG. (2006). *Remote Sensing of Inherent Optical Properties: Fundamentals, Tests of Algorithms, and Applications.* IOCCG, Dartmouth, Canada.

Julian, J. P., Davies-Colley, R. J., Gallegos, C. L., & Tran, T. V. (2013). Optical water quality of inland waters: A landscape perspective. *Annals of the Association of American Geographers, 103*(2), 309-318.

Keith, D. J. (2014). Satellite remote sensing of chlorophyll *a* in support of nutrient management in the Neuse and Tar-Pamlico River (North Carolina) estuaries. *Remote Sensing of Environment, 153*, 61-78.

Kirk, J. T. O. (1994). *Light & Photosynthesis in Aquatic Ecosystems*. (2 ed.). Cambridge: Cambridge University Press.

Kloiber, S. N., Brezonik, P. L., Olmanson, L. G., & Bauer, M. E. (2002). A procedure for regional lake water clarity assessment using Landsat multispectral data. *Remote Sensing of Environment, 82*(1), 38-47.

Leathwick, J. W.-G. (2010). *Freshwater Ecosystems of New Zealand (FENZ) Geodatabase Version One - User Guide.* NIWA, Wellington.

Lee, C. M., Cable, M. L., Hook, S. J., Green, R. O., Ustin, S. L., Mandl, D. J., & Middleton, E. M. (2015). An introduction to the NASA Hyperspectral InfraRed Imager (HyspIRI) mission and preparatory activities. *Remote Sensing of Environment, 167*, 6-19.

Lyu, H., Li, X. J., Wang, Y. N., Jin, Q., Cao, K., Wang, Q., & Li, Y. M. (2015). Evaluation of chlorophyll *a* retrieval algorithms based on MERIS bands for optically varying eutrophic inland lakes. *Science of the Total Environment, 530*, 373-382.

Matthews, M. W. (2011). A current review of empirical procedures of remote sensing in inland and near-coastal transitional waters. *International Journal of Remote Sensing, 32*(21), 6855-6899.

MfE. (2015). *A Draft Guide to Attributes in Appendix 2 of the National Policy Statement for Freshwater Management 2014.* Ministry for the Environment, Wellington.

Mobley, C. D. (1994). *Light and Water: Radiative Transfer in Natural Waters*. San Diego: Academic Press.

Odermatt, D., Giardino, C., & Heege, T. (2010). Chlorophyll retrieval with MERIS Case-2-Regional in perialpine lakes. *Remote Sensing of Environment, 114*(3), 607-617.

Odermatt, D., Gitelson, A., Brando, V. E., & Schaepman, M. (2012). Review of constituent retrieval in optically deep and complex waters from satellite imagery. *Remote Sensing of Environment, 118*, 116-126.

Olmanson, L. G., Brezonik, P. L., & Bauer, M. E. (2011). Evaluation of medium to low resolution satellite imagery for regional lake water quality assessments. *Water Resources Research, 47*.

Olmanson, L. G., Brezonik, P. L., & Bauer, M. E. (2013). Airborne hyperspectral remote sensing to assess spatial distribution of water quality characteristics in large rivers: The Mississippi River and its tributaries in Minnesota. *Remote Sensing of Environment, 130*, 254-265.

Olmanson, L. G., Brezonik, P. L., & Bauer, M. E. (2015). Remote sensing for regional lake water quality assessment: Capabilities and limitations of current and upcoming satellite systems. In T. Younos & T. E. Parece (Eds.), *Advances in Watershed Science and Assessment* (pp. 111-140).

Palmer, S. C. J., Kutser, T., & Hunter, P. D. (2015). Remote sensing of inland waters: Challenges, progress and future directions. *Remote Sensing of Environment, 157*, 1-8.

Politi, E., Cutler, M. E. J., & Rowan, J. S. (2015). Evaluating the spatial transferability and temporal repeatability of remote-sensing-based lake water quality retrieval algorithms at the European scale: a meta-analysis approach. *International Journal of Remote Sensing, 36*(11), 2995-3023.

Roy, D. P., Wulder, M. A., Loveland, T. R., Woodcock, C. E., Allen, R. G., Anderson, M. C., Helder, D., Irons, J. R., Johnson, D. M., Kennedy, R., Scambos, T., Schaaf, C. B., Schott, J. R., Sheng, Y., Vermote, E. F., Belward, A. S., Bindschadler, R., Cohen, W. B., Gao, F., Hipple, J. D., Hostert, P., Huntington, J., Justice, C. O., Kilic, A., Kovalskyy, V., Lee, Z. P., Lymbumer, L., Masek, J. G., McCorkel, J., Shuai, Y., Trezza, R., Vogelmann, J., Wynne, R. H., & Zhu, Z. (2014). Landsat-8: Science and product vision for terrestrial global change research. *Remote Sensing of Environment, 145*, 154-172.

Rudorff, C. M., Novo, E. M. L. M., & Galvao, L. S. (2006). Spectral mixture analysis for water quality assessment over the Amazon floodplain using Hyperion/EO-1 Images. *Revista Ambi-Agua, 1*(2), 65-79.

Schalles, J. F., & Yacobi, Y. Z. (2000). Remote detection and seasonal patterns of phycocyanin, carotenoid and chlorophyll pigments in eutrophic waters. *Archives fur Hydrobiologia - Special Issues Advancements in Limnology, 55*, 153-168.

Scholes, P. (2009). *Rotorua Lakes Water Quality Report.* Environment Bay of Plenty, Whakatane.

Schwarz, A.-M. (1996). *The Role of Light in Determining the Maximum Depth Limits of Characean Algae in New Zealand Lakes.* PhD thesis, University of Auckland, Auckland, New Zealand.

Schwarz, J. N., Pinkerton, M. H., Wood, S., & Zeldis, J. (2010). *Remote Sensing of River Plumes in the Canterbury Bight. Stage II: final report.* NIWA, Christchurch.

Seyhan, E., & Dekker, A. (1986). Application of remote sensing techniques for water quality monitoring. *Hydrobiological Bulletin, 20*(1), 41-50.

Shen, F., Zhou, Y. X., Li, D. J., Zhu, W. J., & Salama, M. S. (2010). Medium resolution imaging spectrometer (MERIS) estimation of chlorophyll *a* concentration in the turbid sediment-laden waters of the Changjiang (Yangtze) Estuary. *International Journal of Remote Sensing, 31*(17-18), 4635-4650.

Simis, S. G. H., Peters, S. W. M., & Gons, H. J. (2005). Remote sensing of the cyanobacterial pigment phycocyanin in turbid inland water. *Limnology and Oceanography, 50*(1), 237-245.

Tan, J., Cherkauer, K. A., & Chaubey, I. (2015). Using hyperspectral data to quantify water-quality parameters in the Wabash River and its tributaries, Indiana. *International Journal of Remote Sensing, 36*(21), 5466-5484.

Teodoro, A. C., Marcal, A. R. S., & Gomez, F. V. (2004) Evaluation of total suspended matter concentration in wave breaking zone using multispectral satellite images. J. Charles R. Bostater & R. Santoleri (Eds.), *Remote Sensing of the Ocean and Sea Ice* (Vol. 5569). Bellingham, WA: SPIE.

Torgersen, C. E., Faux, R. N., McIntosh, B. A., Poage, N. J., & Norton, D. J. (2001). Airborne thermal remote sensing for water temperature assessment in rivers and streams. *Remote Sensing of Environment, 76*(3), 386-398.

Tyler, A. N., Svab, E., Preston, T., Presing, M., & Kovacs, W. A. (2006). Remote sensing of the water quality of shallow lakes: A mixture modelling approach to quantifying phytoplankton in water characterized by high-suspended sediment. *International Journal of Remote Sensing, 27*(8), 1521-1537.

Vant, B. (2015). *Visual Clarity of the Waikato and Waipa Rivers.* Technical Report 2015/13R. Waikato Regional Council, Hamilton, New Zealand. 25p.

Vant, W. N., & Davies-Colley, R. J. (1984). Factors affecting clarity of New-Zealand lakes. *New Zealand Journal of Marine and Freshwater Research, 18*(3), 367-377.

Vermote, E. F., Tanre, D., Deuze, J. L., Herman, M., & Morcrette, J. J. (1997). Second simulation of the satellite signal in the solar spectrum, 6S: An overview. *IEEE Transactions on Geoscience and Remote Sensing, 35*(3), 675-686.

Wang, B., Axe, L., Michalopoulou, Z. H., Riman, R. E., Tan, M. C., & Wei, L. P. (2016). Light absorption properties of the New York/New Jersey Harbor Estuary. *Hydrobiologia, 766*(1), 173-188.

Zhang, Y. C., Ma, R. H., Duan, H. T., Loiselle, S., & Xu, J. D. (2014). A spectral decomposition algorithm for estimating chlorophyll *a* concentrations in Lake Taihu, China. *Remote Sensing, 6*(6), 5090-5106.

Zhao, D. H., Cai, Y., Jiang, H., Xu, D. L., Zhang, W. G., & An, S. Q. (2011). Estimation of water clarity in Taihu Lake and surrounding rivers using Landsat imagery. *Advances in Water Resources, 34*(2), 165-173.

Zhao, D. H., Lv, M. T., Zou, X. X., Wang, P. H., Yang, T. W., & An, S. Q. (2014). What is the minimum river width for the estimation of water clarity using medium-resolution remote sensing images? *Water Resources Research, 50*(5), 3764-3775.

Appendix A: Retrieval Algorithms

Chlorophyll *a*

Type	Algorithm	Equation	Sensor	Chl a range (µg/L)	r^2	RMSE (ug/L)	Original reference	Reference used	Location
Empirical	Regression- B1/B3 Ratio.	*(Summer) Ln(Chl a) = 14.14-5.06(B1/B3) and (Spring) Ln(Chl a) = 24.25-9.28(B1/B3)*	Landsat7 ETM+		0.83 (spring) and 0.91 (summer)			Allan (2008)	Rotorua Lakes
Empirical	Linear Spectral Unmixing	*Chl a = 5.73+2.53 x (Chl endmember percentage)*	Landsat7 ETM+	0 - 120	0.84		Tyler et al. (2006)	Allan (2008)	Waikato Lakes
Semi-Analytical	Bio-optical modelling	*Chl a= 0.3647e $^{44.13}$ B3 and Chl a = 0.00017 e $^{352.95}$*	Landsat 7 ETM+		0.58		Dekker et al. (1997)	Allan (2014)	Rotorua lakes
Empirical	Symbolic Regression, B1/B3 Ratio with B2.	*Chl a = (4618 B2 – 20)/((B1/B3) ^{2})*	Landsat 7 ETM+		0.68	10.32		Allan (2014)	Rotorua lakes
Empirical	Regression B1/B3 Ratio	*Ln(Chl a) = B1/B3 ratio*	Landsat 7 ETM+	0.8-136	0.8	15.5		Allan et al. (2011)	Rotorua Lakes, Lake Taupo
Semi Analytical	Bio-optical modelling	$r_{rs}(\lambda) = \sum_{i=1}^{2} li\left[\frac{b_b(\lambda)}{b_b(\lambda)+a(\lambda)}\right]^{l}$	MODIS	0-3	0.71	0.522	Maritorena et al. 2002	Allan (2014)	Lake Taupo
Empirical	Regression- 2 Band ratios	*705/670* *705/620* *705/592nm*	Hyperspectral	8-830	0.75-0.93	ln0.19-0.43 (~21%)		Olmanson et al. (2013)	Minnesota, Mississippi, St. Croix Rivers
Semi-Analytical	Bio-optical modelling	*Chl a calibrated = 1.3671 x (MERIS chl a values) −11.283*	MERIS	0-130	0.84-0.87	7.6	MERIS case 2 coastal water algorithm	Keith et al. (2014)	Neuse and Tar-Pamlico Estuaries, USA
Empirical + Semi-Analytical	Regression- 2 Band	*Chl a=5.931 (708/664) $^{5.934}$*	MERIS	0 - 250	0.964E	9.8%E		Matthews et al. (2010)	Zeekoevlei (Hippo Lake), South Africa
Semi-Analytical	Synthetic Chlorophyll Index (SCI)	*Chl a (mg/m3) = 179378x2 + 92.934x + 0.2736, where x = SCI (in sr-1)*	MERIS	0-31 (with TSS up to 543)	0.86	2.87		Shen et al. (2010)	Changjiang (Yangtze) Estuary, China

Total suspended solids

Type	Algorithm	Equation	Sensor	TSS range (mg/L)	r^2	RMSE (mg/L)	Original reference	References used	Locations Used
Empirical	Regression, Band 3	*TSS= 0.0388 + 0.0008(B3)*	Landsat 7 ETM+	0 - 350	0.98			Allan (2008)	Waikato Lakes
Empirical	Regression, Band 4	*TSS=-52.8+1449.4xB4*	Landsat 7 ETM+	2 - 344	0.94	21.3		Hicks et al. (2013)	Waikato lakes
Empirical	Regression Band 1	$C_{TR} = exp(2.51\ ln(r_{rs}(B1)) + 12.26)$ *(rrs=subsurface remote sensing reflectance)*	MODIS	50-400TN	0.73	58.9		Allan (2014)	Lake Ellesmere
Semi-analytical	Bio-optical modelling	$C_{TR} = 20.57e^{37.46rrs}$ *(rrs=subsurface remote sensing reflectance)*	MODIS	50-400TN	0.72	58.4		Allan (2014)	Lake Ellesmere
Semi-analytical	Bio-optical modelling	$SS = 1159.6\ r_{rs}(B1) - 0.48$ *(rrs=subsurface remote sensing reflectance)*	MODIS	SS	0.77	58.9	Maritorena et al. 2002	Allan (2014)	Lake Taupo
Empirical	Regression- 1 Band ratio	*Regression using 705nm band*	Hyperspectral	4 to 95	0.77-0.93	ln0.25-0.32		Olmanson et al. 2013	Minnesota, Mississippi, St. Croix Rivers
Empirical	Regression, Band 1 and 2 ratio	*SPM = 12.996 x exp(R21/0.189) where R21 =R(B2)/R(B1)*	MODIS	SPM 0-3500	0.76-0.82		Doxaran et al. 2002	Doxaran et al. (2009)	Gironde Estuary, France
Empirical + Semi-Analytical	Regression- 3 Band	*TSS=–84.428 + 218.329 (708/(559+664))*	MERIS	0.03-50	0.76	14.10%		Matthews et al. (2010)	Zeekoevlei (Hippo Lake), South Africa
Empirical	Regression, Band 4	*ln(SSC) = 3·18236 * ln(ρw,4) – 1·40060 (pw,4=water reflectance at band 4)*	Landsat 7 ETM+	22-2610	0.86	46		Wang et al. (2009)	Yangtze River, China

Secchi depth

Type	Algorithm	Equation	Sensor	SD range (m)	r^2	RMSE (m)	Original reference	References used	Where used
Empirical	Regression- B1/B3 ratio	*Ln(SD) = -2.03+2.75xLn(B1:B3)-0.61xLn(B1)*	Landsat 7 ETM+	0-3	0.67	0.33		Hicks et al. (2013)	Waikato lakes (34 lakes)
Empirical	Regresson- B1/B3 ratio	*Ln(SD) = a(TM1/TM3) + b(TM1) + c*	Landsat 4, 5 TM, and 7 ETM+	0.1-14.6 (modelled)	0.71-0.96		Kloiber et al. (2002)	Olmanson et al. (2008)	Minnesota Lakes
Empirical	Regression- B1/B3 ratio	*Ln SD = -5.2163 + 2.7753*(B1/B3)*	Landsat 7 ETM+	Ln(-0.25 - 3)	0.83		Kloiber et al. (2002)	Allan (2008)	Rotorua Lakes
Empirical	Regression- B1/B3 ratio	*Ln(SDD)=a x Rblue/Rred + b x Rblue + c*	HJ-1A (Similar spectral and spatial resolution to Landsat but temporal resolution of 2 days)	Ln(-3 - 1)	0.94	0.35	Kloiber et al. (2002)	Zhao et al. (2014)	Xitiaoxi River, China
Empirical + Semi-Analytical	Regression - 2 Band	$Z_{SD}=79.469-30.596\ (708/664)$	MERIS		0.801	8.00%		Matthews et al. (2010)	Zeekoevlei (Hippo Lake), South Africa

Turbidity

Type	Algorithm	Equation	Sensor	Turbidity range (NTU)	r^2	RMSE (NTU)	Original reference	References used	Where used
Empirical	Least Squares Regression, Band 4	*Turb=63.7+ 1,587.8xB4*	Landsat 7 ETM+	75-275	0.92	25.9		Hicks et al. (2013)	Waikato lakes (34 lakes)
Empirical	Regression- 1 band	*Regression using 705nm band*	Hyperspectral	2 to 50	0.77-0.92	ln0.23-0.29		Olmanson et al. (2013)	Minnesota, Mississippi, St. Croix Rivers

Coloured dissolved organic matter

Type	Algorithm	Equation	Sensor	CDOM range (m)	r^2	RMSE	Original reference	References used	Where used
Empirical + Semi-Analytical	Gitelson	*aCDOM=25.137 −31.806 ((442−(708/664)−509)/(442+(708/664)+509).)*	MERIS	1.5 - 4	0.751	13%	Gitelson et al. (1993)	Matthews et al. (2010)	Zeekoevlei (Hippo Lake), South Africa

Appendix B: Visibility Statistics for Waikato Lakes

Lakes greater than 1 ha in the Waikato region with characteristics relevant for remote sensing. The lakes are sorted by Land Information New Zealand (LINZ) ID. The maximum number of pixels observed show the observable lake size specific to the sensor used, i.e., 30 m in this case. The total number of successful retrievals (images with at least one pixel in a given lake) indicates the number of observations over the last 16 years. The number of average annual retrievals is the number of partly or entirely cloud free images of the lake divided by the number of years of Landsat 7 and 8 operations (16.25 years at the time of this analysis).

				After Buffer Area (ha)						
LINZ ID	Name	Area (ha)	Isometric inequality	10 m	30 m	60 m	Average number of pixels*	Max. number of pixels*	Number of successful retrievals*	Average annual retrievals*
8265		2.1	0.30	1.2	0.0	-	1.0	1	10	0.6
8266		1.8	0.68	1.3	0.4	-	3.6	4	92	5.7
8302		1.3	0.10	0.1	-	-				
11080		1.3	0.89	0.9	0.3	-				
11084	Lake Orotu	4.7	0.31	3.4	1.4	0.1	12.5	18	74	4.6
11096		1.1	0.25	0.4	-	-				
12585		1.6	0.59	1.0	0.2	-	2.9	4	84	5.2
12588		1.2	0.75	0.8	0.2	-	2.4	4	69	4.2
12591	Lake Parangi	12.0	0.26	9.6	5.4	0.9	53.3	67	98	6.0
12592		1.4	0.54	0.9	0.2	-	2.5	3	90	5.5
12746		1.4	0.32	0.7	0.0	-				
12778		1.8	0.80	1.3	0.5	-				
12780		1.1	0.67	0.7	0.1	-				
12820		1.2	0.19	0.4	-	-				
12830	Lake Harihari	18.4	0.18	14.9	8.5	2.0	84.1	104	107	6.6
12831	Lake Rototapu	2.0	0.90	1.5	0.7	0.0	7.1	8	93	5.7
12872	Lake Rotoroa	22.6	0.43	20.1	15.5	9.5	158.6	181	98	6.0
12873	Lake Numiti	15.8	0.54	13.9	10.6	6.3	102.8	121	97	6.0
12876	Lake Taharoa	216.5	0.31	207.2	189.6	164.7	1649.9	2144	109	6.7
12984		1.0	0.32	0.4	-	-				

				After Buffer Area (ha)						
LINZ ID	Name	Area (ha)	Isometric inequality	10 m	30 m	60 m	Average number of pixels*	Max. number of pixels*	Number of successful retrievals*	Average annual retrievals*
12988		1.1	0.74	0.7	0.1	-				
13017		2.0	0.45	1.3	0.2	-				
13147		3.0	0.34	2.0	0.4	-	4.0	4	1	0.1
13148	Lake Kuratau	103.1	0.24	95.8	81.8	62.7	694.2	863	94	5.8
13149		6.6	0.48	5.4	3.0	0.9	7.9	27	75	4.6
13222		3.7	0.07	1.4	0.1	-				
13268		1.0	0.45	0.5	-	-				
13276		15.2	0.08	10.5	4.1	0.8	39.7	51	88	5.4
13277	Lake Hinemaiaia	21.8	0.29	18.8	13.0	6.2	85.5	107	90	5.5
13278	Lake Rotongaio	34.2	0.51	31.4	25.8	18.2	262.6	295	93	5.7
13284	Pukuriri Lagoon	3.6	0.69	2.9	1.5	0.2	9.9	20	28	1.7
13687		1.5	0.74	1.0	0.3	-	2.7	3	7	0.4
13736	Lake Rotokotuku	1.2	0.93	0.8	0.3	-	3.8	4	10	0.6
13764		3.7	0.60	2.9	1.4	0.2	12.5	18	11	0.7
13768		1.2	0.59	0.8	0.0	-	1.0	1	50	3.1
13832		1.1	0.43	0.6	-	-				
13833		1.5	0.30	0.8	0.0	-				
13837		1.6	0.32	0.8	0.1	-	1.5	2	39	2.4
13857	Lake Waipapa	116.6	0.09	103.5	77.7	41.6	617.9	900	204	12.6
13863		1.2	0.60	0.7	0.1	-	1.0	1	70	4.3
13873	Lake Whakamaru	539.0	0.05	503.7	434.6	336.4	3680.4	4886	112	6.9
13876	Lake Maraetai	400.6	0.05	367.7	308.4	240.0	1841.4	3480	205	12.6
13877	Lake Maraetai	18.0	0.09	12.9	5.5	0.7	52.2	62	88	5.4
13882		1.4	0.43	0.8	0.2	-	2.3	3	133	8.2
13883		7.9	0.28	6.0	3.0	0.4	4.6	29	104	6.4
13886		2.7	0.59	2.0	1.0	0.1	3.6	11	30	1.8

				After Buffer Area (ha)						
LINZ ID	Name	Area (ha)	Isometric inequality	10 m	30 m	60 m	Average number of pixels*	Max. number of pixels*	Number of successful retrievals*	Average annual retrievals*
13904		2.2	0.58	1.6	0.5	-	5.5	7	70	4.3
13907		1.5	0.34	0.8	0.0	-				
13909	Lake Aratiatia	45.1	0.09	37.0	21.3	5.8	197.3	255	90	5.5
13915	Lake Rotokawa	65.5	0.78	62.3	56.1	47.2	498.5	630	87	5.4
13930		1.4	0.22	0.6	-	-				
13941		1.3	0.12	0.3	-	-				
13950		3.9	0.25	2.5	0.7	-	12.1	14	66	4.1
13957	Lake Atiamuri	203.5	0.03	176.4	125.0	66.6	754.1	1417	214	13.2
13970	Lake Ohakuri	940.2	0.02	860.2	714.0	538.5	5774.2	8022	104	6.4
14011		1.1	0.56	0.7	0.0	-				
14071	Lake Tutaeinanga	3.1	0.51	2.3	1.0	0.1	9.8	11	87	5.4
14082	Lake Ngakoro	7.0	0.47	5.6	3.2	0.6	34.1	37	70	4.3
14092		1.2	0.71	0.8	0.1	-	1.0	1	19	1.2
14121		1.6	0.83	1.2	0.4	-	5.1	7	96	5.9
14146		1.6	0.65	1.1	0.3	-	2.1	4	70	4.3
14150		1.1	0.43	0.5	0.0	-				
14157	Lake Whangioterangi (Echo Lake)	3.6	0.32	2.4	0.5	-	5.5	6	70	4.3
14179	Lake Ngapouri	21.3	0.52	19.1	15.0	10.1	144.8	173	88	5.4
14204	Ngakoro	1.3	0.70	0.9	0.2	-	1.6	2	17	1.0
14205	Rotowhero (Green Lake)	2.6	0.69	1.9	0.9	0.0	9.4	11	77	4.7
14208	Lake Ngahewa	8.4	0.53	7.1	4.5	1.7	47.7	54	81	5.0
14334		1.7	0.91	1.2	0.5	0.0	4.7	5	85	5.2
14343		2.7	0.45	1.9	0.6	-	6.4	9	90	5.5

				After Buffer Area (ha)						
LINZ ID	Name	Area (ha)	Isometric inequality	10 m	30 m	60 m	Average number of pixels*	Max. number of pixels*	Number of successful retrievals*	Average annual retrievals*
14405	Lake Mangakaware	14.6	0.32	12.2	8.0	3.6	73.8	90	111	6.8
14406	Lake Ngaroto	91.8	0.46	86.8	77.0	63.1	682.8	865	114	7.0
14407	Lake Ngarotoiti	3.3	0.51	2.4	0.9	0.0	10.0	12	97	6.0
14408	Lake Ruatuna	11.8	0.63	10.3	7.6	4.2	77.7	89	112	6.9
14418	Lake Mangahia	7.9	0.52	6.6	4.3	1.9	42.5	47	99	6.1
14420		2.3	0.85	1.7	0.9	0.1	8.1	9	99	6.1
14422	Lake Maratoto	17.9	0.49	15.7	11.7	6.2	108.3	135	112	6.9
14423	Lake Rotopataka	1.1	0.36	0.5	0.0	-				
14424	Lake Serpentine E	1.4	0.67	0.9	0.2	-	2.6	3	97	6.0
14425	Lake Serpentine W	4.3	0.15	2.5	0.4	-	5.7	8	101	6.2
14426	Lake Serpentine N	4.6	0.84	3.8	2.4	0.8	24.1	29	107	6.6
14427		6.1	0.51	4.9	2.8	0.6	27.7	33	108	6.6
14428	Lake Rotomanuka	13.6	0.74	12.2	9.4	5.9	90.9	104	108	6.6
14430		1.3	0.59	0.8	0.2	-	1.0	1	127	7.8
14436		2.0	0.59	1.4	0.4	-	2.8	4	135	8.3
14450		1.6	0.55	1.0	0.2	-	2.0	3	3	0.2
14464		3.4	0.68	2.6	1.4	0.2	13.2	18	149	9.2
14472		1.7	0.54	1.1	0.1	-	1.0	1	1	0.1
14541	Lake Rotongata	6.1	0.46	4.8	2.5	0.7	21.6	29	172	10.6
14542		1.6	0.66	1.1	0.2	-	1.8	3	123	7.6
14546	Lake Arapuni	828.2	0.06	785.0	700.4	584.8	5773.1	7766	221	13.6
14559		1.7	0.63	1.2	0.3	-	2.6	3	139	8.6

				After Buffer Area (ha)						
LINZ ID	Name	Area (ha)	Isometric inequality	10 m	30 m	60 m	Average number of pixels*	Max. number of pixels*	Number of successful retrievals*	Average annual retrievals*
14562		2.6	0.20	1.4	0.1	-	1.8	2	5	0.3
14573		1.6	0.39	0.9	0.0	-				
14586	Lake Moananui	7.9	0.19	5.7	2.1	0.1	15.4	24	166	10.2
14587		1.0	0.64	0.6	0.1	-	1.0	1	15	0.9
14631		2.3	0.43	1.6	0.2	-	3.5	4	138	8.5
14657		1.7	0.46	1.1	0.3	-	2.0	3	2	0.1
14661		1.2	0.20	0.4	-	-				
14678		1.5	0.22	0.6	-	-				
14680	Lake Karapiro	770.3	0.02	696.2	559.8	391.5	3194.0	6296	221	13.6
14718		9.1	0.13	6.2	2.0	0.2	18.1	22	102	6.3
14720	Lake te ku utu	4.6	0.66	3.7	2.1	0.4	20.4	24	96	5.9
14723		1.1	0.84	0.7	0.2	-	3.3	4	80	4.9
14772		1.2	0.87	0.8	0.3	-	3.0	3	83	5.1
14783		1.0	0.79	0.6	0.1	-	1.0	1	1	0.1
14792		1.0	0.45	0.6	0.0	-				
14793		1.3	0.70	0.9	0.2	-	3.2	4	83	5.1
14802		1.7	0.39	1.0	0.2	-	2.2	3	77	4.7
14820		1.1	0.32	0.5	0.0	-				
14838		1.0	0.20	0.3	-	-				
14852		1.3	0.35	0.7	0.0	-				
14860	Hamareha Lakes	4.4	0.39	3.2	1.3	0.1	1.9	16	28	1.7
14866		1.4	0.64	0.9	0.2	-	1.8	3	61	3.8
14885		1.0	0.24	0.3	-	-				
14888	Lake Okoroire	3.5	0.32	2.3	0.7	-	4.4	8	62	3.8
14897		1.9	0.16	0.8	-	-				
14902		1.5	0.30	0.8	0.0	-	1.0	1	62	3.8
14904		1.4	0.22	0.5	0.0	-				

				After Buffer Area (ha)						
LINZ ID	Name	Area (ha)	Isometric inequality	10 m	30 m	60 m	Average number of pixels*	Max. number of pixels*	Number of successful retrievals*	Average annual retrievals*
14917		1.0	0.46	0.6	0.0	-				
14922		1.2	0.34	0.6	0.0	-				
14998		2.2	0.13	0.8	-	-				
14999		2.5	0.52	1.7	0.5	-	1.6	6	48	3.0
15004		2.3	0.44	1.5	0.5	-	4.8	6	84	5.2
15005	Lake Pataka	4.8	0.68	3.9	2.4	0.8	20.9	30	89	5.5
15007	Lake Koromatua	4.9	0.76	4.1	2.5	0.7	24.8	29	91	5.6
15008	Lake Cameron	4.7	0.60	3.8	2.0	0.3	17.5	22	102	6.3
15009		1.9	0.55	1.3	0.3	-	3.3	5	89	5.5
15013	Lake Rotokauri	38.0	0.52	35.0	29.3	21.4	220.7	340	104	6.4
15020	Horseshoe Lake	3.4	0.46	2.5	1.0	0.1	10.5	14	70	4.3
15022	Lake Rotoroa	52.0	0.48	48.3	41.3	31.4	291.7	467	113	7.0
15025		1.0	0.61	0.6	0.0	-				
15029		1.1	0.44	0.6	0.0	-	1.0	1	28	1.7
15032	Lake Pikopiko	4.7	0.67	3.8	2.2	0.4	25.0	27	97	6.0
15033	Lake Hotoananga	15.6	0.87	14.2	11.4	7.8	98.1	119	100	6.2
15034	Lake Areare	30.4	0.50	27.7	22.5	15.2	220.3	259	107	6.6
15035	Lake A	2.8	0.94	2.2	1.3	0.3	13.7	17	87	5.4
15036	Lake E	3.1	0.39	2.1	0.7	-	7.8	9	96	5.9
15037	Lake D	27.2	0.36	24.2	18.4	11.4	175.4	210	112	6.9
15038	Lake B	9.7	0.57	8.3	5.7	2.9	58.3	68	104	6.4
15039	Lake C	1.6	0.38	0.9	0.0	-	1.0	1	91	5.6
15060		1.0	0.68	0.6	0.0	-	1.0	1	75	4.6
15061		3.5	0.47	2.6	1.3	0.2	15.5	17	89	5.5
15106		1.5	0.71	1.0	0.3	-	2.6	4	5	0.3
15112		1.4	0.26	0.6	0.0	-				

				After Buffer Area (ha)						
LINZ ID	Name	Area (ha)	Isometric inequality	10 m	30 m	60 m	Average number of pixels*	Max. number of pixels*	Number of successful retrievals*	Average annual retrievals*
15122		3.0	0.86	2.4	1.3	0.2	11.1	14	90	5.5
15140		1.8	0.31	1.0	0.0	-	1.0	1	63	3.9
15141		1.4	0.33	0.7	0.0	-				
15163		2.0	0.56	1.4	0.3	-	3.7	5	84	5.2
15165		1.1	0.68	0.7	0.2	-	1.3	3	32	2.0
15170		1.0	0.78	0.7	0.1	-	1.1	2	51	3.1
15176		7.0	0.35	5.5	3.0	0.7	25.1	34	91	5.6
15240		1.2	0.34	0.6	0.0	-				
15257		1.4	0.69	1.0	0.2	-	2.5	3	77	4.7
15270		1.0	0.79	0.6	0.1	-	1.2	2	10	0.6
15339		1.6	0.20	0.7	-	-				
15341		1.6	0.68	1.1	0.3	-	2.2	4	6	0.4
15396		1.2	0.17	0.3	-	-				
15634		1.4	0.34	0.7	-	-				
15651		2.4	0.15	1.1	0.0	-				
20846	Lower Tama	21.1	0.92	19.4	16.3	12.1	128.0	187	79	4.9
20851	Upper Tama	31.4	0.59	28.8	24.0	17.4	202.2	276	75	4.6
20852		1.1	0.89	0.7	0.2	-	2.8	4	4	0.2
20853		3.3	0.61	2.5	1.2	0.0	8.3	16	25	1.5
20857	Blue Lake	17.2	0.94	15.7	12.9	9.3	91.0	148	63	3.9
20858	Beggs Pool	1.1	0.30	0.5	0.0	-				
21356		5.3	0.35	3.9	1.5	0.0	7.6	20	27	1.7
21367	Lake Rotoaira	1,567.8	0.41	1,545.9	1,502.8	1,440.3	13836.3	16672	97	6.0
21370	Lake Rotopounamu	85.1	0.73	81.3	73.9	63.3	717.3	830	90	5.5
21371		1.3	0.49	0.8	0.0	-				

				After Buffer Area (ha)						
LINZ ID	Name	Area (ha)	Isometric inequality	10 m	30 m	60 m	Average number of pixels*	Max. number of pixels*	Number of successful retrievals*	Average annual retrievals*
21383	Lake Otamangakau	156.4	0.07	140.2	112.3	84.7	1037.8	1276	94	5.8
21384	Lake Rotokura	2.7	0.78	2.1	1.0	0.1	8.0	14	42	2.6
21422		1.3	0.20	0.4	-	-				
34200		1.6	0.38	0.9	0.1	-	1.0	1	31	1.9
41314	Lake Waahi	444.7	0.26	430.1	401.9	362.7	3417.3	4453	117	7.2
41327		1.0	0.57	0.6	0.1	-	1.3	2	81	5.0
41328		3.5	0.67	2.7	1.4	0.2	2.6	17	67	4.1
41335		1.4	0.44	0.8	0.1	-	2.1	3	35	2.2
41470		4.5	0.82	3.7	2.3	0.8	25.1	27	95	5.8
41471		2.8	0.47	2.0	0.8	0.0	9.1	12	89	5.5
41472		1.7	0.69	1.2	0.4	-	6.6	7	86	5.3
45975		1.5	0.03	0.0	-	-				
45979		1.1	0.75	0.7	0.2	-				
45980		2.4	0.13	1.0	-	-				
49076		2.2	0.53	1.5	0.4	-	4.3	6	91	5.6
49089		2.7	0.81	2.1	1.1	0.1	14.0	14	1	0.1
49090	Lake Ohinewai	17.1	0.59	15.2	11.7	6.9	112.9	135	98	6.0
49091	Lake Rotokawau	14.8	0.41	12.7	8.7	3.8	85.4	105	107	6.6
49147		1.0	0.49	0.6	-	-				
49148		3.6	0.16	2.0	0.6	-	5.6	7	78	4.8
49151		1.5	0.53	1.0	0.1	-	1.0	1	15	0.9
49152		2.1	0.57	1.5	0.5	-	4.0	4	1	0.1
49156		3.5	0.82	2.8	1.6	0.4	15.2	20	66	4.1
49169		18.5	0.47	16.3	12.4	8.1	108.7	141	99	6.1
49176	Lake Okowhao	7.5	0.57	6.2	4.1	1.7	43.8	49	98	6.0
49180	Lake Whangape	1,078.9	0.15	1,049.1	990.9	906.9	7251.5	10771	127	7.8

				After Buffer Area (ha)						
LINZ ID	Name	Area (ha)	Isometric inequality	10 m	30 m	60 m	Average number of pixels*	Max. number of pixels*	Number of successful retrievals*	Average annual retrievals*
49181		1.1	0.79	0.7	0.2	-	1.4	3	16	1.0
49186	Lake Rotongaro	283.9	0.41	274.6	256.3	229.6	2104.0	2878	120	7.4
49187	Lake Rotongaroiti	44.5	0.34	40.5	33.7	24.3	290.4	389	111	6.8
49189		3.2	0.39	2.3	0.8	-	4.3	11	59	3.6
49194		2.1	0.77	1.6	0.7	0.0	10.1	11	90	5.5
49196	Lake Waiwhata	1.3	0.53	0.8	0.1	-	1.0	1	78	4.8
49198		1.8	0.43	1.1	0.2	-	1.0	1	5	0.3
49199		2.1	0.70	1.5	0.6	0.0	7.4	9	88	5.4
49200	Lake Hakanoa	56.4	0.63	53.1	46.9	38.5	415.7	530	107	6.6
49228		2.7	0.51	1.9	0.6	-	3.3	7	75	4.6
49238		3.6	0.37	2.5	0.7	-	6.0	7	93	5.7
49239	Lake Kimihia	48.8	0.51	45.4	38.7	29.3	285.4	427	115	7.1
49254		3.1	0.49	2.2	0.9	-	2.9	7	8	0.5
49257		1.7	0.31	0.9	0.1	-	1.5	2	2	0.1
49258		1.4	0.60	0.9	0.1	-	3.5	4	2	0.1
49259		1.7	0.44	1.1	0.2	-	1.3	2	3	0.2
49291	Lake Otamatearoa	4.9	0.86	4.1	2.6	1.0	23.8	28	90	5.5
49295	Lake Puketi	5.9	0.64	4.9	3.0	0.7	26.4	36	91	5.6
50254		3.6	0.65	2.8	1.4	0.0	11.1	17	82	5.0
50255		1.2	0.61	0.7	0.1	-	1.2	2	11	0.7
50462		1.5	0.28	0.7	0.0	-				
50464		4.7	0.61	3.8	2.4	0.9	23.8	30	92	5.7
50466		2.1	0.56	1.5	0.5	-	5.8	9	87	5.4
50469		1.1	0.23	0.4	-	-				
50470	Lake Kopuera	44.9	0.58	41.8	35.9	27.7	312.4	408	106	6.5

				After Buffer Area (ha)						
LINZ ID	Name	Area (ha)	Isometric inequality	10 m	30 m	60 m	Average number of pixels*	Max. number of pixels*	Number of successful retrievals*	Average annual retrievals*
50493		1.3	0.29	0.6	-	-				
50768		1.2	0.79	0.8	0.2	-	1.1	2	9	0.6
50781		3.1	0.53	2.3	0.9	0.0	5.0	7	79	4.9
50782	Lake Waikare	3,438.7	0.24	3,396.2	3,312.0	3,187.2	25845.2	36766	127	7.8
50783		1.9	0.47	1.2	0.3	-	1.2	2	60	3.7
50786		1.1	0.12	0.1	-	-				
51150		1.4	0.50	0.8	0.1	-	1.0	1	2	0.1
51282		1.0	0.81	0.7	0.1	-	2.8	4	78	4.8
51368	Mangatangi Reservoir	154.5	0.03	129.2	86.6	45.8	604.9	1046	108	6.6
51371	Upper Mangatawhiri Reservoir	123.9	0.09	111.2	89.6	64.5	615.3	1023	108	6.6
51380		11.1	0.31	9.1	5.4	1.9	37.4	56	99	6.1
51382		2.5	0.27	1.5	0.3	-	1.5	3	4	0.2
51383		1.5	0.17	0.5	0.0	-	1.0	1	78	4.8
51430		8.6	0.42	7.0	4.2	0.9				
51440		1.5	0.87	1.0	0.4	-				
50496		1.5	0.81	1.1	0.4	-				
51404		1.8	0.55	1.2	0.2	-	1.9	5	60	3.7
51406		1.5	0.34	0.8	0.1	-				
51413		1.6	0.43	1.0	0.1	-	1.6	2	67	4.1
54734	Lake Taupo (Taupomoana)	61,334.9	0.25	61,159.5	60,813.8	60,308.4	591817.8	674976	101	6.2

*no entry in some cells indicates that there have been no successful retrievals to date. This may be due to lake size, shape or processing difficulties.

Appendix C: Estuary Maps

Air photos of Waikato estuaries (WRAPS 2012). Red line is derived from LCDB estuary shape by applying an inside buffer of 30 m.

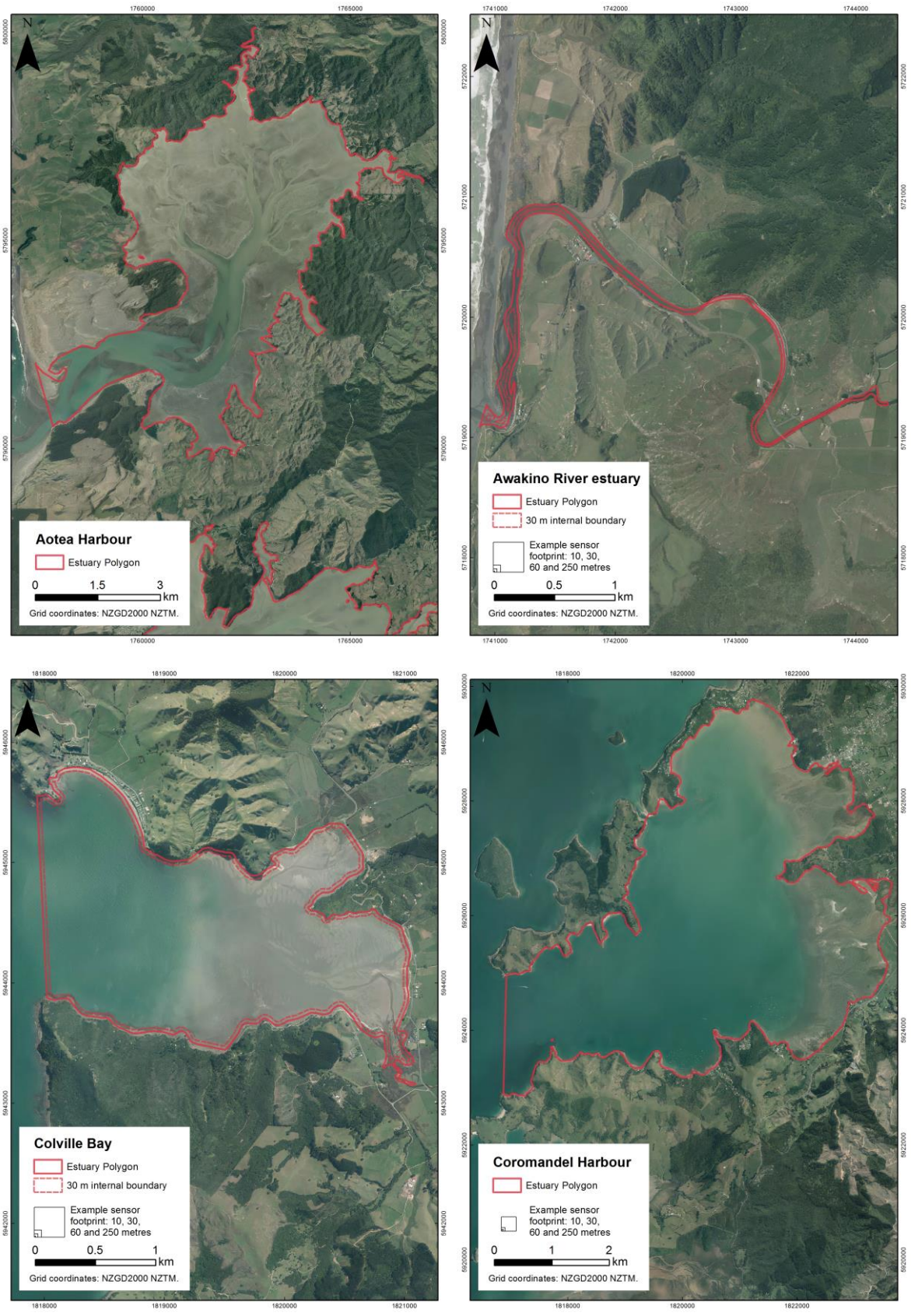

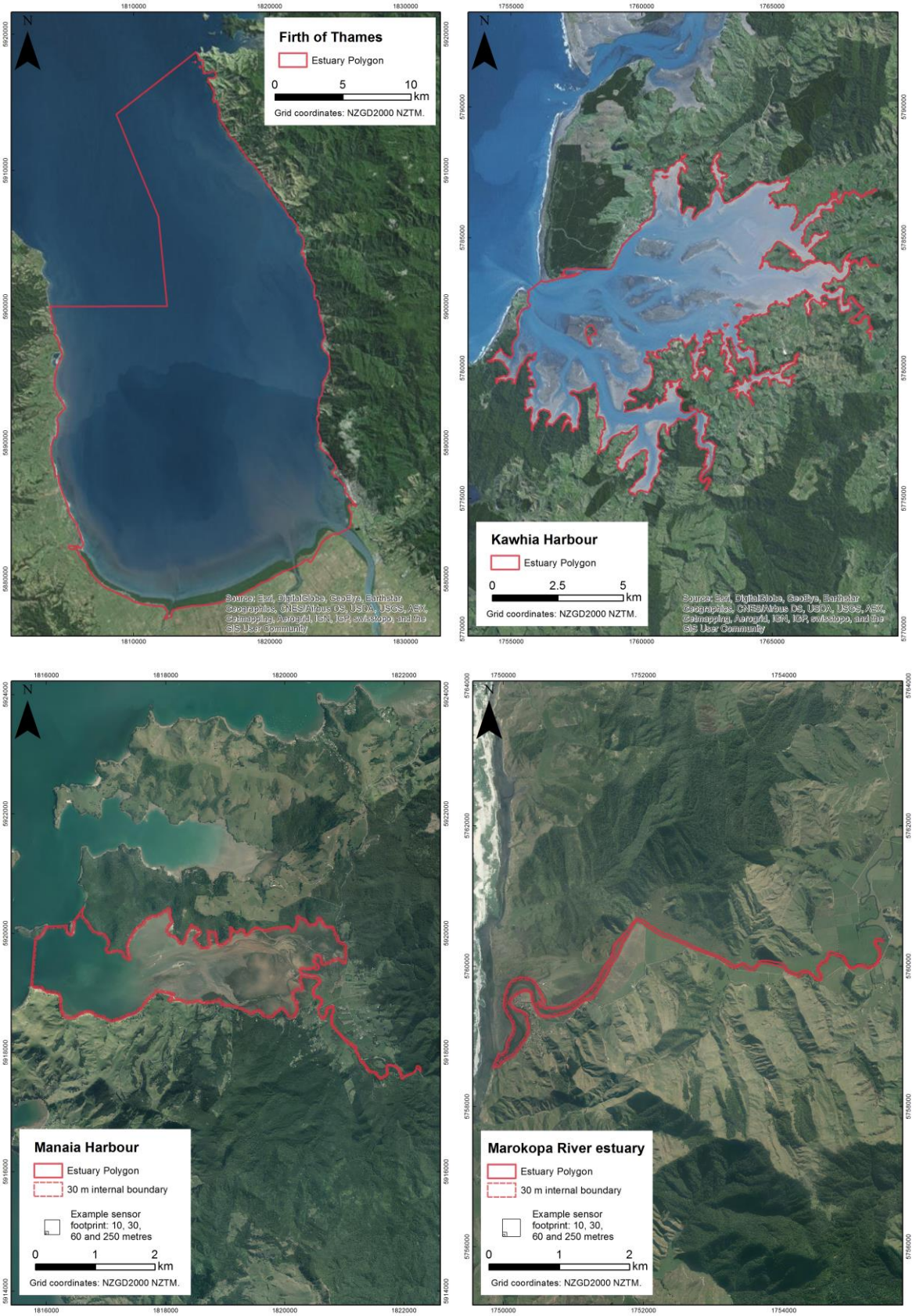
Firth of Thames
Estuary Polygon
0 5 10
km
Grid coordinates: NZGD2000 NZTM.
Kawhia Harbour
Estuary Polygon
0 2.5 5
km
Grid coordinates: NZGD2000 NZTM.
Manaia Harbour
Estuary Polygon
30 m internal boundary
Example sensor footprint: 10, 30, 60 and 250 metres
0 1 2
km
Grid coordinates: NZGD2000 NZTM.
Marokopa River estuary
Estuary Polygon
30 m internal boundary
Example sensor footprint: 10, 30, 60 and 250 metres
0 1 2
km
Grid coordinates: NZGD2000 NZTM.

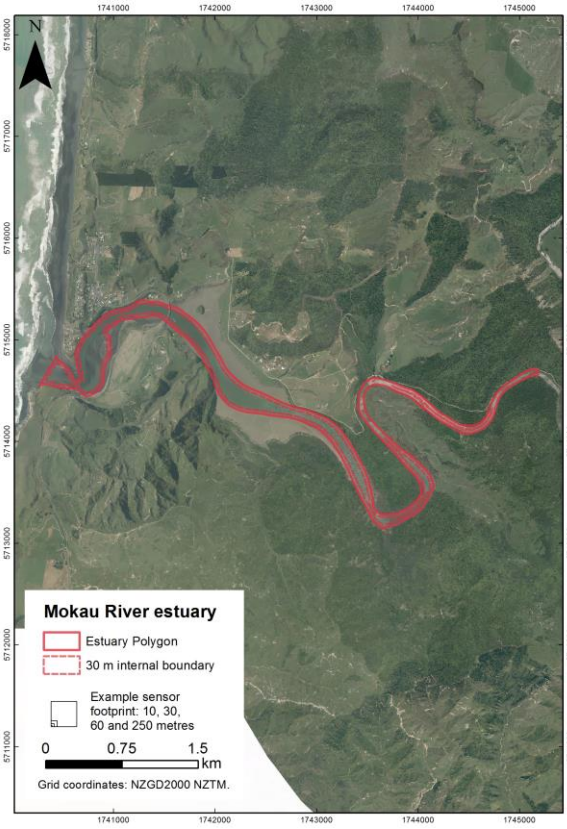
Mokau River estuary
Estuary Polygon
30 m internal boundary
Example sensor footprint: 10, 30, 60 and 250 metres
0 0.75 1.5 km
Grid coordinates: NZGD2000 NZTM.

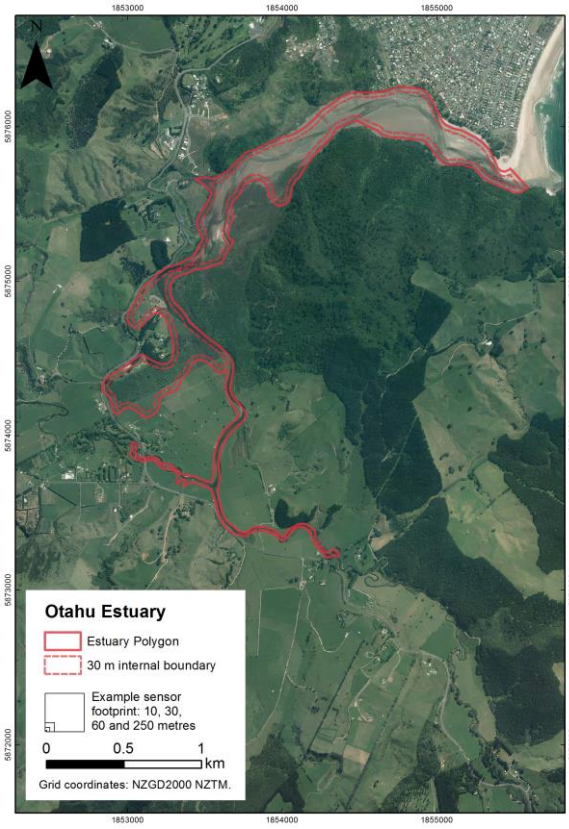
Otahu Estuary
Estuary Polygon
30 m internal boundary
Example sensor footprint: 10, 30, 60 and 250 metres
0 0.5 1 km
Grid coordinates: NZGD2000 NZTM.

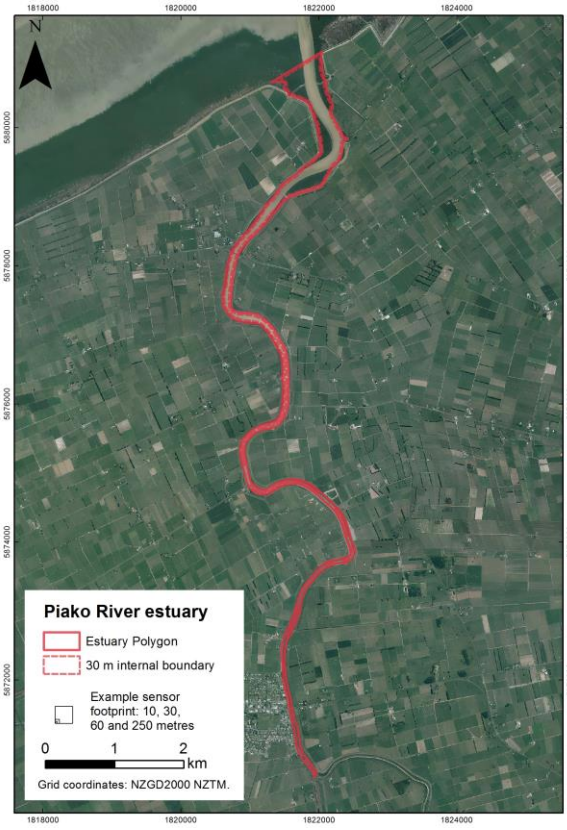
Piako River estuary
Estuary Polygon
30 m internal boundary
Example sensor footprint: 10, 30, 60 and 250 metres
0 1 2 km
Grid coordinates: NZGD2000 NZTM.

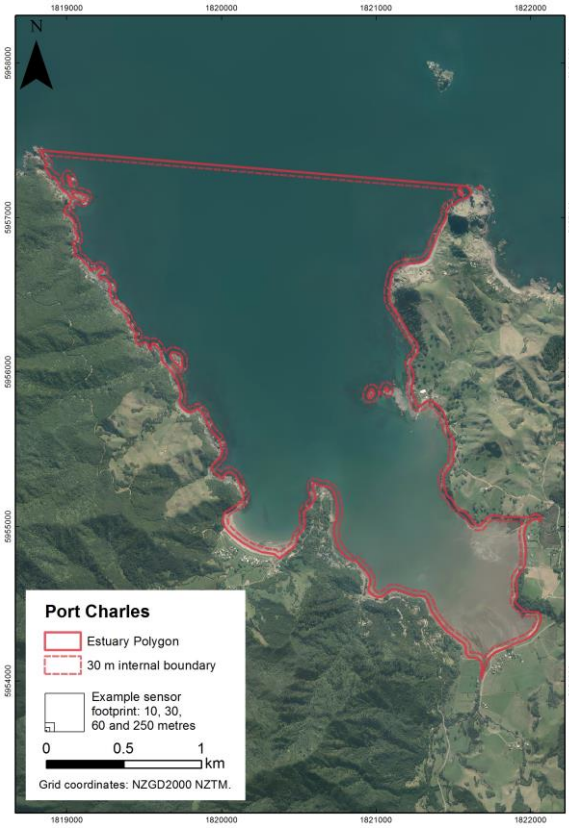
Port Charles
Estuary Polygon
30 m internal boundary
Example sensor footprint: 10, 30, 60 and 250 metres
0 0.5 1 km
Grid coordinates: NZGD2000 NZTM.

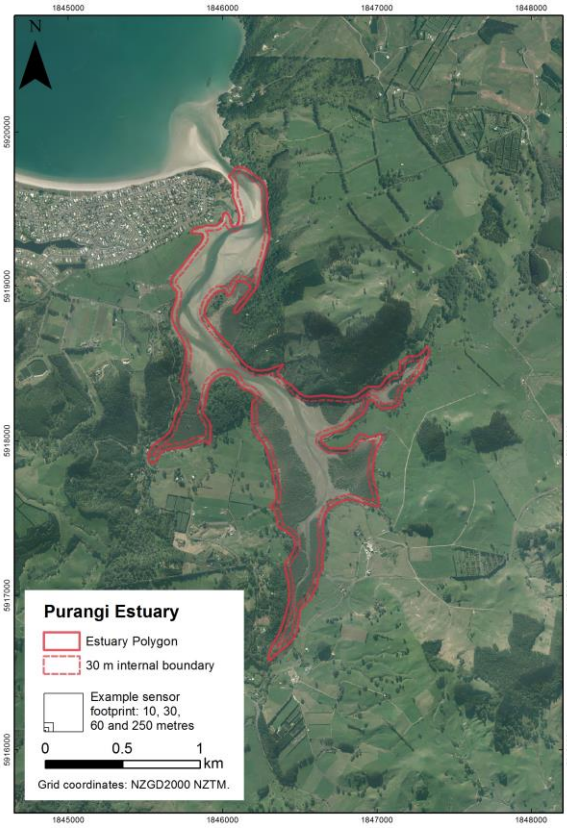
Purangi Estuary
Estuary Polygon
30 m internal boundary
Example sensor footprint: 10, 30, 60 and 250 metres
0 0.5 1 km
Grid coordinates: NZGD2000 NZTM.

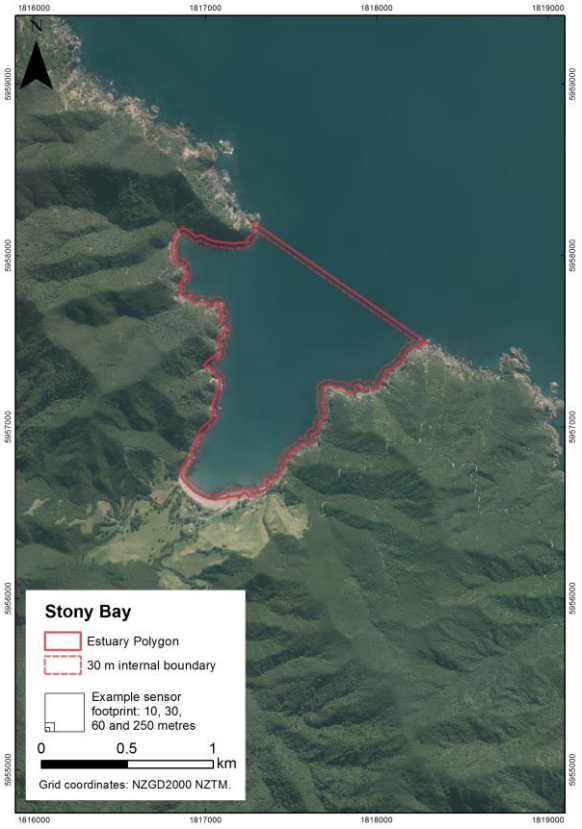
Stony Bay
Estuary Polygon
30 m internal boundary
Example sensor footprint: 10, 30, 60 and 250 metres
0 0.5 1 km
Grid coordinates: NZGD2000 NZTM.

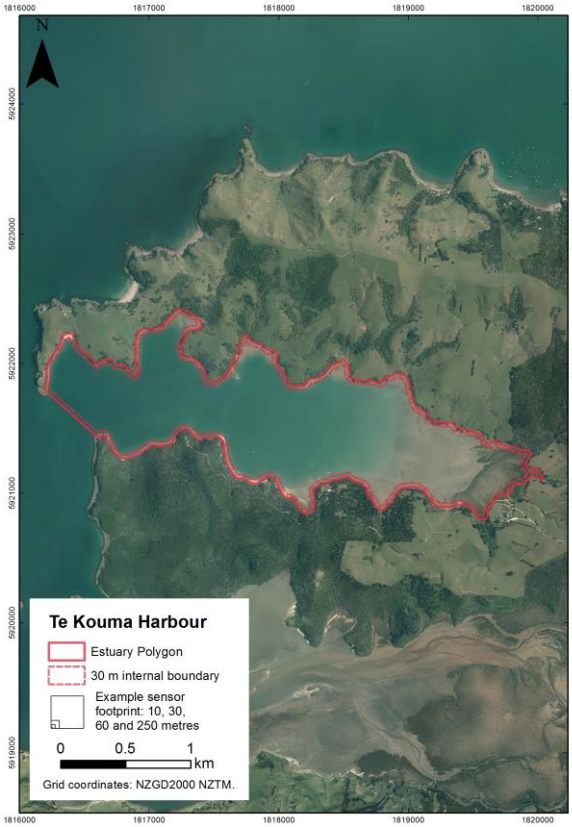
Te Kouma Harbour
Estuary Polygon
30 m internal boundary
Example sensor footprint: 10, 30, 60 and 250 metres
0 0.5 1 km
Grid coordinates: NZGD2000 NZTM.

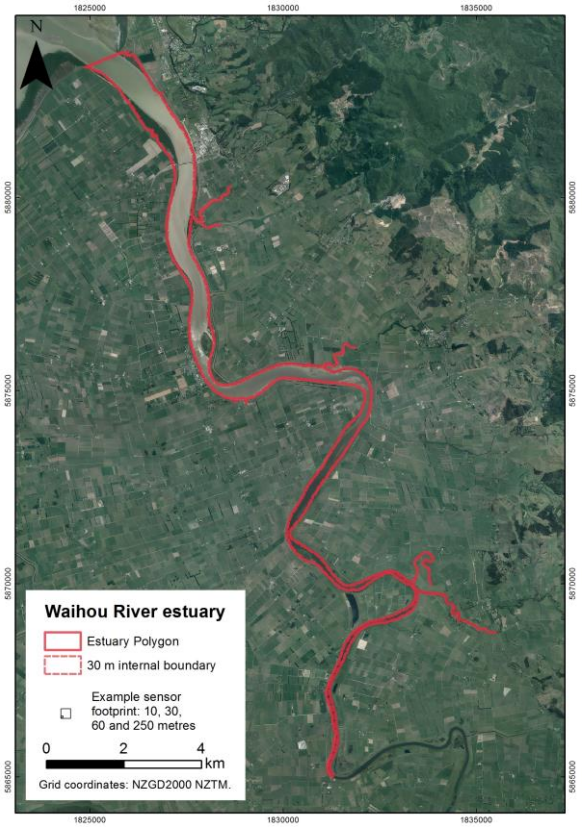
Waihou River estuary
Estuary Polygon
30 m internal boundary
Example sensor footprint: 10, 30, 60 and 250 metres
0 2 4 km
Grid coordinates: NZGD2000 NZTM.

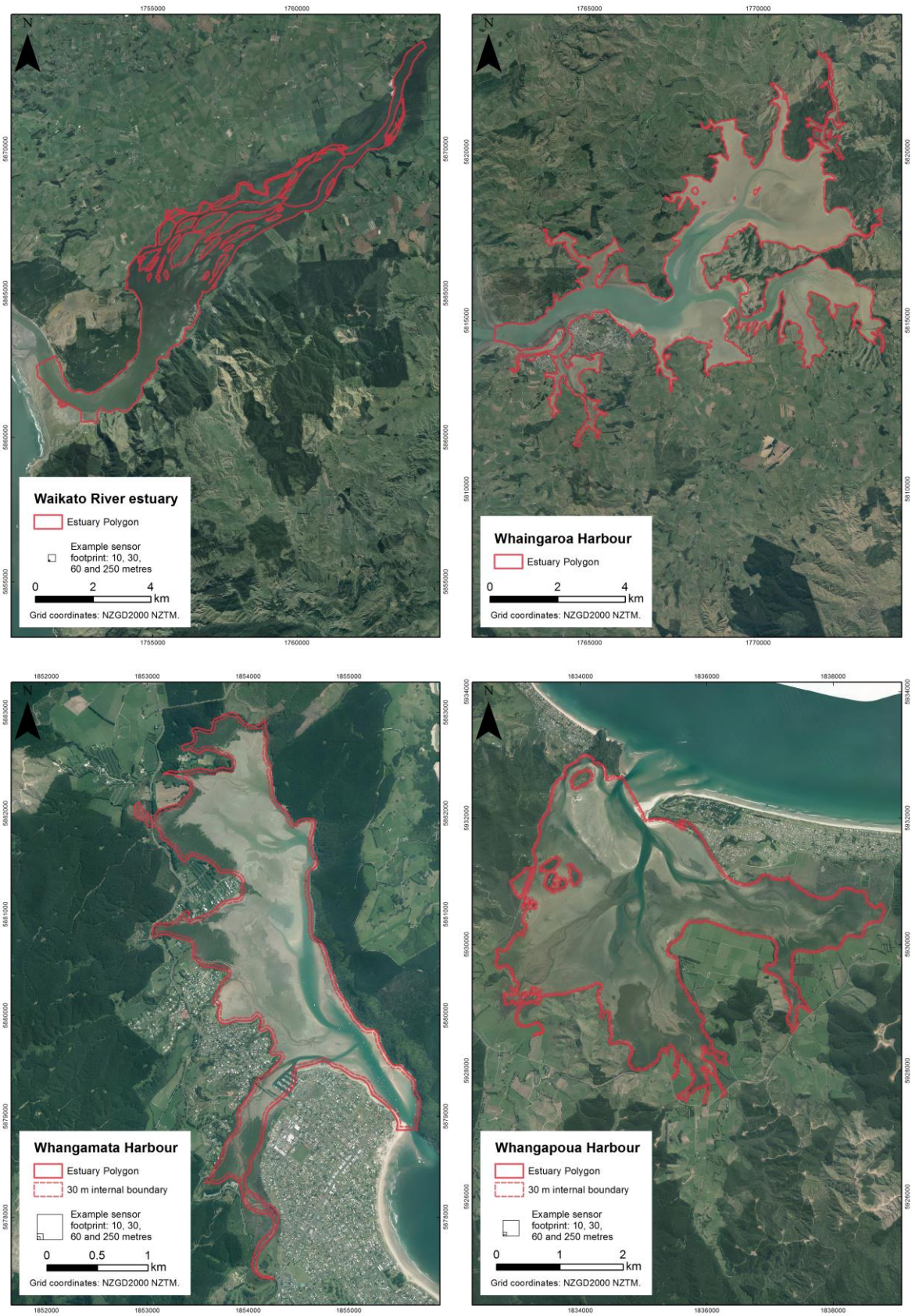
Waikato River estuary
Estuary Polygon
Example sensor footprint: 10, 30, 60 and 250 metres
0 2 4 km
Grid coordinates: NZGD2000 NZTM.
Whaingaroa Harbour
Estuary Polygon
0 2 4 km
Grid coordinates: NZGD2000 NZTM.
Whangamata Harbour
Estuary Polygon
30 m internal boundary
Example sensor footprint: 10, 30, 60 and 250 metres
0 0.5 1 km
Grid coordinates: NZGD2000 NZTM.
Whangapoua Harbour
Estuary Polygon
30 m internal boundary
Example sensor footprint: 10, 30, 60 and 250 metres
0 1 2 km
Grid coordinates: NZGD2000 NZTM.

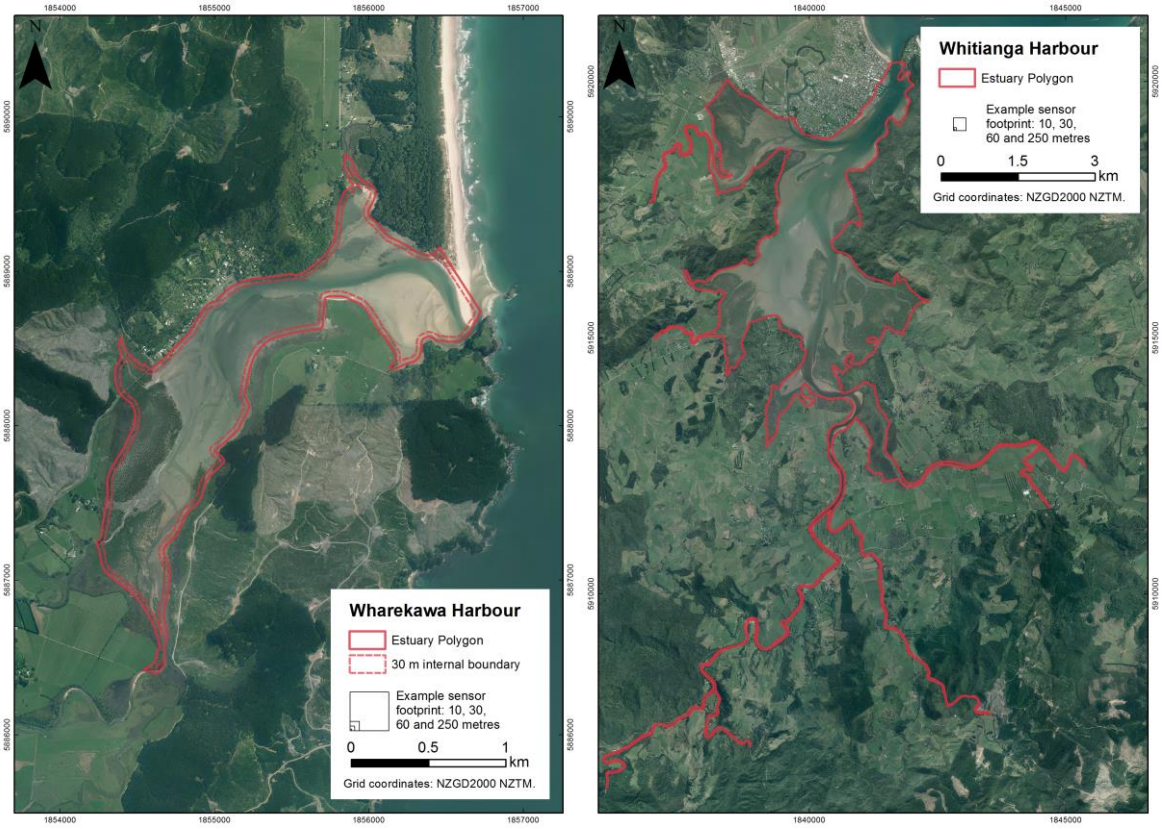
Wharekawa Harbour
Estuary Polygon
30 m internal boundary
Example sensor footprint: 10, 30, 60 and 250 metres
0 0.5 1 km
Grid coordinates: NZGD2000 NZTM.
Whitianga Harbour
Estuary Polygon
Example sensor footprint: 10, 30, 60 and 250 metres
0 1.5 3 km
Grid coordinates: NZGD2000 NZTM.